Petra Christöfl, BSc

Investigation of mechanical strength of iron containing NTC ceramics

MASTER'S THESIS

to achieve the university degree of

Diplom-Ingenieurin

Master's degree programme: Advanced Materials Science

submitted to

Graz University of Technology

Supervisor

Ao.Univ.Prof. Dipl.-Ing. Dr.techn. Klaus Reichmann

Institute for Chemistry and Technology of Materials

Graz, May 2017

Kurzfassung

Festigkeitsanalysen von eisenhaltigen NTC Keramiken

In der Firma EPCOS OHG, einem Mitglied der TDK Gruppe, werden NTC (Negative Temperature Coefficient Thermistors) Temperatursensoren auf Basis von kermischen $NiMn_2O_4$ Spinellen hergestellt. Während des Fertigungsprozesses kam es dabei öfters zu Kantenausbrüchen an den Substraten. Kantenausbrüche sind nicht nur optische Fehler, sondern verändern auch die elektrischen Eigenschaften der NTCs. Ziel dieser Master Arbeit war es die Ursachen der Kantenausbrüche näher zu betrachten und in einem zweiten Schritt sollten diese Kantenausbrüche bei einer eisenhältigen Keramik verringert werden.

Nach Analyse des Produktionsprozesses nach Six Sigma Methoden stellte sich heraus, dass die mechanische Festigkeit der NTCs zu gering ist. Als Ursache der geringen Festigkeit konnte die Porosität der Keramiken ausgeschlossen werden. Vielmehr konnte gezeigt werden, dass die NiO Ausscheidungen und deren Verteilung im Substrat einen wesentlichen Einflussfaktor auf die Festigkeit darstellen.

Zur Verbesserung der mechanischen Festigkeit wurden die Sinterparameter "Haltezeit", "Maximaltemperatur" und "Abkühlrate" in einer Statistischen Versuchsplanung (DoE) variiert. Somit konnte die Festigkeit von 32 MPa auf 43 MPa verbessert werden.

Abstract

Investigation of mechanical strength of iron containing NTC ceramics

In the company of EPCOS OHG, a TDK group company, NTC temperature sensors (Negative Temperature Coefficient Thermistors) on the basis of ceramic $NiMn_2O_4$ Spinels are produced. During manufacturing process, edge breakouts on the substrates occured frequently. Edge breakouts are not only optical flaws, they also change electrical parameters of NTCs. It was the goal of this master thesis to investigate the reasons of the edge breakouts and in a second step to reduce edge breakouts for one specific iron containing composition.

After analysis of the production process with Six Sigma methods it was obvious, that the mechanical strength was too low. Porosity of the ceramics could be excluded as possible reason for the reduced strength. Furthermore it could be shown, that NiO precipitations

and their distribution within the substrate are a main influencing factor on mechanical strength.

To improve the mechanical strength, the sinter parameters "Hold Time", "Maximum Temperature" and "Cooling Rate" were varied according to a Design of Experiments (DoE) plan. Hence the mechanical strength could be improved from 32 MPa to 43 MPa.

Contents

1. Introduction

Temperature sensors are widely integrated in our daily lives and can be found in households, laboratories, medical devices and also in industrial equipment. Their main purpose is to deliver an electrical signal in dependence of temperature.

Nevertheless four types of temperature sensors can be found on the market: thermocouples, RTDs (*resistance temperature detectors*), sensors and thermistors such as NTCs. [6]

Thermocouples consist of two different metals and use the Seebeck effect to translate a temperature difference in an electrical current. They are small, cheap, tough and cover a wide temperature range from $-270°C$ to $2300°C$. But as a disadvantage they are prone to corrosion and have a lower sensitivity than NTCs.[6]

RTDs are Platinium components, which are able to convert a temperature signal in a resistance signal, due to a linear resistance to temperature dependency. To produce a signal output, a current excitation is needed. In comparison to NTC, the RTD has the highest sensitivity. The main disadvantage is that RDTs are expensive and have a slow response time. The temperature range lies between $-50°C$ to $1000°C$. [6]

Semiconductors based on Si and Ge are often integrated into IC sensors and offer a highly linear resistance temperature dependency, furthermore low costs, higher stability and the fastest response time. The main disadvantage is the limited temperature range from $-50°C$ to $150°C$. [6]

In an NTC (*Negative Temperature Coefficient*) thermistor, based on ceramics, the resistance decreases with growing temperature. NTCs can be used in a temperature range from $-50°C$ to $1000°C$. Furthermore they can be produced in small sizes and with low cost. Another benefit of NTCs is their high sensitivity. On the other hand the temper-

ature dependency is non linear and as for ICs and RTDs, a current source is needed. [6]

NTC resistors can be used as temperature sensors or heat abstraction sensors. They can also be used for compensation or safety in electronic circuits.[18]

Temperature sensors are often applied for temperature measurement of gases in fire detectors. In automotive industry often metal encapsulated NTCs are used to have a good heat conduction e.g for control of temperature of engine block, cooling water, oil and brake fluid.[18]

NTCs are also used in medical devices like in clinical thermometers, where they replace mercury thermometers for safety reasons.[18]

Another field of application is as sensor for thermal conductivity. Therefore the NTCs are operated under constant current and the heat dissipation is measured by a changing heat dissipation coefficient, which is dependent from the ambient medium. The sensor detects a changing aggregate state or a changing gas pressure. This is used e.g. in gas chromatography.

In electronic circuits, NTCs are used for limitation of inrush currents. [18]

In the company of EPCOS, NTCs are produced with emphasis on electrical parameters employing strict quality management, as these are the main customer requirements. For a manufacturing company it's also necessary to avoid or minimize scrap. Edge breakouts are responsible for a big part of this scrap as they are not only optically visible defects. Edge breakouts change the geometry of a NTC component and therefore change also the electrical parameters. The main goal of this diploma thesis is to investigate the causes of the edge breakouts and their influencing factors during the process. As the analysis of the manufacturing process with Six Sigma tools comes to the result, that the mechanical strength of the NTCs is too low, the mechanical strength of various types of NTC ceramics had to be investigated. Mainly iron containing NTCs should be investigated and non iron containing NTCs served as reference. Furthermore the mechanical strength of one certain iron containing ceramic should be improved within electrical specifications by variation of sinter parameters.

2. Fundamentals and State of the Art

2.1. Fundamentals of NTC Ceramics

NTC thermistors are ceramic semiconductors based on one of three Crystal structures: Spinels, Perovskites or Pyrochlores. In this diploma thesis, only Spinel structured materials are examined and therefore the emphasis is put on the Spinel.

Mn_3O_4 with the mineral name "'Hausmannite"' is a transition metal oxide and a so called normal Spinel with Mn^{2+} on tetrahedral sites and Mn^{3+} on octahedral sites. This Spinel is not very conductive. By substituting Mn^{3+} with Ni^{2+}, Ni^{2+} is able to occupy octahedral sites. This leads to a conversion of Mn^{3+} to Mn^{4+},which compensates the lower charge of Ni. That is the basis for polaron hopping. Polaron hopping needs ions of the same element with different charges on similar sites. So the electrons are able to move. [12]

The electronic band structure is an energy model, where electrons can stay in electronic states with special energy niveaus. There are also energy ranges, where electrons can never exist (gaps). Electrons in an ionic crystal are experiencing a strong electron-lattice interaction. This leads to a breakdown of the band structure and produces localized charge carriers, the polarones (see figure 2.1). The movement of the polarones is thermally activated and the specific resistance decreases exponentially due to activation energy of Arrhenius type. [11]

Spinel can generally be divided into two groups: normal and inverse Spinel. The general formula of normal Spinel is $A[B_2]O_4$. It can be described by the cubic space group Fd3m with the number 228 in the International table of x-ray crystallography. It has a cubic close packing of O^{2-} and A^{2+} occupying the tetrahedral interstices and B^{3+} occupying

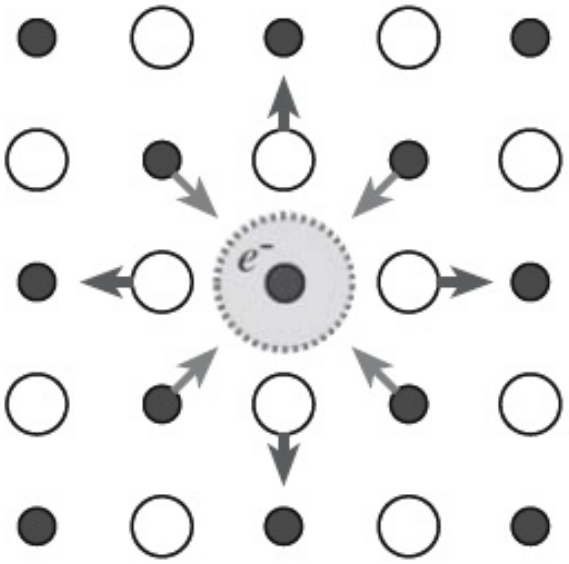

Figure 2.1.: polaron, which shows the distortion of the lattice around an electron after [2]

the octahedral interstices. The structure offers 64 tetrahedral and 32 octahedral interstices. Each unit cell contains of eight AB_2O_4 formula units and therefore consists of 32 O^{2-}, 8 A^{2+} and 16 B^{3+} ions. Therefore only half of the octahedral interstices and a quarter of the tetrahedral interstices are filled. The B-B bond length is represented by $\frac{\sqrt{2}a_0}{4}$, whereas the A-A bond length amounts to $\frac{\sqrt{3}a_0}{4}$ and A-B is $\frac{\sqrt{11}a_0}{8}$. As B-B is the shortest bond length, this bond plays an essential role in the electrical conductivity. [12]

There also exists the so called inverse spinel $B[AB]O_4$. In an inverse spinell half of the B cations occupy tetrahedral sites and all the other B cations occupy the octahedral sites together with the A cations. B ions moving to tetrahedral sites change their valency from 3+ to 2+, whereas B ions on an octahedral site, can change their valency from 3+ to 4+. So the B ions on octahedral states have mixed valences depending on the number of A^{2+} ions on the octahedral sites. This influences the concentration of polarons and therefore influences the resistance. The most common spinel for NTC ceramics is $NiMn_2O_4$.

The exact allocation of cations in the inverse spinel is still matter of research. Furthermore the degree of inversion depends on temperature. It decreases with increasing

temperature. Also in a less studies spinel like $NiFe_2O_4$ there is no agreement in exact valence distribution. [6]

In figure 2.2 the phase diagram for the system Ni-Mn-O can be seen. The compositions of investigated NTCs are around R=0.3. The phase named "$Spl + Ni_xMn_{1-x}O$" is a region consisting of the two phases spinel and $Ni_xMn_{1-x}O$. The structure of this phase is NaCl type. On the left side next to this phase one can find the spinel phase which is a one phase region. At lower temperatures and Mn richer composition the phase $Spl + \alpha - Mn_2O_3$ builds another two phase region. Also the phase "$Spl + NiMnO_3$" is a two phase region.

Sintering a green body of composition 0.3 up to about 1200°C leads to the two phase area, where Ni enriched precipitations are built in the Spinel phase.

However, in a NTC the resistivity ρ depends on the temperature T represented in formula 2.1, where ρ_∞ is approximately independent from temperature and the constant B is related to the activation energy of the electrons.

$$\rho(T) = \rho_\infty \exp(\frac{B}{T}) \tag{2.1}$$

Differentiating equation 2.1 leads to the temperature coeffiecient of restistance α_R represented in equation 2.2.

$$\alpha_R = \frac{1}{\rho}\frac{d\rho}{dT} = -\frac{B}{T^2} \tag{2.2}$$

One can see, the larger the value of B, the higher the temperature coefficient. Furthermore the resistivity will be high at low temperatures as can also be seen in figure 2.3.[12]

$$T - T_0 = k_{th}UI = k_{th}P \tag{2.3}$$

On load the NTC behaves like described in formula 2.3, where P is the power, I is the current, U the voltage drop along the NTC and k_{th} is the constant depending on mounting, shape and surface finish of the NTC as well as environmental conditions.

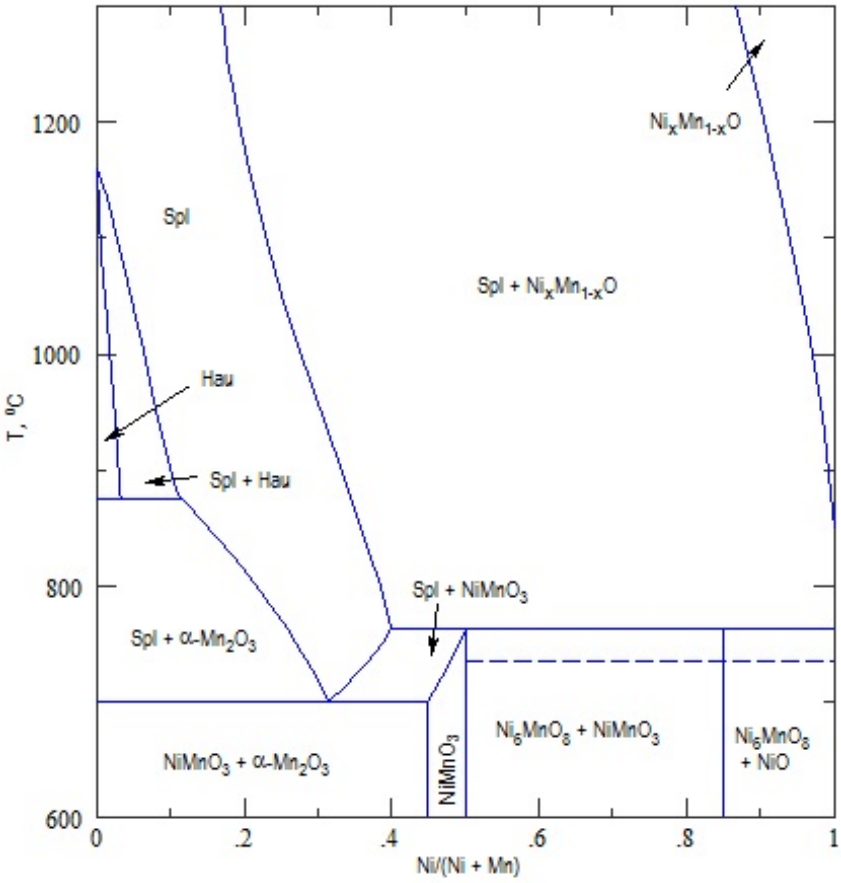

Figure 2.2.: Phase diagram for the system Ni-Mn-O after [8]

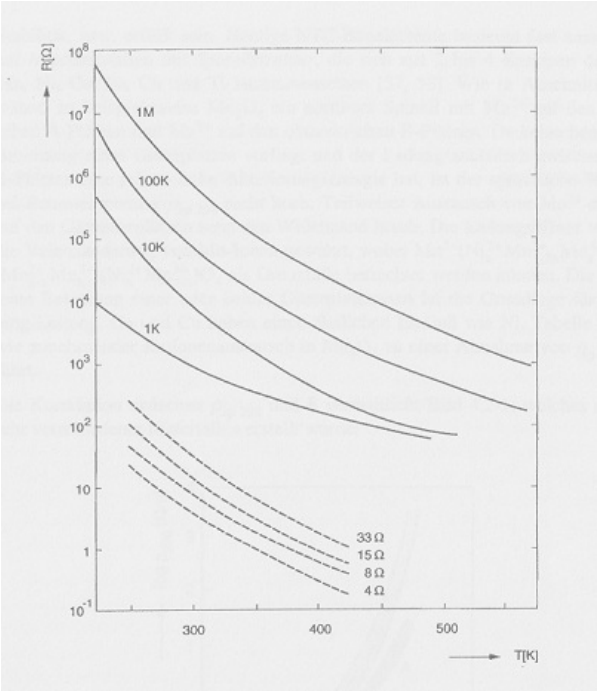

Figure 2.3.: temperature dependency of restistance R of different commercially used NTC thermistors: solid line for NTC as temperature sensor and dashed line for NTC as current pulse protection [18]

Finally the resistance R can be determined by using formula 2.4.

$$R(T) = R_\infty \exp\left(\frac{B}{T_0 + k_{th}P}\right) \tag{2.4}$$

2.2. Mechanical Strength of Ceramic Materials

The following chapter gives a main overview of mechanical strength in ceramics and their measurements methods. Most parts of this chapter are taken from Munz et. al.[13].

NTCs are so called functional ceramics, where the temperature dependent electric conductivity is in focus. But also the NTC has to face mechanical load, for example in a rotating application. As ceramics are brittle materials, they can react to localized and timely short overload with fracture. Furthermore fracture triggering structure failures are randomly distributed which make them even less predictable.

The biggest disadvantage of ceramics is their brittleness, in other words they break without plastic deformation. Another big disadvantage is the big variation of strength in ceramics, because the error size is statistically distributed. The density of the most important ceramics lies between 2.5 - 5 g/cm^3. If the ceramics are porous, the density is lower. The modulus of elasticity for ceramics is much higher than the E-module of metals. It depends on density and porosity, whereas volume and form of the pores are influencing the elastic constant. The higher the porosity is, the lower the E-module will be.

Fracture in ceramics is always the cause of failures. These failures arise during manufacturing in form of pores, cracks or inclusions or they develop during surface treatment, where failures in form of cracks arise which can lead to breakage of ceramics. Ceramics behave with low resistivity against crack propagation and are therefore brittle.

Strength in ceramic materials is usually characterized as resistance against tensile stress (tensile strength). Any other strength like compressive strength is not that important. Tensile strength measurement in ceramics may be performed with tensile test or bending test, depending on the form of the ceramics. Cylindric samples are tested with tensile test and rectangular samples with a bending test. In this present diploma thesis, rectangular samples are investigated; therefore the bending test will be described in the following section.

The 4-point bending test is the most commonly used bending test, because it has a bigger measuring range and a more constant bending moment than the 3-point bending test. By reason of statistical influences the strength data of 4-point bending test are at a lower level than of the 3 point bending test. This has to be considered when comparing data.

The bending strength can be calculated according to fomula 2.5, where F is the failure load, S_1 and S_2 are the distances between the load rolls, W is the height of the sample and b is the width of the sample. A sketch of the 4 point bending test can be seen in figure 2.4. [13]

$$\sigma_c = \frac{3(S_1 - S_2)F}{2W^2 b} \tag{2.5}$$

The development of the tensions near the top of the crack at tensile load perpendicular

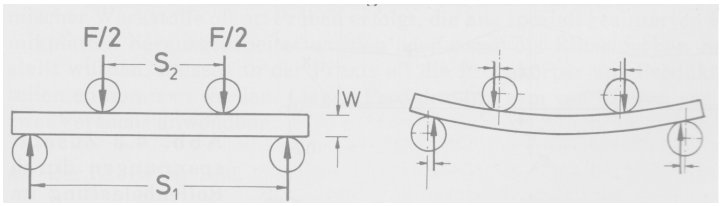

Figure 2.4.: sketch of the 4-point bending test before and after loading situation after [13]

to the crack area can be described with the fracture toughness K_{Ic}. It depends on the mechanical strength σ_c, the size of the failure a and the geometry factor of the sample Y.

$$K_{IC} = \sigma_c Y \sqrt{\pi a} \tag{2.6}$$

Four factors are mainly influencing the measurement error of the 4-point bending test. The first to be mentioned is the friction. If the rolls are affixed, friction occurs between sample and roll. The strength seems higher than it is. To minimize this failure the rolls should be freely movable. The second measurement error is the displacement of the contact line between roll and sample at higher deflexion. The measuring error depends on the proportion from roll diameter to the height of the sample. Excessive tension can be seen as the third measurement error. Loading force is transferred via a contact line between roll and sample. These tensions cause tensile stress to the inner load rolls, which superimposes the bending stress. That is why so many samples break directly under one of the inner rolls. The last measurement failure occurs, if a sample has different elastic constants in case of compressive or tensile stress.

Another way of strength testing is the ball on three balls test (see figure 2.5). It's done by 3 balls contacting each other and a load summoned up by a fourth ball. The advantage of this buildup is that the points of load transfer are well defined, even for imperfect geometry samples. Also sliding friction is replaced by rolling friction. Moreover friction is reduced to a minimum, because the supporting balls are able to roll outwards if the sample bends. After measurement the force data has to be converted into stress data, where numerical tools based on the software Mathematica can be used. To get precise stress data it's very important to measure the thickness in the middle of the sample exactly. The big advantage of the ball on three balls test is that it's possible to test

small components [3]

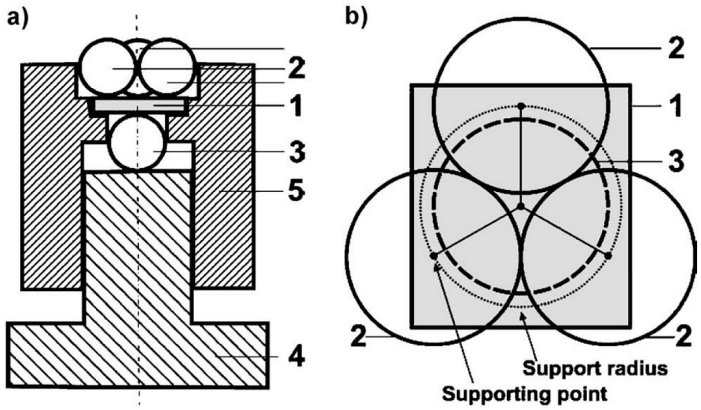

Figure 2.5.: sketch of the ball on three balls test: (a) cross section of the ball on three balls test, (b) top view sketch after [4]

As mentioned earlier, the variance of the mechanical strength is higher than in metals, which is a cause of the fracture reason. Fracture can be running out of the surface or the volume. In the following section it is assumed that only one type of flaw is causing the collapse. Crucial for collapse is the biggest failure in the sample, if there is a homogeneously distributed tension gradient.

2.3. Processing of NTC Ceramics

Processing of NTC ceramics is carried out by usual ceramic production techniques. There are various production types depending on geometry, favored accuracy and application of the ceramic. Anyway there are three main steps in the ceramics production:

1. preparation of ceramic powder via mixed oxide route

2. forming of green ceramic samples with either tape casting or pressing

3. heat treatment (sintering) to get a dense microstructure of the material and desired electrical properties

2.3.1. Powder Synthesis

Raw materials for NTC ceramics are oxides, carbonates, hydroxides and also spray dried salts. After weighing of the required proportions of the raw materials they get wet milled, dried and calcined. In many cases the raw material mixture is calcinated by temperatures between 900 to 1300 K to get a chemical homogeneous and compressed oxide mixture. Moreover phase formation takes place. Another milling process adjusts the particle size of the powder. Normally ceramic powders are milled to μm dimensions to achieve a high sintering activity afterwards. Dried powders are processed to a slurry from which ceramic tapes are casted. To optimize the flowability and to increase the bulk density, the powder is getting granulated. In ceramic processing, spray drying is the most common form of granulation, where the ceramic slurry is sprayed in droplets and dried afterwards in a hot gas flow. [18], [16], [10]

2.3.2. Forming

To get the form of a disc, the granulate is uniaxially cold pressed. Extrusion of oxide powder charged with binder leads to rod shaped NTCs. To get rectangular chips, the powder is processed to a slurry and afterwards tape casted. In tape casting the slurry is spread over a surface covered with a removable sheet. After drying, the sheet is removed and the green bodies are cut to shape. Compared with other production techniques, tape casting has the advantage, that it leads to a uniform packing density in the green body. To reach the desired thickness of the component, foils are laminated. After that the green bodies (substrated from tapes and discs) have to be debindered with a certain temperature program. [18], [16], [10]

2.3.3. Sintering

During sintering the ceramic compound gets its ultimate strength and all the other desired properties. Most ceramic components are sintered with temperatures between 1.500 and 2.200 K. Nowadays dilatometric tests are used to find out the right sintering temperature. It's often wanted to have a preferably low sintering temperature. This can be realized with sinteractive raw materials, milling of the raw materials to very fine

grains or through addition of flux material. Flux material reacts with the matrix phase of the raw material and speeds up the sintering. This leads to a lowering of the sintering temperature. With lower sintering temperature the sintering is more cost economical because of the lower energy and material (machines) costs. Furthermore a low sintering temperature influences strength of the ceramic, because at low sintering temperature grain growth does not occur or it occurs only a little. Strength is a function of grain size. The smaller the grains, the higher the strength.

Furthermore for a good strength of a ceramic compound the density of the sintered body has to be high. The higher the density is, the higher the strength of a sintered ceramic. During sintering a ceramic compound suffers a certain amount of shrinkage, which has to be considered in the planning of the process. Shrinkage often lies between 15-25% depending on the kind of compound and on the used raw materials. Often shrinkage is different in the three directions in space. With an increase of density the shrinkage increases too.

Sintering process can occur between solid particles, so called solid state reaction. But also fluid phases are involved in sintering, whereas the reaction velocity is much higher. During fluid phase sintering various amounts of fluid phases take part, depending on the type of composition and the ratio between the components. Those components, which lead to the fluid phases have to be distributed homogeneously over the green body to avoid inhomogeneous densification. If fluid phases are localized somehow in the compound, instead of shrinkage dilatation can occurs, because the fluid phase diffuses in the grain boundaries and pushes the grains apart. At that places where the fluid phase developed at first, a pore stays behind. Mostly this pore does not disappear during the rest of the sintering process, which leads to a lowering of strength in the compound.

Sintering in NTC ceramics occurs in temperature ranges between 1250 and 1600 K. At these top temperatures, densification, complete building of the spinel phase and grain growth takes place. Typical NTC grain sizes are in between 4 and 30 μm. Most NTCs are drafted as single-phase spinell systems. Somehow in the cooling phase oxidation of the spinel occurs and leads to formation of a new phase. This could be avoided with higher cooling rates. [18]

2.3.4. Electrodes

After sintering the NTCs are coated with silver and gold paste through screen printing and burned in afterwards. In other cases also vacuum deposition techniques are used. Because of the band structure of the spinels and the high carrier density there is no depletion layer of barrier at the grain boundaries or at the boundary layer of the electrodes. Therefore resistive transitions occur. Multilayer wafers are diced after electrode deposition to obtain single components. [18]

2.4. Six Sigma Tools

Six Sigma is a quality management tool and it's main goal is the improvement of processes. The optimization runs through following phases and is therefore called the DMAIC method: **D**efine, **M**easure, **A**nalyze, **I**mprove and **C**ontrol. In figure 2.1 the main goals, functions and tools of Six the Six Sigma Phases are represented.

In the Define phase the parameters, which have to be improved, are determined. In the Measure Phase the actual condition of the process is described. In the Analyze phase the relationship between command variable and influence factors are identified. Within the Improvement phase a solution is determined and practically operated. In the Control phase the optimized solution gets implemented sustainable.[22]

2.4.1. Design of Experiments

Design of experiments (DoE) is a useful method for optimization and development of products and processes and therefore part of the Analyze step of the Six Sigma Roadmap (see table 2.1. When planning experiments, resources are limited and it's the responsibility of the designer to get accurate and reliable results. The main goal of design of experiments is to find out the relationship between influencing factors and target factors with as little experiments as possible. To get a reliable proposition the target values have to be normally distributed.

Table 2.1.: Six Sigma Roadmap after [7]

Phase	goals	main functions	tools
Define	definition of the improvement project	description of the initial situation, getting an overview of the process, determine customer requirements, defining the project	work breakdown structure, project results plan
Measure	determination of the current state	detailing the processes, interpret existing data, capture and evaluate data, check suitability of the measuring system, detect process power	measuring system analysis, Pareto analysis
Analyze	identification of relevant reasons	identify main influencing factors, identify cause-effect relationships	cause-effect analysis, correlation and regression, statistical design of experiments
Improve	development and testing of Solutions	develop solution variants, evaluate solution and choice of solution, testing of chosen solution and evidence of effectiveness, planning of implementation	creativity techniques, FMEA
Control	sustainable implementation of optimizes solution	establishing of the solution in the organisation, secure improvements sustainable, closing of the project	process flow chart, Process control card, training

So the first issue of DoE is to find out the influencing factors and the target factors, which can be found out with process mapping, paired comparison, Critical two Matrix, Pareto analysis and Ishikawa diagrams. Influencing factors should be adjustably targeted and reproducible. DoE furthermore requires a processing of the plan without gaps. But the main factor of success is the right selection of the target values.

The settings of the factors are called steps or levels. Each factor is tested at least at two levels. The effect of one factor depends mainly on it's step distance. Little steps have usually little impacts. If the step is too narrow, maybe the impact cannot be measured. Therefore it is necessary to have bigger steps in an earlier phase of the project.

It is usual, when having three influencing factors, to just change one parameter in every experiment. So every effect can be back warded to an influencing factor. This experimental setup has a big disadvantage. It assumes that the effect only depends on the one changed influencing factor. But practically the effect depends often on more than one influencing factor. DoE assures that the combination of influencing factors can be shown. An orthogonal DoE ensures that no combination of two columns correlates to each other (see also table 2.2). In other words, the setting pattern of all factors have to be independent [20].

In figure 2.6 a full factorial DoE with 3 factors and 2 steps can be seen. This DoE contains $2^3 = 8$ experiments (corner points).

If the factors do not depend linearly from each other, the full factorial DoE can be expanded to a so-called central composite design. It enables the possibility to add so called star points to the corner points of the cube. A star enables the variation of the factors outgoing the center point. The step distance is now higher that the step distance of the cube (see figure 2.7). With this design three factors can be observed with 15 experiments at five steps (see table 2.2). The correlation coefficient is depending on the amount of factors. At three factors it amounts 0.47. The quotient of the step size is the extension factor. If a DoE is orthogonal and rotatable, the extension factor has to be given in dependency of the amount of factors. A design is rotatable, if the variance of the prediction is only depending on the distance to the central point and not from the direction. [20]

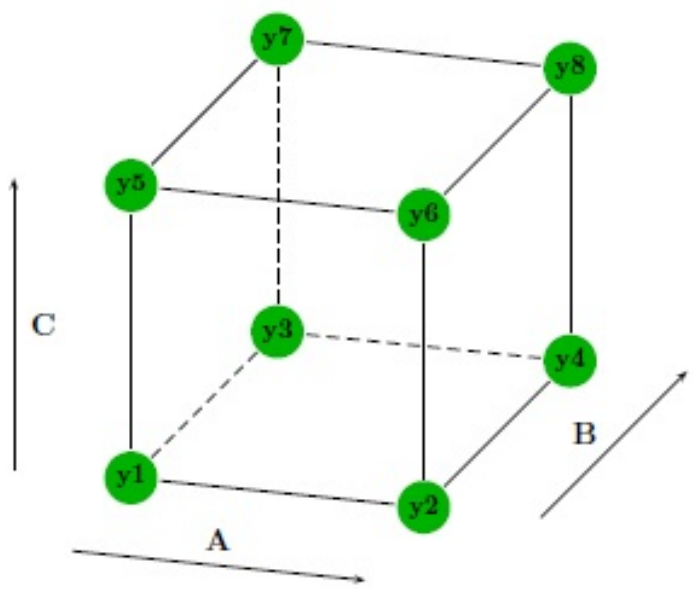

Figure 2.6.: fullfactorial DoE after [20]

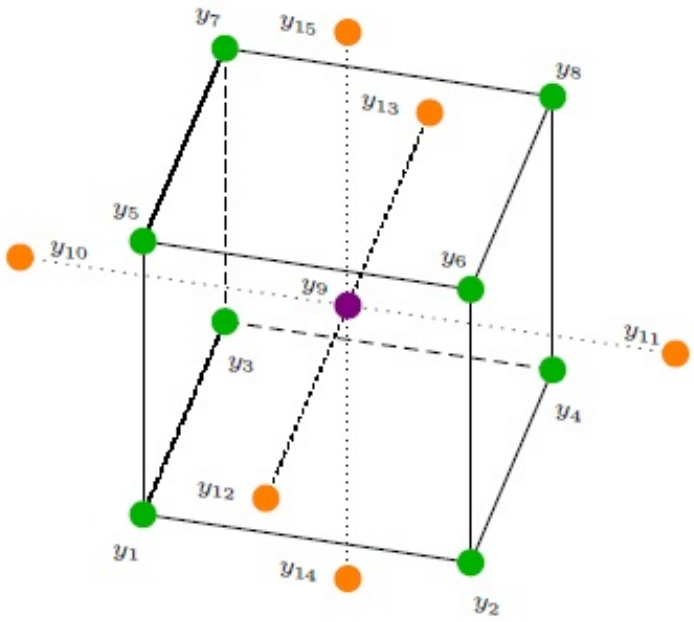

Figure 2.7.: fullfactorial DoE with center and star points after [20]

Table 2.2.: Central Composite Design of DoE [20]

A	B	C	y
-	-	-	y1
+	-	-	y2
-	+	-	y3
+	+	-	y4
-	-	+	y5
+	-	+	y6
-	+	+	y7
+	+	+	y8
0	0	0	y9
–	0	0	y10
++	0	0	y11
0	–	0	y12
0	++	0	y13
0	0	–	y14
0	0	++	y15

2.5. Statistic Evaluation

In the daily life in companies, decisions are often made following a good feeling or due to long term experiences. With Six Sigma decisions are made on the basis of numbers, data and facts. If somebody wants to apply Six Sigma for project and process management, it is essential to understand basic statistics. Statistics, which are used in this diploma thesis, are described in the following section.

In every experiment, statistically random events occur due to environment or irregularities in process or raw material. Because of that, it is necessary to describe the influence of this randomness properly with statistical tools. In this diploma thesis the Software Minitab and Microsoft Excel were used for statistical evaluation.

2.5.1. Statistic Distributions

There are two main distributions to be considered: the discrete and the continuous distribution. Discrete distributions are applied, when characteristics are countable and continuous distributions are used for measurable characteristics (see fig. 2.8).

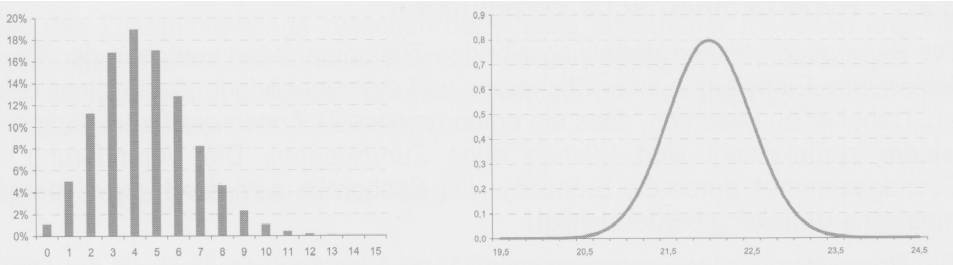

Figure 2.8.: types of statistic distributions: descrete distribution: characteristsics can only take well defined values (left), continuous distribution: characteristis can take any value (right) after [22]

In the following section, only statistic distributions, which are used in this diploma thesis, are described.

2.5.1.1. Normal Distribution

The normal distribution is a continuouse distribution and is also often called "Gauss's bell curve", named after the German mathematician Johann Carl Friedrich Gauss. Main parts of this chapter are taken from [22]. There are several reasons for the frequent usage of the normal distribution [22]:

- According to the central limit theorem, characteristics, which are resulting of many independently non dominating random variables, are about normal distributed. Therefore many characteristics are normally distributed theoretically.

- Sometimes not normal distributed characteristics can be transformed in normal distributed variables. Then the laws of normal distribution can be used.

In fig.2.9 the normal distribution is shown. Two parameters are determining the normal distribution: The arithmetic mean μ determines the location of the bell curve. This value defines the biggest density of measured values and is also called the expected value. The standard deviation σ is the degree of the spread width of the Gaussian bell curve and corresponds to the distance from μ to the inflection point. Both parameters are usually unknown and are estimated from a sample.

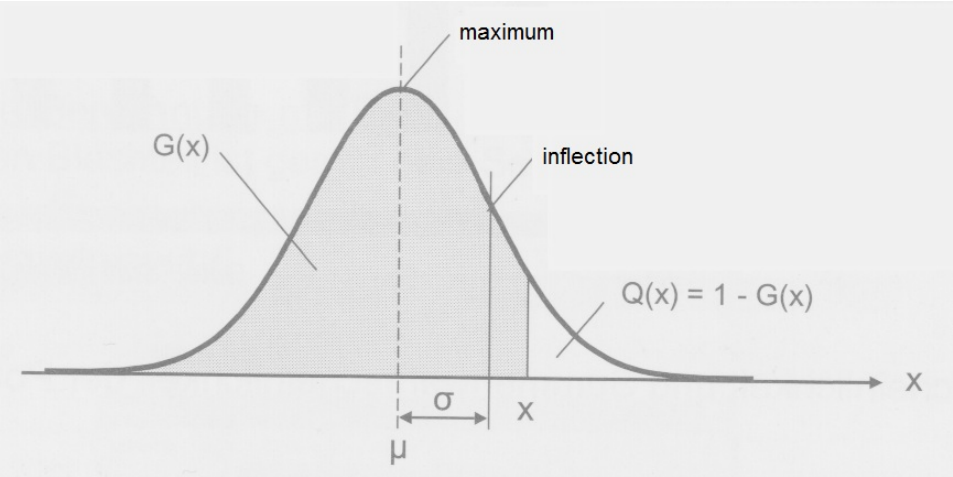

Figure 2.9.: density function of the normal distribution after [22]

The density function of the normal distribution is a symmetrical function. The graph turns bell-like to both sides and draws closer to the abscissa, which it touches in infinity.

The area under the curve corresponds to the probability, where G(x) is the probability that a measured value turns out the be x at maximum. This is in accordance to the area under the bell curve from $-\infty$ to x. The rest of the area from x to $+\infty$ is defined as Q(x). The sum of G(x) and Q(x) equals to 100%, which means that

$$G(x) + Q(x) = 1 \tag{2.7}$$

The probability that a normal characteristic equals exactly x, is zero. It is more useful to formulate questions about intervals. The probability that a measured value lies in between a and b equals to G(b)-G(a) and corresponds to the area under the bell curve between a and b. The area from $-\infty$ to $+\infty$ is 1 or 100%. The area in between $-\sigma$ to $+\sigma$ equals to 68.27% (see also fig. 2.10).

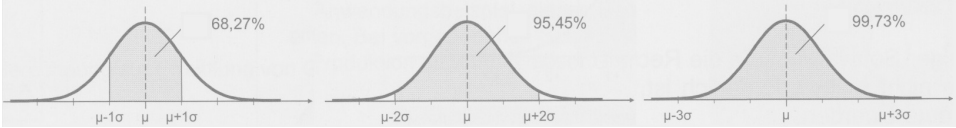

Figure 2.10.: area under the Normal distribution after [22]

For the usage of the normal distribution in practical, the normal distribution has to be converted to the so called standardized normal distribution, where $\mu = 0$ and $\sigma = 1$. The so called z-transformation can be carried out with formula 2.8:

$$z = \frac{X - \mu}{\sigma} \tag{2.8}$$

For the so calculated z, the area under the Gaussian bell curve can be looked up in so called z tables in every mathematic formula collection.

2.5.1.2. Weibull Distribution

It could be derived, that for a bigger class of density function of the flaw size, the strength distribution can be approximated with Weibull distribution, which is named after the swedish professor and engineer Waloddi Weibull. The Weibull distribution is also a continuous distribution and can be adjusted for many forms of frequency distributions. The Weibull distribution is identified by three parameters [22]:

- characteristic life time
- breakdown steepness
- breakdown free time

Therefore the Weibull distribution belongs to the main distributions to evaluate the life time of products, because it depicts the whole life time behavior.

The distribution of mechanical strength can be represented with the Weibull distribution according to equation 2.9, where F is the density function, σ_c is the variation of the mechanical strength and m is the Weibull modulus.

$$F(\sigma_c) = 1 - \exp[-(\frac{\sigma_c}{\sigma_0})^m] \tag{2.9}$$

σ_0 can be represented as

$$\sigma_0 = \frac{K_{Ic}}{Y\sqrt{a_0}(zV)^{1/m}} \tag{2.10}$$

The parameter a is the length of the initial crack size and a_0 is the smallest assumed crack size. Y is a constant parameter and equals to one in most cases. K_{Ic} is the fracture toughness.

The representation of the results is represented in a Weibull diagram, where on the axis of abziscissae one can find $\ln \sigma_c$ and on the axis of ordinates one can find $\ln \ln 1/(1-F)$, where F is the probability of failure. To determine the Weibull strength σ_0 and the Weibull modulus m graphically, first of all, the measured tensile strength data are sorted and enumerated ascending from 1 to n. After that the probabilities of failure F_i are related, with calculation according to equation 2.11.

$$F_i = \frac{i - 0.5}{n} \tag{2.11}$$

The parameter m is the slope of the best fit line and the Weibull strength σ_0 is the strength at $\ln \ln 1/(1-F) = 0$ or F=0.632, which can be seen in figure 2.11.

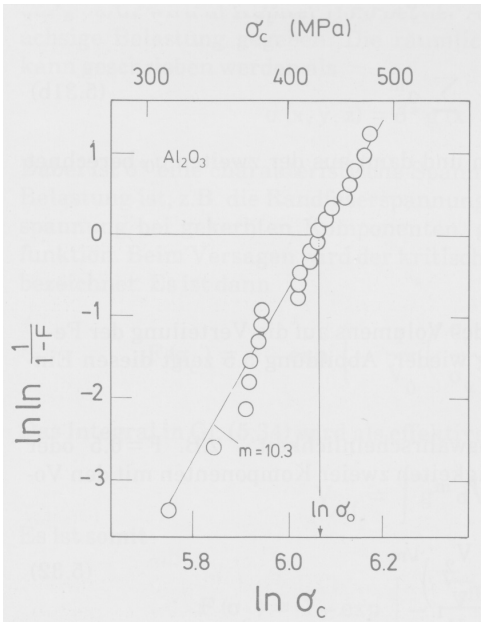

Figure 2.11.: variation of mechanical strength of Al_2O_3 in a Weibull diagramm after [13]

2.5.2. Statistical Hypothesis Testing

Statistical hypothesis testing is a useful tool to make decisions on a reliable basis. First of all a hypothesis has to be set up. Main goal of statistical hypothesis testing is to find out, if a hypothesis is true with a certain probability. The initial assumption of the test is called the null hypothesis (H_0). The opposing assumption is called the alternative hypothesis (H_1). Also a confidence interval has to be set up. In this confidence interval the true value can be found with a certain percentage. A good overview of hypothesis testing can be found in [22] or also in the mathematical form collection of [14].

There are two testing options: the unilateral test and the bilateral test. If there exists an upper or a lower delimitation because of physical reasons, the unilateral test should be used. For example it could be a physical reason that negative values are not allowed. For problems with upper and lower limit the bilateral test should be used. To find out if the null hypothesis has to be accepted or rejected, a test for significance has to be carried out. As a result of the test, the p-value shows, if the null hypothesis should be accepted or the alternative hypothesis should be accepted. In most cases a confidence interval of 95% is chosen (see figure 2.12). So the level of significance is $\alpha = 5\%$. The confidence interval is an area, which includes with infinitely repetition of a random experiment a defined prevalence of the true value. If the confidence interval is 95%, the true value lies in between the confidence interval with 95%. So if the calculated p-value is bigger than 0.05, the null hypothesis has to be accepted. If the p-value is smaller or even to 0.05, the null hypothesis has to be declined and the alternative hypothesis has to be accepted. So the probability to make a wrong decision is 5%. [22],[14]

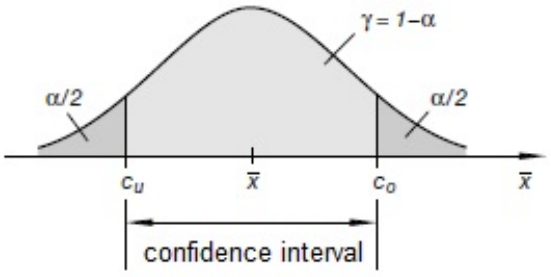

Figure 2.12.: confidence interval after [14]

2.5.3. t-Test

There are two tests which are able to compare two samples to determine if they are significantly distinguishable or not: They are called t-test and u-test. The u test has relatively weak requirements. The characteristic has to be steady and the sample has to be independent. Furthermore the standard deviation should be known. The t test on the other hand, estimates the standard deviation of the sample. Furthermore a sample should be normally distributed to use the t test.

The one sample t test checks on the basis of the mean of a sample if the mean of a basic population differs from a specified value. The two sample t test checks on the basis of the mean of two independent samples, how the mean of two basic populations behave to each other. This test is often used in current diploma thesis to find out, if a characteristic of two samples is significantly different or not. For testing more than two samples, a multiple t-test could be applied. But it should be considered, that with this testing method the probability of an incorrect decision increases, where the null hypothesis is wrongly rejected. [22]

2.5.4. Regression Analysis

To determine, if causes have actual influence on characteristics to be optimized, a regression analysis can be used. To be more precisely, the relationship between product characteristics or between product characteristsics and their influencing values could be investigated. In a scatter plot characteristic one of a product is plotted on the x-axis and characteristic two is plotted on the y-axis. Every data point illustrates two depending parameters. Different forms of correlation can be seen in figure 2.13. Positive correlation between two variables one and two means that, big values of variable one often go together with big values of variable two, whereas small variables of variable one occur often in connection with small variables of variable two. But only with positive correlation it cannot be assumed that a cause and effect dependency exists.[22]

The correlation coefficient r is a value to estimate, if there is a dependency between variable one and variable two and it lies between -1 and 1. The algebraic sign defines the direction of the correlation. If r is positive, variable two rises with variable one. If

r is negative, variable two falls while variable one is rising. As a rule of thumb, if r lies between 0.5 and 0.8, a correlation is given and if r lies between 0.8 and 1, the correlation is strong.

To evaluate the extent of correlation, it is necessary to look at the correlation coefficient as well as at the data plot. A small correlation coefficient could also be a sign for a non linear dependency.[22]

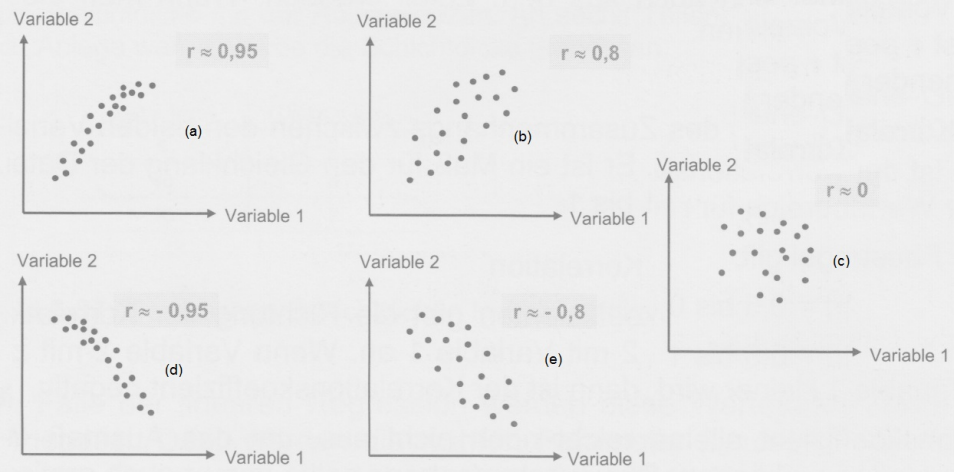

Figure 2.13.: excamples for correlation: (a) positive correlation, (b) weak positive correlation, (c) no correlation, (d) negative correlation, (e) weak negative correlation after [22]

Three main points characterize the procedure for regression analysis [22]:

- determination of the mathematical model (e.g. linear model)
- adaption of the model to the data with the model parameters
- analysis of the residuals to assess the quality of the model

If the mathematical model behind regression is linear, the so called "'best line"' gets fitted into the data points. Therefore the least squares method could be used, where the sum of the quadratic distances between actual value and estimated value is a minimum. If the fit has good quality, the residuals should only scatter randomly. A residual is the deviation of the observed value to the value of the model.

3. Experimental Methods

Following section describes all the experimental methods used for this diploma thesis.

3.1. Sample Taking

The NTC's are taken directly out of the production line after sintering as 30x30 mm square shaped plated with a thickness between 0.4 and 0.8 mm. Afterwards they are cut with a saw also in the production department in 5 mm broad stripes. For this diploma thesis, seven kinds of substrates with different composition, thickness or sintering procedure were taken as reference NTC's. Moreover, one of these kinds of substrates was chosen for further investigation with DoE. This NTC type was taken from a production batch after debindering and then sintered in a laboratory sintering furnace (AMI III asset number 34907) with defined parameters for DoE (see also 4.3.1). Afterwards these samples were also cut in 5 mm stripes. For electrical investigations samples were metallized with Ag paste. Sintered, metallized and sliced substrates can be seen in figure 3.1.

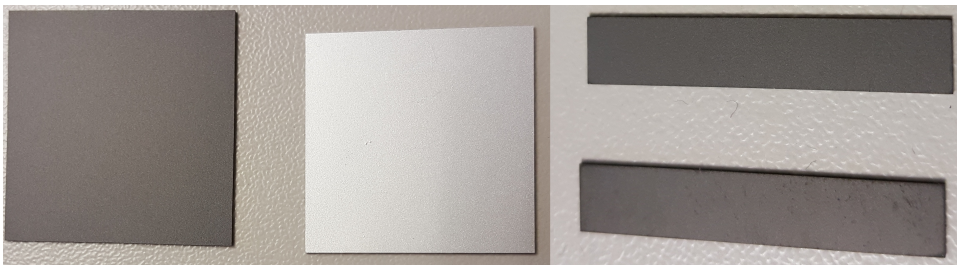

Figure 3.1.: NTC samples: left: sintered substrate, middle: metallized substrate, right: sliced substrate

3.2. Measurement System Analysis

Several kinds of measuring devices come into use in this diploma thesis. All of them are calibrated according to DIN ISO standard specification. Another critical point is the knowledge of the measuring technology characteristics of the measuring devices and their statistical behavior under process conditions. For every kind of measuring system, statistical investigations to analyze the spreading of the measuring devices are necessary. Measuring System Analysis (MSA) are statistical methods to evaluate measuring processes and moreover to estimate the measurement error. Information in this chaper is mainly taken from [7].

Main goal of MSA in this diploma thesis is to proof, if a measuring system is capeable for a given measuring task or not. That's why MSA is performed as follows: Firstly, ten samples are measured sequentially with a distinct measuring device. After that, these ten samples are measured randomly another two times. As a next step, the same procedure is performed by another operator. Afterwards an analysis of variance (ANOVA) estimates separated and together the repeatability and the reproducibility (R&R) of the measuring system.

The measured data was analyzed by statistical software Minitab with the Gage R&R ANOVA method.

The evaluation of the data with Minitab firstly shows the "Two-Way ANOVA Table With Interaction". It arranges the significance of the independent variables (Part number and Operator) to the dependent variable (e.g. length) and the interaction between the dependent variables. As the tolerance level of significance is settled with 5%, the p value of a certain variable has to be equal or smaller than 0.05 to be significant.

The second part of the evaluation is called "‘ Gage R&R"’. In the first column the Standard Deviation (StdDev) of a certain source is printed. The second column, named "‘Study Var"’ is the Standard Deviation multiplied by six, because of the six sigma concept. The third column shows the "‘%Study Var"’, where the percentage of the individual standard deviations of the total standard deviation is shown. This is also graphically illustrated.

The %Study Var of the Total Gage R&R is an indicator for the assessment of a measuring

process. The %Study Var has to be smaller than 10% to call a measuring system capable.

3.2.1. Calliper Gauge

3.2.1.1. Length Measurement

The Two-Way Anova Table with Interaction for the Calliper gauge (Mitutoyo Absolute Digimatic, asset number 07026777, ME-01821, calibration date 3.6.16-3.12.16) length measurement and the Gage R&R can be seen in table 3.1 and in table 3.2. The graphical illustration is visible in figure 3.2.

The p value in table 3.1 shows, that the samples itself are significant, but the tester and also the connection between tester and sample is not significant, because the p- value is bigger than 0.05. According to table 3.2 the Gage R&R of the calliper gauge length measurement is 10.51% and therefore the calliper gauge is valued limited measurable for the length.

Table 3.1.: Two-Way Anova Table with Interaction for the Calliper gauge length measurement

Source	DF	SS	MS	F	p
Samples	9	0.247800	0.0275333	489.079	0.000
tester	1	0.000027	0.0000267	0.474	0.509
samples*tester	9	0.000507	0.0000563	1.126	0.368
repeatability	40	0.002000	0.0000500		
total	59	0.250333			

Table 3.2.: Gage R&R for the Calliper gauge length measurmenet

Source	StdDev	Study Var	%Study Var
R&R (total)	0.0071524	0.042914	10.51
repeatability	0.0071524	0.042914	10.51
reproduceability	0.0000000	0.0000000	0.00
tester	0.0000000	0.0000000	0.00
between the samples	0.0676784	0.406070	99.45
total spreading	0.0680553	0.408332	100.00

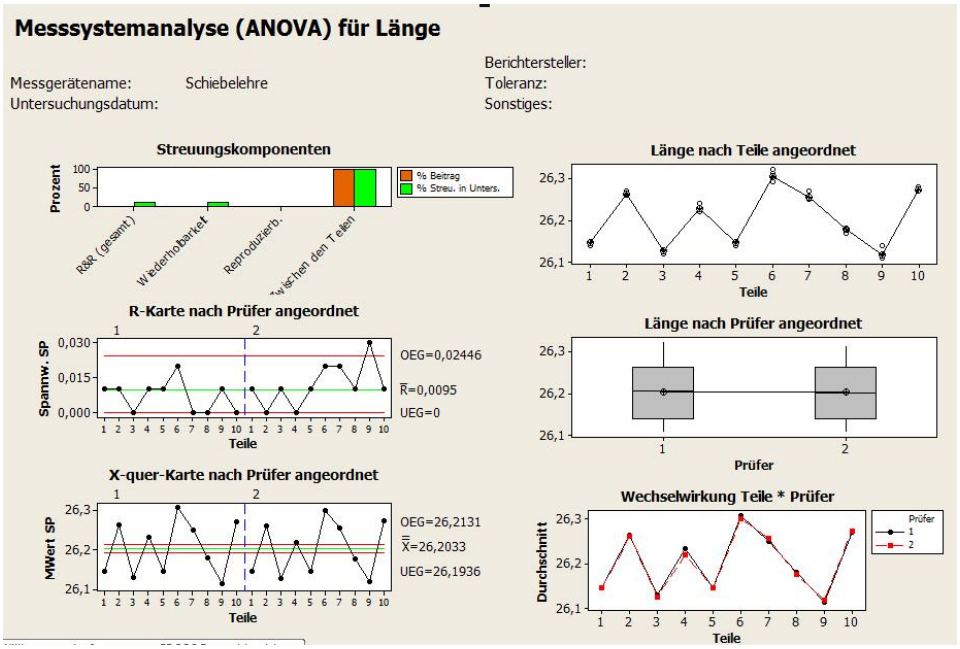

Figure 3.2.: MSA for the calliper gauge for the length

3.2.1.2. Width Measurement

The Two-Way Anova Table with Interaction for the Calliper gauge width measurement and the Gage R&R can be seen in table 3.3 and in table 3.4. The graphical illustration is visible in figure 3.3.

The p value in table 3.3 shows, that only the tester is significant. The samples and the connection between sample and tester are not significant, because the p-value is bigger than 0.05. According to table 3.4 the Gage R&R of the calliper gauge width measurement is 100.00% and therefore the calliper gauge is valued not measurable for the width.

Table 3.3.: Two-Way Anova Table with Interaction for the Calliper gauge width measurement

Source	DF	SS	MS	F	p
Samples	9	0.0005017	0.0000557	0.70163	0.697
tester	1	0.0007350	0.0007350	9.25175	0.014
samples*tester	9	0.0007150	0.0000794	0.74479	0.666
repeatability	40	0.0042667	0.0001067		
total	59	0.0062183			

Table 3.4.: Gage R&R for the Calliper gauge width measurmenet

Source	StdDev	Study Var	%Study Var
R&R (total)	0.0110805	0.0664831	100.00
repeatability	0.0100830	0.0604979	91.00
reproduceability	0.0045947	0.0275681	41.47
tester	0.0045947	0.0275681	41.47
between the samples	0.0000000	0.0000000	0.00
total spreading	0.0110805	0.0664831	100.00

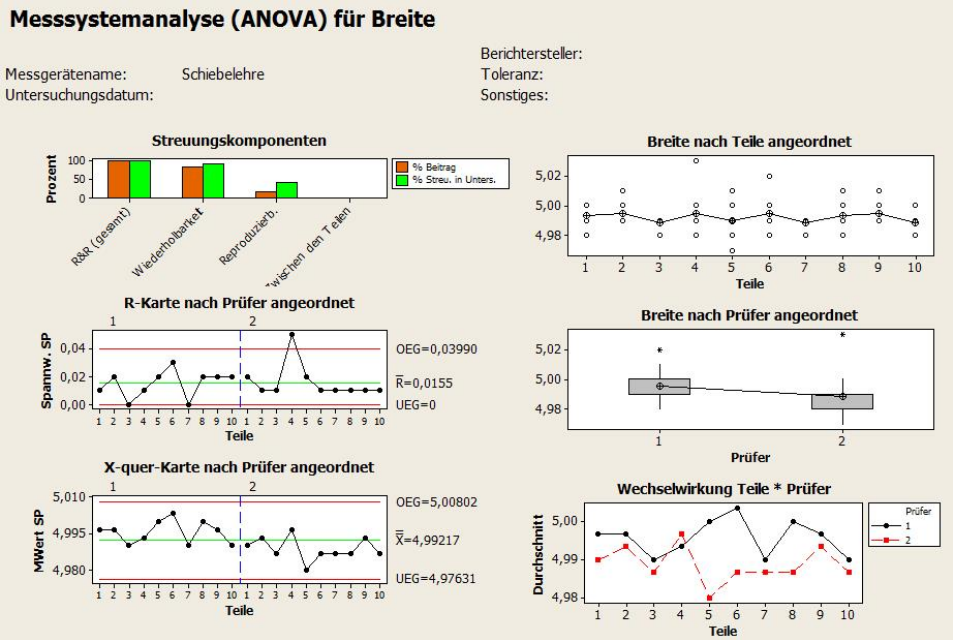

Figure 3.3.: MSA for the calliper gauge for the width

3.2.1.3. Height Measurement

The Two-Way Anova Table with Interaction for the Calliper gauge height measurement and the Gage R&R can be seen in table 3.5 and in table 3.6. The graphical illustration is visible in figure 3.4.

The p value in table 3.5 shows, that neither the samples nor the connection between sample and tester are significant, because the p-value is bigger than 0.05. The tester is significant.

According to table 3.6 the Gage R&R of the calliper gauge width measurement is 94.07%

and therefore the calliper gauge is valued not measurable for the height.

Table 3.5.: Two-Way Anova Table with Interaction for the Calliper gauge height measurement

Source	DF	SS	MS	F	p
Samples	9	0.0003667	0.0000407	2.89474	0.065
tester	1	0.0001067	0.0001067	7.57895	0.022
samples*tester	9	0.0001267	0.0000141	0.60317	0.787
repeatability	40	0.0009333	0.0000233		
total	59	0.0015333			

Table 3.6.: Gage R&R for the Calliper gauge heigth measurment

Source	StdDev	Study Var	%Study Var
R&R (total)	0.0049464	0.0296785	94.07
repeatability	0.0046511	0.0279065	88.45
reproduceability	0.0016836	0.0101015	32.02
tester	0.0016836	0.0101015	32.02
between the samples	0.0017846	0.0107074	33.94
total spreading	0.0052585	0.0315510	100.00

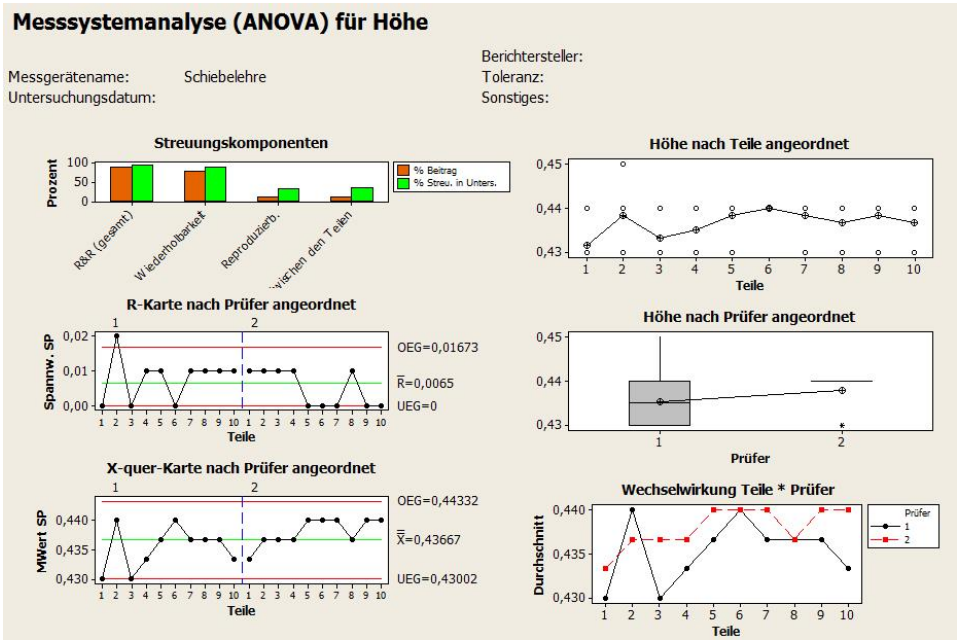

Figure 3.4.: MSA for the calliper gauge for the height

3.2.2. Micrometer Gauge

3.2.2.1. Length Measurement

The Two-Way Anova Table with Interaction for the Micrometer gauge (Mitutoyo Digimatic, ME-03208,calibration date 1.8.16-1.2.17) length measurement and the Gage R&R can be seen in table 3.7 and in table 3.8. The graphical illustration is visible in figure 3.5.

The p value in table 3.7 shows, that the samples itself are significant, but the tester and also the connection between tester and sample is not significant, because the p-value is bigger than 0.05. According to table 3.8 the Gage R&R of the calliper gauge length measurement is 7.71% and therefore the calliper gauge is valued measurable for the length.

Table 3.7.: Two-Way Anova Table with Interaction for the Micrometer gauge length measurement

Source	DF	SS	MS	F	p
Samples	9	0.190682	0.0211869	1765.58	0.000
tester	1	0.000060	0.0000600	5.00	0.052
samples*tester	9	0.000108	0.0000120	0.56	0.822
repeatability	40	0.000859	0.0000215		
total	59	0.191710			

Table 3.8.: Gage R&R for the Micrometer gauge length measurmenet

Source	StdDev	Study Var	%Study Var
R&R (total)	0.0045917	0.027550	7.71
repeatability	0.0044431	0.026659	7.46
reproduceability	0.0011584	0.006951	1.94
tester	0.0011584	0.006951	1.94
between the samples	0.0593958	0.356375	99.70
total spreading	0.0595730	0.357438	100.00

3.2.2.2. Width Measurement

The Two-Way Anova Table with Interaction for the Micrometer gauge width measurement and the Gage R&R can be seen in table 3.9 and in table 3.10.

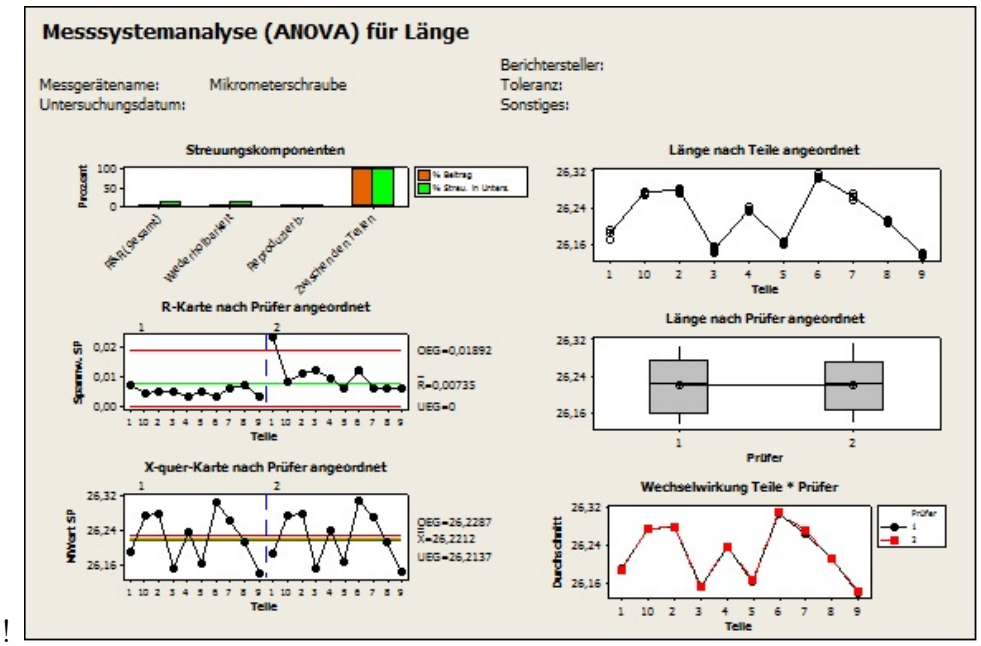

Figure 3.5.: MSA for the micrometer gauge for the length

The graphical illustration is visible in figure 3.6.

The p value in table 3.9 shows, that the samples itself are significant, but the tester and also the connection between tester and sample is not significant, because the p-value is bigger than 0.05. According to table 3.10 the Gage R&R of the calliper gauge width measurement is 9.90% and therefore the calliper gauge is valued measurable for the width.

Table 3.9.: Two-Way Anova Table with Interaction for the Micrometer gauge width measurement

Source	DF	SS	MS	F	p
Samples	9	0.0007604	0.0000845	931.122	0.000
tester	1	0.0000000	0.0000000	0.184	0.678
samples*tester	9	0.0000008	0.0000001	0.605	0.785
repeatability	40	0.0000060	0.0000002		
total	59	0.0007673			

Table 3.10.: Gage R&R for the Micrometer gauge Width measurmenet

Source	StdDev	Study Var	%Study Var
R&R (total)	0.0003730	0.0022379	9.90
repeatability	0.0003730	0.0022379	9.90
reproduceability	0.0000000	0.0000000	0.00
tester	0.0000000	0.0000000	0.00
between the samples	0.037495	0.0224969	99.51
total spreading	0.0037680	0.0226079	100.00

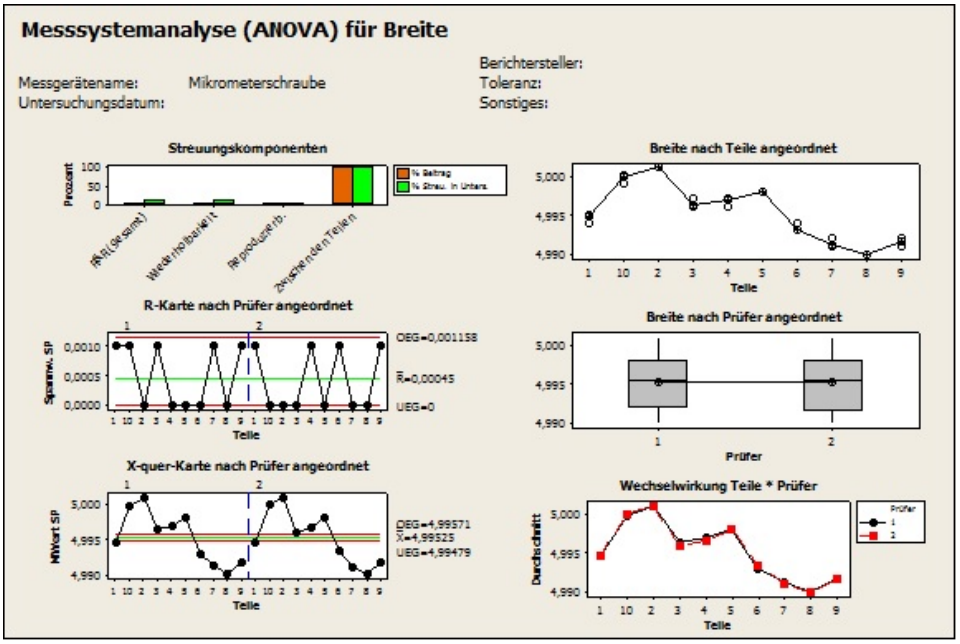

Figure 3.6.: MSA for the micrometer gauge for the width

3.2.2.3. Height Measurement

The Two-Way Anova Table with Interaction for the Micrometer gauge height measurement and the Gage R&R can be seen in table 3.11 and in table 3.12. The graphical illustration is visible in figure 3.7.

The p value in table 3.11 shows, that the samples itself are significant, but the tester and also the connection between tester and sample is not significant, because the p-value is bigger than 0.05. According to table 3.12 the Gage R&R of the calliper gauge height measurement is 7.71% and therefore the calliper gauge is valued measurable for the height.

Table 3.11.: Two-Way Anova Table with Interaction for the Micrometer gauge height measurement

Source	DF	SS	MS	F	p
Samples	9	0.0008867	0.0000985	950.000	0.000
tester	1	0.0000001	0.0000001	0.643	0.443
samples*tester	9	0.0000009	0.0000001	0.622	0.771
repeatability	40	0.0000067	0.0000002		
total	59	0.0008943			

Table 3.12.: Gage R&R for the Micrometer gauge height measurmenet

Source	StdDev	Study Var	%Study Var
R&R (total)	0.0003938	0.027550	7.71
repeatability	0.0044431	0.026659	7.46
reproduceability	0.0011584	0.006951	1.94
tester	0.0011584	0.006951	1.94
between the samples	0.0593958	0.356375	99.70
total spreading	0.0595730	0.357438	100.00

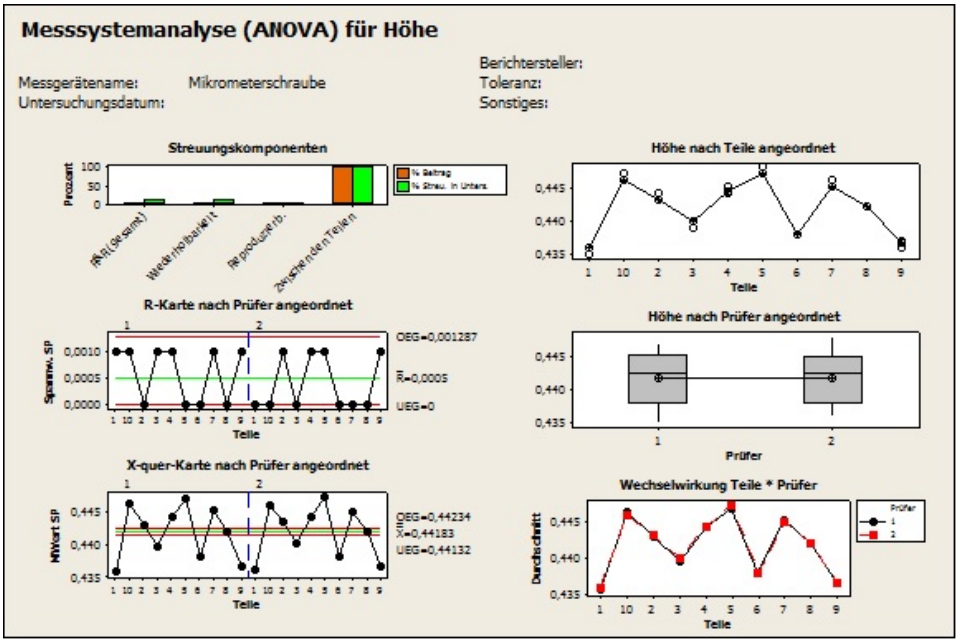

Figure 3.7.: MSA for the micrometer gauge for the height

3.2.3. Laboratoy Balance

The Two-Way Anova Table with Interaction for the Laboratory Balance measurement(artorius, asset number:46995) and the Gage R&R can be seen in table 3.13 and in table 3.14. The graphical illustration is visible in figure 3.8.

The p value in table 3.13 shows, that neither the tester, nor the tester in connection with the samples are significant, because the p-value is bigger than 0.05. The samples on the other hand are significant.

According to table 3.14 the Gage R&R of the Laboratory Balance measurement is 6.81% and therefore the Laboratory Balance is valued measurable for the mass.

Table 3.13.: Two-Way Anova Table with Interaction for the laboratory balance measurement

Source	DF	SS	MS	F	p
Samples	9	0.0001501	0.0000167	1322.56	0.000
tester	1	0.0000000	0.0000000	0.65	0.442
samples*tester	9	0.0000001	0.0000000	0.97	0.479
repeatability	40	0.0000005	0.0000000		
total	59	0.0001508			

Table 3.14.: Gage R&R for the laboratory balance measurmenet

Source	StdDev	Study Var	%Study Var
R&R (total)	0.0001137	0.0006822	6.81
repeatability	0.0001137	0.0006822	6.81
reproduceability	0.0000000	0.0000000	0.00
tester	0.0000000	0.0000000	0.00
between the samples	0.0016666	0.0099998	99.77
total spreading	0.0016705	0.0100231	100.00

3.2.4. Displacement Indicator

The Two-Way Anova Table with Interaction for the dismplacement indicator measurement and the Gage R&R can be seen in table 3.15 and in table 3.16. The graphical illustration is visible in figure 3.9.

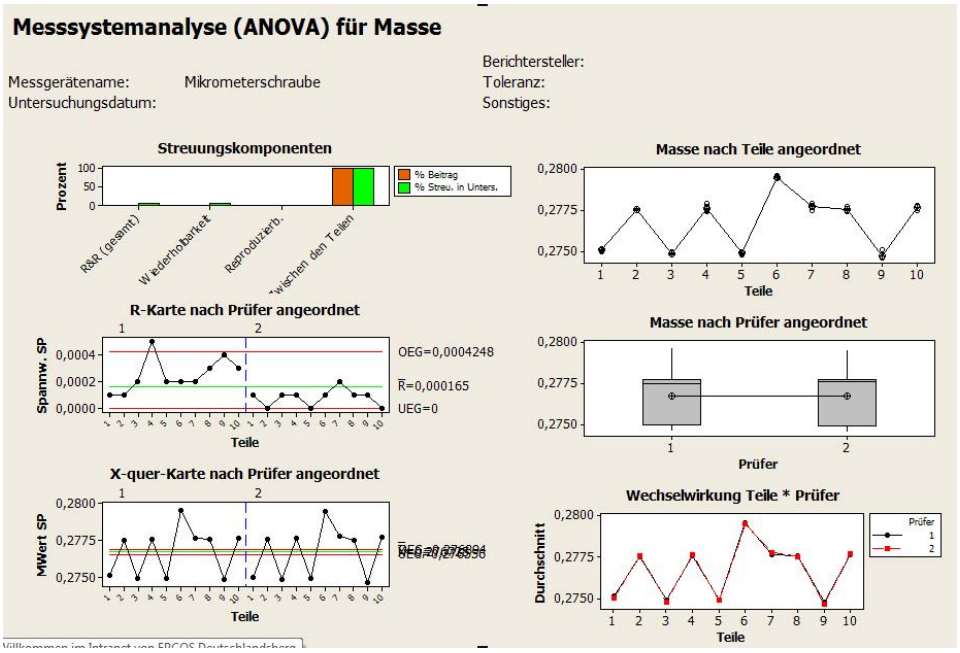

Figure 3.8.: MSA for the laboratory balance

The p value in table 3.15 shows, that the samples and the samples in connection with the tester are significant, because the p-value is smaller than 0.05. The tester is not significant.

According to table 3.16 the Gage R&R of the displacement indicator measurement is 9.83% and therefore the displacement indicator is valued measurable for the thickness of a sample.

Table 3.15.: Two-Way Anova Table with Interaction for the displacement indicator measurement

Source	DF	SS	MS	F	p
Samples	9	0.0955750	0.0106194	395.483	0.000
tester	1	0.0000417	0.0000417	1.552	0.244
samples*tester	9	0.0002417	0.0000269	2.302	0.034
repeatability	40	0.0004667	0.0000117		
total	59	0.0963250			

Table 3.16.: Gage R&R for the displacement indicator measurmenet

Source	StdDev	Study Var	%Study Var
R&R (total)	0.0041500	0.024900	9.83
repeatability	0.0034157	0.020494	8.09
reproduceability	0.0023570	0.014142	5.58
tester	0.0007027	0.004216	1.66
between the samples	0.0420170	0.252102	99.52
total spreading	0.0422215	0.253329	100.00

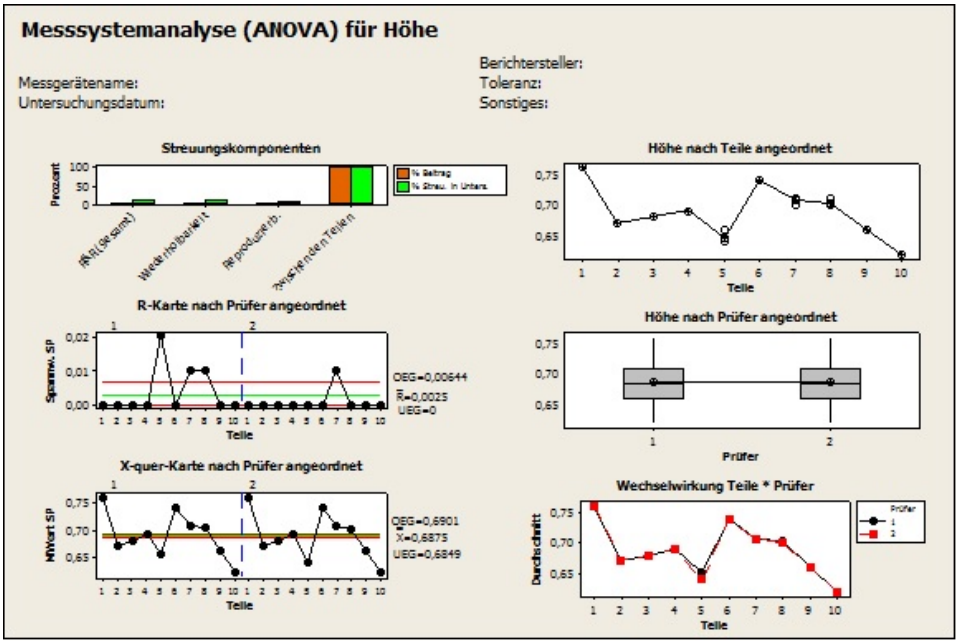

Figure 3.9.: MSA for the displacement indicator

3.2.5. 4-point Bending Strength

MSA for the Zwick four point bending strength measurement (asset number 40158, calibration from 10.2.16-10.2.17) was performed by the laboratory.

3.2.6. He-Pycnometer

MSA for the He-Pycnometer measurement (AccuPyc 1340,asset number 87 114, calibration from) was performed by the laboratory.

3.3. Propagation of Uncertainty

In some experiments, uncertainties from the measurement are estimable directly from the measurement. Other parameters have to be calculated and therefore also the uncertainty has to be calculated. A common method to estimate uncertainties is the "propagation of unceraintty".

Every measured variable X_k has an uncertainty s_{x1} mostly coming from limited instrumental precision. If another parameter Y is calculated from these measured variables, also the uncertainty s_Y has to be calculated according to formula 3.1 from uncertainty theory, whereas the derivation has to be calculated at mean of the measured parameter X_k

$$s_Y = \sqrt{\sum_{k=1}^{m} \left(\frac{\partial Y}{\partial X_k} s_{X_k} \right)^2} \tag{3.1}$$

In most cases the simplified estimation with the so called maximum error is also appropriate:

$$s_Y \approx \sum_{k=1}^{m} \left| \frac{\partial Y}{\partial X_k} \right| \Delta \overline{X_k} \tag{3.2}$$

The calculaton of the maximum error is used in this diploma thesis.

3.4. Density Measurement

The measurement of geometric density, open porosity and total porosity was performed according to DIN 993-1. The geometric density is the relationship between the mass of a dry and porous body and its total volume. Open porosity is the relationship between the volume of the open pores of a porous body and its total volume. The total porosity is the relationship between the open and the closed pores and the total volume of the sample.

First of all, 10 samples were picked from every NTC type to be investigated. From every sample, length, width and height was measured with the micrometer gauge. Afterwards, mass (m_{sample}) was recorded with the laboratory balance (asset number 46995). From this data, the geometrical density was calculated. Afterwards the samples were immersed in distilled water and put in a vacuum bell for 15 minutes. After that, samples were measured separately in the Archimedes balance, where the samples are firstly weighed in a water bath (m_{water}) and then shortly dried with a humid cleaning cloth. Then they are weighed again in air (m_{air}). The determination of the density of a sample follows the principle of Archimedes. The difference of the masses (in air and in water) yields the mass of the replaced water. If this mass is divided by the fluid desity it results in the volume of the immersed sample. The Archimedes density of the sample $\rho_{Archimedes}$ can be calculated with a division of the mass of the immersed sample through the volume of the sample.

$$V_{sample} = \frac{m_{air} - m_{water}}{\rho_{water}} \tag{3.3}$$

$$\rho_{Archimedes} = \frac{m_{sample}}{V_{sample}} \tag{3.4}$$

The open porosity is calculated according to formula 3.5:

$$\pi_a = \frac{m_{air} - m_{sample}}{m_{air} - m_{water}} \tag{3.5}$$

The total porosity is calculated according to formula 3.6:

$$\pi_t = \frac{\rho_t - \rho_{Archimedes}}{\rho_t}.100 \tag{3.6}$$

The determination of the theoretical density of an NTC ρ_t was carried out with NTC powder material in a He-Pycnometer (AccuPyc 1340, asset number 87 114). For this purpose, NTC substrates were pestled with a mortar to a fine powder. Then this powder was sieved through a sieve. Afterwards the NTC powder samples were filled in a 1 ccm sample cylinder and measured with the measuring program of the He-Pycnometer.

3.5. 4-point Bending Strength Measurement

To determine the bending strength, the 4 point bending strength measurement device from Zwick/Roell (asset number 40 158) was used.

From each NTC type, 30 samples were taken and enummerated. Stripes according to chapter 3.1 were taken. The width and the height was measured with the micrometer gauge. Every sample was placed one after another at the sample plating of the strength measurement device (see figure 3.10). Pressing at the start button of the Zwick/Roell software, the automatic measurement of strength began. The output parameters of this measurement was the fracture force and the elongation at fracture, as well as the stress/strain curve for every sample. The evaluation of this data was carried out as described in section 2.5.1.2.

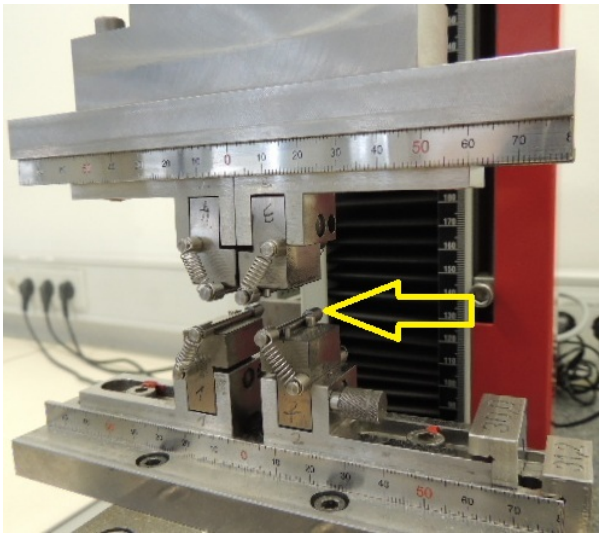

Figure 3.10.: picture 4 point bending strength test device: Zwick/Roell

3.6. Measurement of the Warping

Since edge breakouts are caused in many cases by residual stresses in surface regions, the so called measurement of warping or bimetal test war performed in order to find out if stress exists between surface layers and intermediate layers. For this purpose the height of one substrate of each NTC DoE type, the height was measured with a displacement

indicator Mitutoyo Absolute (asset number ME-01180) from both sides. The higher the difference of the height, the more a substrate is warped. This way the warping of the sintered NTC bodies could be determined. After the warpage measurement one surface layer of each substrate was grinded down. The heights of the substrates were measured again from both sides with the displacement indicator after drying. If a difference between the height on both sides showed a warping after grinding(see figure 3.11) this could be taken as evidence for stress within the substrate.

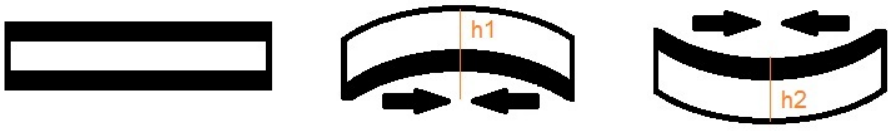

Figure 3.11.: schematic of the warping measurement: the surface layer under compressive stress is shown in black

3.7. Methods for Analysis of Microstructure

3.7.1. Light Optical Microscope

For investigation with the Light optical microscope (LoM) samples from every NTC type were embedded upright in epoxy resin, grinded and polished. Afterwards samples were investigated by the reflected light microscope Olympus BX51M (asset number 87139) with white light. Furthermore the fracture surface of the samples was investigated with Stereo microscope Leica (asset number:38801).

3.7.2. Scanning Electron Microscope

The surfaces of the embedded samples were coated with carbon by vapour deposition to avoid electrical charges during the measurement. Afterwards samples were investigated with the Zeiss Merlin VP (asset number 87139) electron microscope. The BSE (backscattered electrons) mode delivers information about the material (phase) contrast. The brigther a local position appears in a BSE mode picture, the higher the atomic number of the investigated element. Pictures with the Secondary electrons (SE) mode give

information about the topography of a sample. The detector for the Secondary electrons is fixed sidewards of the samples [19].

The measurement of the grain sizes was carried out with EBSD (Electron Backscattered Diffraction). This is a Scanning electron microscope scanning technique, which allows cristallographic information to be obtained. A stationary electron beam gets defracted at a tilted crystallographic sample. The defracted electrons are viewable at a flouescent screen as the so called Kikuchi patterns. This diffraction pattern can be used to measure the crystal orientation, grain boundary misorientations and can also provide information about local crystalline imperfections. [1]

The measurement of the precipitations and the porosity was also performed with Scanning Electron Microscope in BSE mode. Afterwards precipitation and porosity was evaluated with the Software Analyze, for what every sample was subdivided into 10μm bars (see figure 3.12). The amount of precipitation (or porosity) of every bar was then plotted in a graphic.

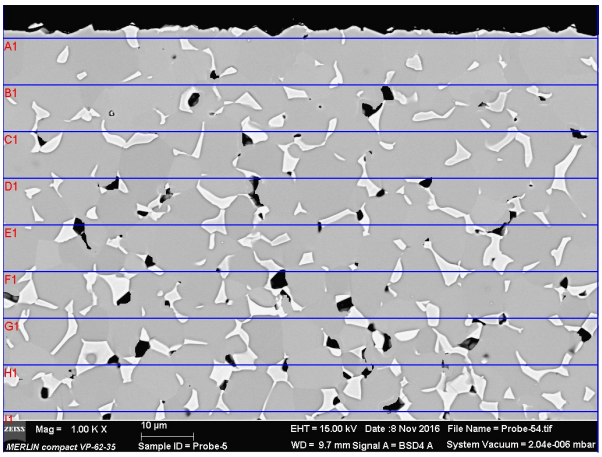

Figure 3.12.: Example for the screening in the porosity and precipitation measurement: bars with a width of 10μm were classified

3.8. Measurement of Electrical Properties

To evaluate the electrical properties, four substrates of each type were taken. Each substrate was metalized with silver paste on every side. The substrates were cut to the same size and then sorted in a special sample holder for the electrical measurement.

This sample holder gets immersed in an oil bath and with a certain setting of current and voltage, the resistance gets measured with a Keithley 2002 measurement device at 25 °C and 100 °C. The B value gets calculated according to fundamental section.

4. Results and Discussion

4.1. Process Analysis

The phase Measure of Six Sigma is featured of following activities:

- Choose a key product
- Define the process for the product and it's performace features and characteristics
- Validate the measuring system and choose representative data for the performance features

In following diploma thesis NTC substrates were chosen as key product. The definition of the performance features and the choise of representative features of the performance features follows in this chapter. Profound literature for process analysis can be found in [7].

4.1.1. Process Flow Chart

A process flow chart is a tool to visualize the sequence of the single process steps when manufacturing a concrete product. Therefore both value-adding and non value-adding processes like transport, storage and testing are visualized. The process flow in this diploma thesis is represented with standardized symbols.[7] The flow chart itself is performed with Microsoft Power Point and can be seen in figure 4.1

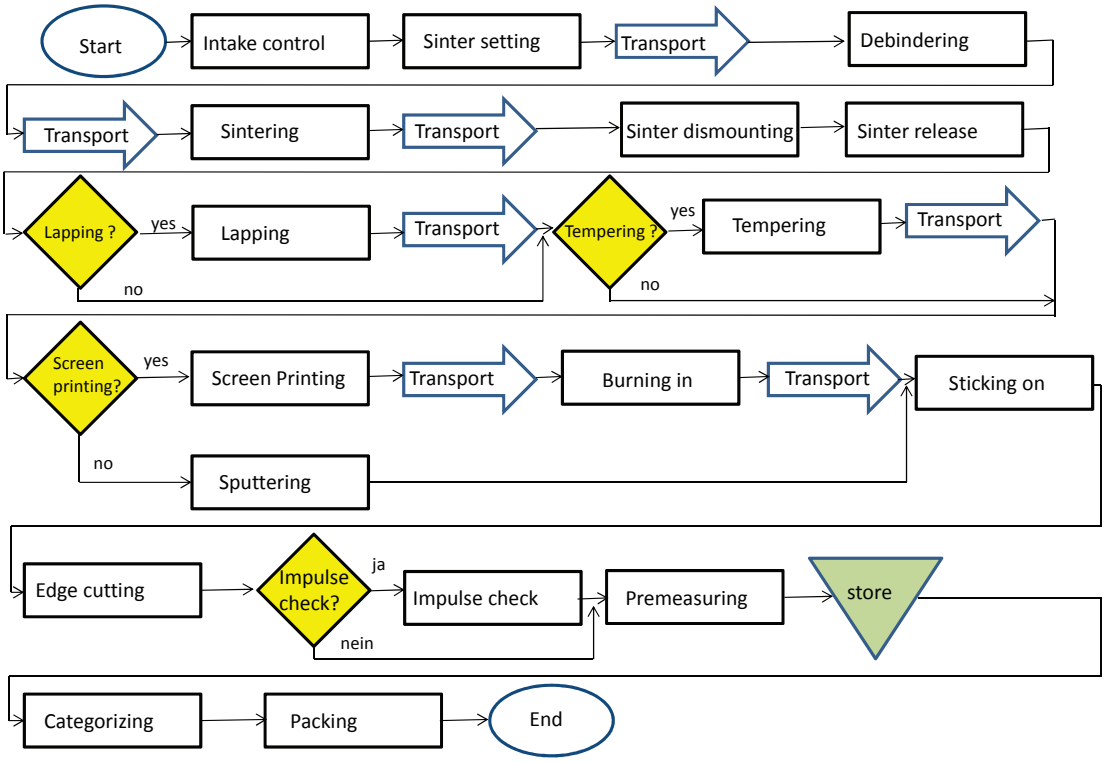

Figure 4.1.: Process flow chart

4.1.2. Process Mapping

Another goal in process analysis is to identify the relevant process parameters for the single process steps after [7]. To achieve this, a process mapping for the process step Sintering was performed, because according to definition of the project, the mechanical strength should be improved via sintering. The process mapping was performed in a team with employees of the production line and illustrated afterwards in figure 4.2.

Legend:
X: These are the input parameters of the following process step, e.g. the product- or quality characteristics of the processing step.
Y: These are the output parameters of the last process step, e.g. the product- or quality characteristics of the processing step.

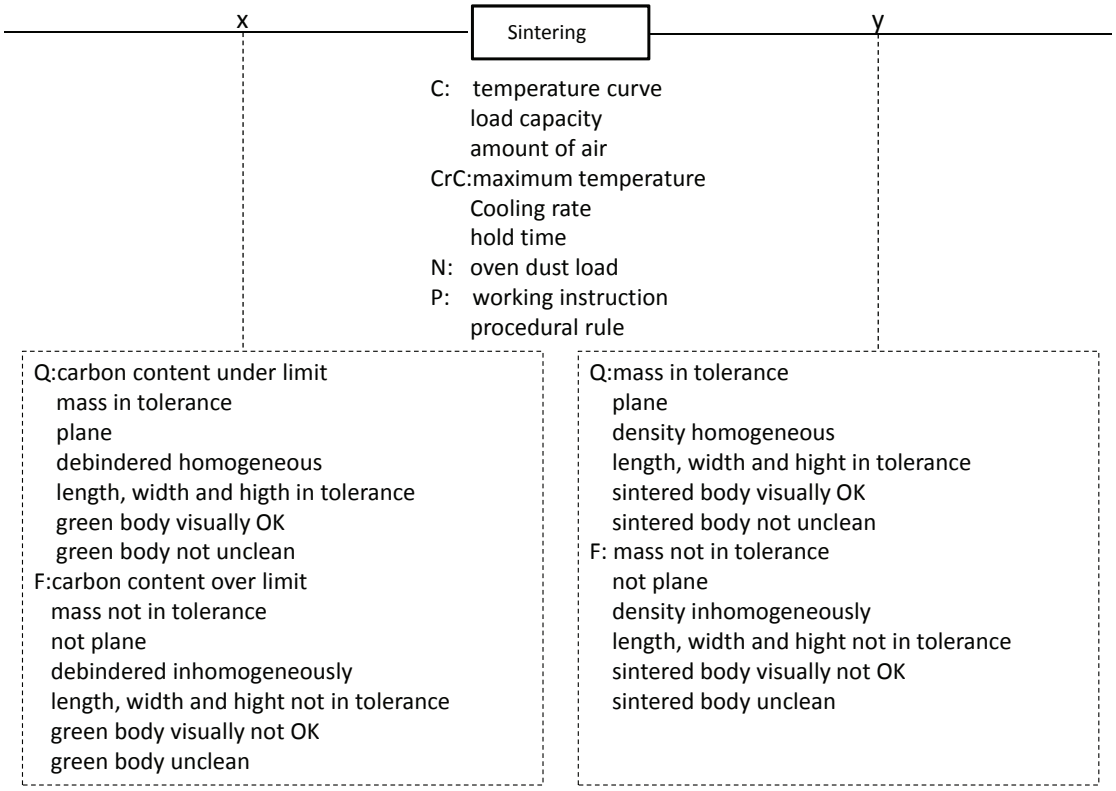

Figure 4.2.: Process Mapping

C: These are the controllable factors, which are changeable during the process step.
CrC: These are the critical controllable factors. These factors have particular wide influence on the process outcome.
N: The disturbance value N (Noise) has bad influence especially on the spreading of the product characteristics.
P: The procedure parameters are influence values on the whole process, which are operating through regulations or computer programs.
Q: This parameter describes desired results according to quality standards.
F: This parameter describes undesired and faulty but possible process results.

4.1.3. Ishikawa Diagram

As a next step a so called Ishikawa diagram (cause and effect diagram) was performed. It's main goal is to illustrate the relationship between an effect and it's possible causes. The possible causes are divided into main- and sub-category. In this diploma thesis it was mainly used to describe the relationship between quality criteria and their main influencing factors. Therefore it was a necessary condition to perform design of experiments. In this method it is expected, that the cause of every possible effect is counted among the five cause groups: Personnel, Material, Measurements, Environments, Methods and Machines. The solution of this problem is represented in a so-called fishbone diagram, where the associated influencing values are registered on the branches. Ishikawa diagrams were performed in team work. The diagram for the key effect "'mechanical strength not enough"' is illustrated in figure 4.3.

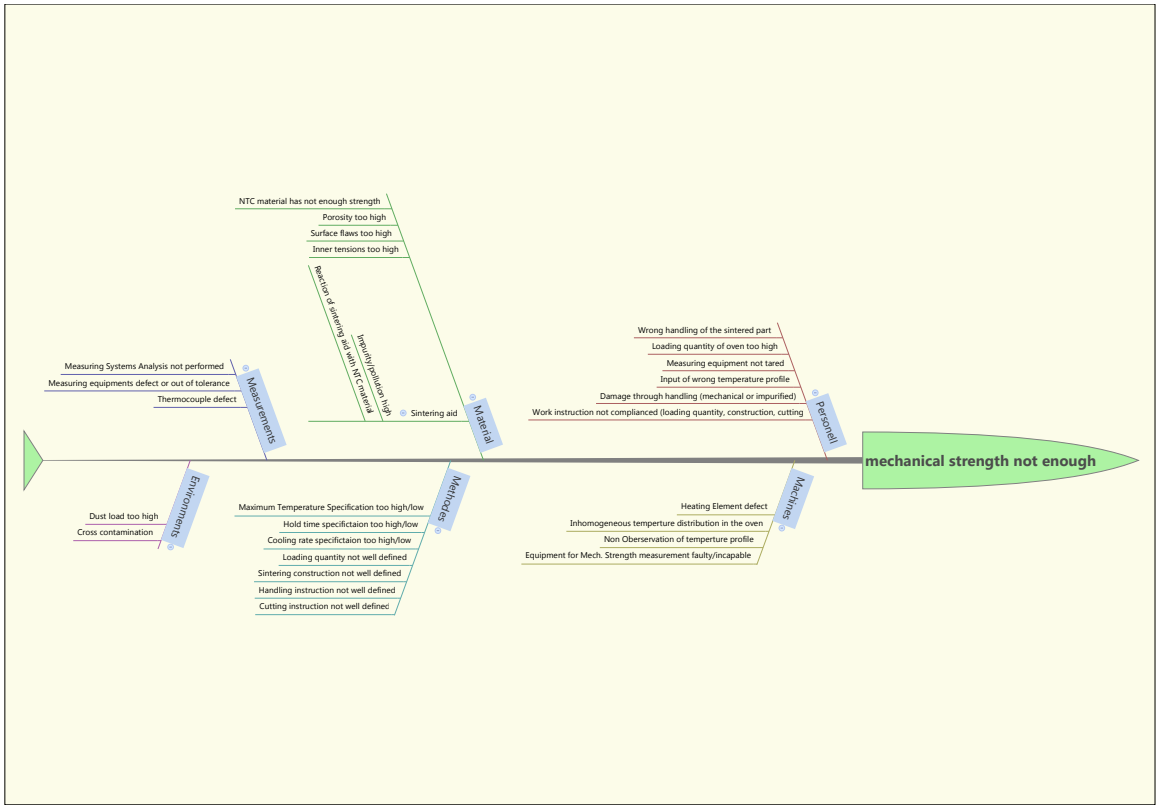

Figure 4.3.: Ishikawa diagram for the key effect: Mechanical strength too low

4.1.4. Comparison of Pairs

To rank and measure the target values of the sintered substrates the comparison of pairs tool has been used. This tool enables to evaluate and rank target and influence values among each other.

All items on the list of target values are then compared with each other, one by one. The weighing is carried out according to following assignment:

- 0: the column is preferred
- 1: the equality of column and row
- 2: the row is preferred

After that the scores of every row are summarized. The sum of every row indicates the importance of the actual target or influence value. A higher sum indicates a higher importance. Now a ranking can be done with rank one for the highest score and the last rank for the lowest score.

The comparison of pairs for the target values of sintered substrates can be seen in figure 4.4.

According to figure 4.4 the most important target values of sintered substrates are "'electrical resistance not in tolerance"' and "'mechanical strength not enough"'. The main goal of this diploma thesis is to improve the mechanical strength. Because of that, another comparison of pairs for the target value "'mechanical strength not enough"' was performed (see figure 4.5). The influence values were determined with the Ishikawa diagram in figure 4.3.

The evaluation of the comparison of pairs in figure 4.5 follows in chapter 4.1.5

target values of sintered (metalized) substrates		1	2	3	4	5		
		dust load of sintered part too high	electrical resistance not in tolerance	thickness out of tolerance	mechanical strength not enough	area of the part is not in tolerance	sum	Ranking
1	dust load of sintered part too high	-	0	0	0	2	2	3
2	electrical resistance not in tolerance	2	-	2	1	2	**7**	1
3	thickness out of tolerance	2	0	-	0	2	4	2
4	mechanical strength not enough	2	1	2	-	2	**7**	1
5	area of the part is not in tolerance	0	0	0	0	-	0	4

Figure 4.4.: Comparison of pairs for the target values of sintered substrates

4.1.5. Pareto Analysis

The reporting of the comparison of pairs is examinated in the Pareto analysis. The summarized ranking of the comparison of pairs can be seen in table 4.1.

In figure 4.6 the Pareto analysis is graphically illustrated. It shows, that the biggest influencing value is the NTC material itself. Therefore in this diploma thesis only one material was used for the DoE. "'Input of the wrong temperature profile"' is ranked number three. This was avoided with double checking of the input parameter at the sintering oven.

	Influence values for mechanical strength	1	2	3	4	5	6	7	8	9	10	11	12	13	14	15	16	17	18	19	20	21	22	23	24	25	26	27	28	sum	Rang
1	wrong handling of the sintered part	-	2	0	0	1	0	0	0	0	0	0	0	0	0	1	0	0	0	0	0	0	0	0	0	0	0	0	0	7	18
2	loading quantity of oven too high	0	-	0	0	1	0	0	0	0	0	0	0	0	0	1	0	0	2	0	0	0	0	0	0	0	0	0	0	7	18
3	measuring equipment not tared	0	0	-	1	1	1	1	2	1	1	1	1	1	1	1	1	1	2	1	1	1	1	1	1	1	2	1	0	33	8
4	input of wrong temperature profile	0	0	1	-	1	1	1	2	1	1	1	1	1	1	2	1	1	2	1	1	1	1	1	1	2	2	2	0	42	3
5	damage through handling (mechanical or impurified)	1	1	1	1	-	1	0	2	0	2	0	0	0	0	1	1	1	2	1	1	1	1	0	1	1	1	2	2	27	12
6	Work instruction not complianced (loading quantity, construction, cutting)	2	2	1	0	1	-	2	1	0	0	0	0	0	0	2	1	1	2	1	1	1	1	0	0	0	1	0	0	15	15
7	Heating Element defect	2	2	1	1	2	2	-	1	1	1	1	1	1	2	2	2	2	2	2	2	2	2	1	0	0	0	1	1	27	12
8	inhomogeneous temperture distribution in the oven	2	2	0	1	0	2	1	-	1	1	0	0	0	0	2	2	2	2	2	2	2	2	1	0	0	0	2	2	28	11
9	actual temp profile not according to input profile	2	2	1	1	2	2	1	1	-	2	1	1	1	2	2	2	2	2	2	2	1	2	1	0	1	1	2	2	40	5
10	Equipment for Mech. Strength measurement faulty/incapable	2	2	1	0	0	2	1	1	2	-	0	0	0	2	2	2	2	2	2	2	1	1	0	1	0	0	2	2	29	10
11	Maximum Temperature Specification too high/low	2	2	1	1	2	2	1	2	1	2	-	1	0	1	2	2	2	2	2	2	2	2	1	0	0	0	2	2	44	2
12	Hold time specification too high/low	2	2	1	1	2	2	1	2	1	2	1	-	1	1	2	2	2	2	2	2	2	2	1	0	0	0	2	2	42	3
13	Cooling rate specification too high/low	2	2	1	1	2	2	1	2	1	2	1	1	-	1	2	2	2	2	2	2	1	2	0	1	0	0	2	2	41	4
14	loading quantity not well defined	2	1	0	0	0	1	0	0	0	0	0	0	0	-	1	1	1	2	1	1	1	1	0	0	0	0	1	1	14	16
15	sintering construction not well defined	1	1	1	0	0	1	0	0	0	0	0	0	0	1	-	1	1	2	2	2	2	2	1	0	0	0	1	1	13	17
16	handling instruction not well defined	1	2	1	0	1	1	2	0	0	0	0	0	0	1	1	-	1	2	1	0	0	0	0	0	0	0	1	1	16	14
17	cutting instruction not well defined	2	2	1	1	1	1	1	1	1	1	1	1	1	2	2	1	-	2	2	1	1	1	0	0	0	0	1	2	31	9
18	dust load too high	0	0	0	0	0	0	0	0	0	0	0	0	0	0	0	0	0	-	0	0	0	0	0	0	0	0	0	0	0	19
19	cross contamination	2	2	0	0	0	0	0	0	0	0	0	0	0	0	0	0	0	2	-	0	0	0	0	0	0	0	0	0	7	18
20	Measuring Systems Analysis not capeable	2	2	1	0	0	0	0	0	0	0	0	0	0	0	0	0	0	2	2	-	0	0	0	0	0	0	0	0	8	8
21	Measuring equipments defect or out of tolerance	2	2	1	0	2	2	1	1	1	1	0	1	1	1	1	1	1	2	2	1	-	1	0	0	0	0	0	0	8	8
22	thermocouple defect	2	2	1	1	1	2	1	1	1	0	0	0	1	1	1	1	1	2	2	2	1	-	1	0	0	0	0	0	7	18
23	NTC material has not enough strength	2	2	1	2	2	2	2	2	2	1	2	2	2	2	2	2	2	2	2	2	2	2	-	0	1	2	2	2	34	7
24	porosity too high	2	1	1	1	1	2	2	2	1	2	1	1	1	1	1	1	1	2	2	2	2	2	1	-	0	1	2	2	40	1
25	surface flaws too high	2	2	1	0	1	2	2	2	1	2	0	0	0	1	1	1	1	2	2	2	2	2	1	0	-	1	2	2	38	6
26	inner tensions too high	2	1	1	0	1	2	2	2	1	2	1	0	0	0	0	0	0	2	2	2	2	2	1	0	0	-	2	2	38	6
27	sintering aid:impurity/pollution high	2	2	0	0	0	2	1	2	0	0	0	0	0	0	0	0	0	2	2	2	2	2	1	0	0	0	-	0	13	17
28	reaction of sintering aid with NTC material	2	2	1	0	0	1	0	1	0	0	0	0	0	0	0	0	0	2	2	2	2	2	1	0	0	0	2	-	19	13

Figure 4.5.: Comparison of pairs for the influence values for mechanical strength

Table 4.1.: Pareto Analysis for the comparision of pairs for the influence values for mechanical strength

Influence value	sum	rank
NTC material has not enough strength	49	1
Maximum temperature Specification too high/low	44	2
Input of wrong temperature profile	42	3
Hold time specification too high/low	42	3
Cooling rate specification too high/low	41	4
Actual temperature profile not according to input profile	40	5
Porosity too high	38	6
Surface flaws too high	38	6
Inner tensions too high	38	6
Thermocouple defect	34	7
Measuring equipment not tared	33	8
MSA not capeable	33	8
Measuring equipment defect or out of tolerance	33	8
Cutting instruction not well defined	31	9
Equipment for Mechanical Strength measurement faulty/incapeable	29	10
Inhomogeneous temperature distribution in the oven	28	11
Damage through handling (mechanical or impurified)	27	12
Heating element defect	27	12
Reaction of sintering aid with NTC material	19	13
Handling Instruction not well defined	16	14
Work instruction not complianced	15	15
Loading quantity not well defined	14	16
Sintering construction not well defined	13	17
Sintering aid: impurity/pollution high	13	17
Wrong handling of the sintered part	7	18
Loading quantity of oven too high	7	18
Cross contamination	7	18
Dust load too high	0	19

The effects ranked at two, three and four, "‘Maximum temperature "’,"’Hold time"’ and "‘Cooling rate"’ were selected to be changed in the DoE.

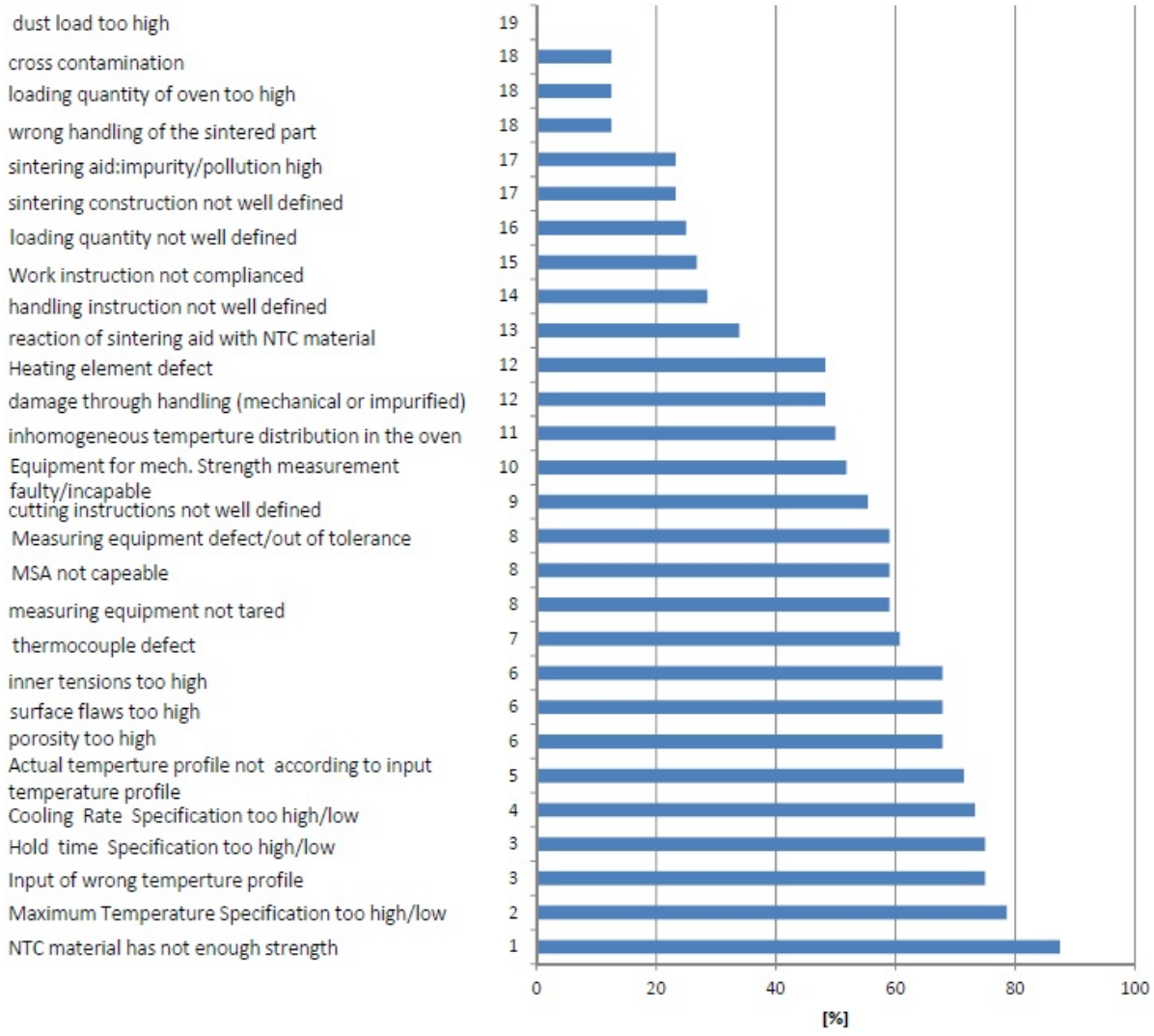

Figure 4.6.: graphical illustration of the Pareto Analysis for the comparision of pairs for the influence values for mechanical strength

4.2. Properties of Iron Containing and Reference NTC Ceramics

In following chapter, properties of as sintered NTC ceramics from production line like density, porosity, mechanical strength and microstructure are discussed. The samples are devided into two groups: iron containing and non iron containg ceramics, because the strength of an iron containing ceramic should be improved and the non iron containing ceramics should serve as reference. Each type of NTC has got a sample ID from the

writer. Samples 1a, 1b and 2 are the non iron containing samples. Sample 1a and 1b have the same composition and are sintered with the same parameters. The only difference between sample 1a and 1b is the thickness (amount of stacked layers), whereas sample 1b is nearly twice as thick as sample 1a. Samples 3, 4, 5a and 5b are iron containing ceramics, in which samples 5a and 5b contain of the same material and are sintered with the same parameters. The only difference between them is the thickness. Furthermore sample 5b is lapped.

4.2.1. Density

Following section describes the density of iron containing and non iron containing NTCs as well as their influence on the mechanical strength.

The geometric density, the Archimedes density and the total porosity of samples 1a and 1b in table 4.2 are not significantly different. The theoretical density is measured with the gas pycnometer because the material is inhomogeneous and the powder measurement delivers the mean density of a material without pores. That is the reason why the raw density is the highest density for all samples in the tables 4.2 and 4.3. The total porosity is calculated from the proportion of theoretical density and geometric density. Sample 2 has a higher total porosity than sample 1a and 1b. In general it could be said, that the iron containing samples have a higher total porosities than the non iron containing samples. Sample 3 has the highest total porosity among all investigated samples. The open porosity is lower than 1% for all samples, so it can be assumed that the samples are sintered dense.

Table 4.2.: density properties of non iron containing NTCs

Sample ID	1a	1b	2
Geometric density $[g/cm^3]$	5.16 ± 0.01	5.17 ± 0.01	5.22 ± 0.03
Archimedes density $[g/cm^3] \Delta\rho = 0.002 g/cm^3$	5.252	5.217	5.155
Theortical density $[g/cm^3]$	5.273 ± 0.004	5.278 ± 0.005	5.579 ± 0.008
Open porosity [% of the volume]	0.71 ± 0.06	0.46 ± 0.04	0.71 ± 0.06
Total porosity [%]	2.1 ± 0.2	2.1 ± 0.2	6.4 ± 0.6

Table 4.3.: density properties of iron containing NTCs

Sample ID	3	4	5a	5b
Geometric density $[g/cm^3]$	4.78 ± 0.02	5.14 ± 0.02	5.14 ± 0.01	5.3 ± 0.3
Archimedes density $[g/cm^3] \Delta\rho = 0.002 g/cm^3$	4.753	5.041	5.143	5.105
Theoretical density $[g/cm^3]$	5.257 ± 0.006	5.250 ± 0.005	5.380 ± 0.005	5.398 ± 0.006
Open porosity [% of the volume]	0.25 ± 0.06	0.48 ± 0.07	0.26 ± 0.05	0.25 ± 0.05
Total porosity [%]	9.1 ± 0.3	2.1 ± 0.2	4.4 ± 0.2	4.6 ± 0.3

4.2.2. Mechanical Properties

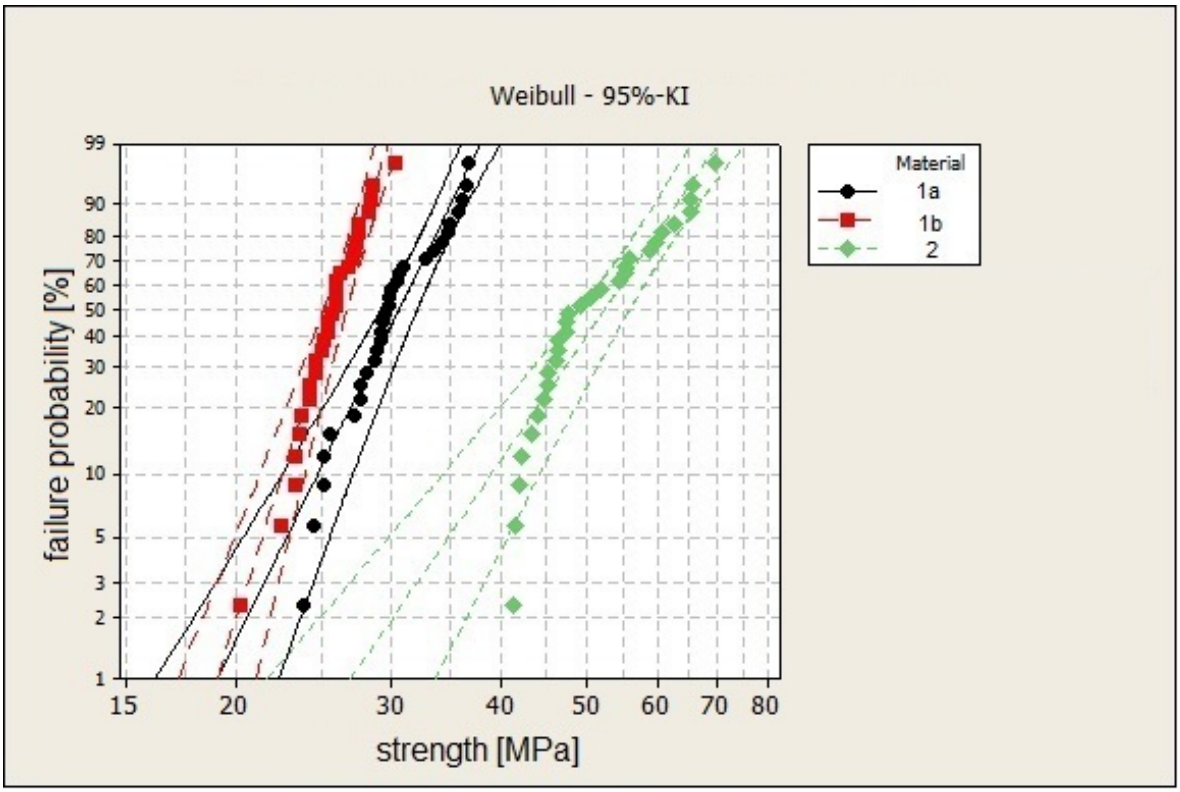

Figure 4.7.: Weibull diagram for the non iron containing reference NTC materials: 1a:black, 1b red, 2:green

In the following section the Weibull strength of iron containing and non iron containing NTCs are presented.

Looking at figure 4.7, it can be seen that the Weibull strength of 1a with 32 ± 5 MPa and 1b with 27 ± 5 MPa are rather low. On the contrary the Weibull module of 1b is 15.0,

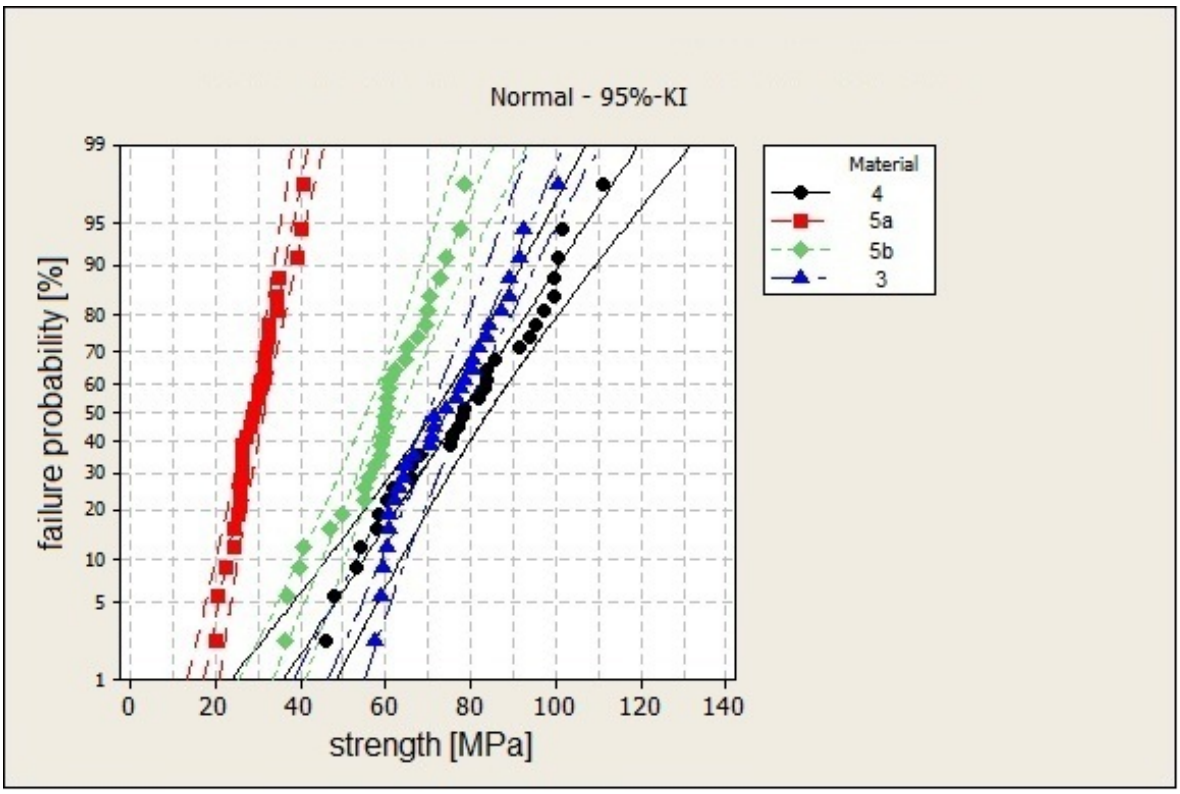

Figure 4.8.: Weibull diagram for the iron containing reference NTC materials: 3:blue, 4:black, 5a:red, 5b:green

this indicates that the material seems to be homogeneous. On the other hand, sample 2 with a Weibull strength of 55 ± 5 MPa has two different slopes within the curve. This could be a hint of two different failure causes in the ceramic. Therefore the Weibull module of sample 2 with 7.1 is not very meaningful. Weibull strength and modules can be found in table 4.6 and 4.7.

Figure 4.8 shows the iron containing NTC ceramics. The main difference between 5a and 5b ceramic is, that 5b is lapped on both sides of the sample, so that the sintered skin is lapped off. Sample 5a has a rather low strength of 32 ± 2 MPa and the slope seems to be quite constant, which is a hint, that sample 5a is a homogeneous ceramic. On the contrary, sample 5b has a strength of 64 ± 2 MPa, although it consists of the same material but has another thickness. It's also obvious, that sample 5b has more than one slope, so there are more than one failure causes. Sample 3 has a strength of 79 ± 2 MPa and sample 4 has a strength of 85 ± 2 MPa, but the Weibull moduli of both samples are quite low, so the materials are not very homogeneous.

Looking at figure 4.9 and table 4.4, it is obvious that the lapped sample of 5a has a much higher strength with 78 ± 2 MPa in contrast to the as sintered sample 5a, which has a strength of 38 ± 2 MPa. So it can be assumed that another factor reducing mechanical strength could be found in the sintered skin. Moreover table 4.4 shows that the Archimedes density and the total porosity of both samples are not significantly different. So it could be assumed that porosity and density are not significantly different in the stressed layer and the inner side of the ceramic. The Weibull module of the unlapped sample is higher that that of the lapped sample. Reason could be scratches introduced by the lapping process acting as early failure source.

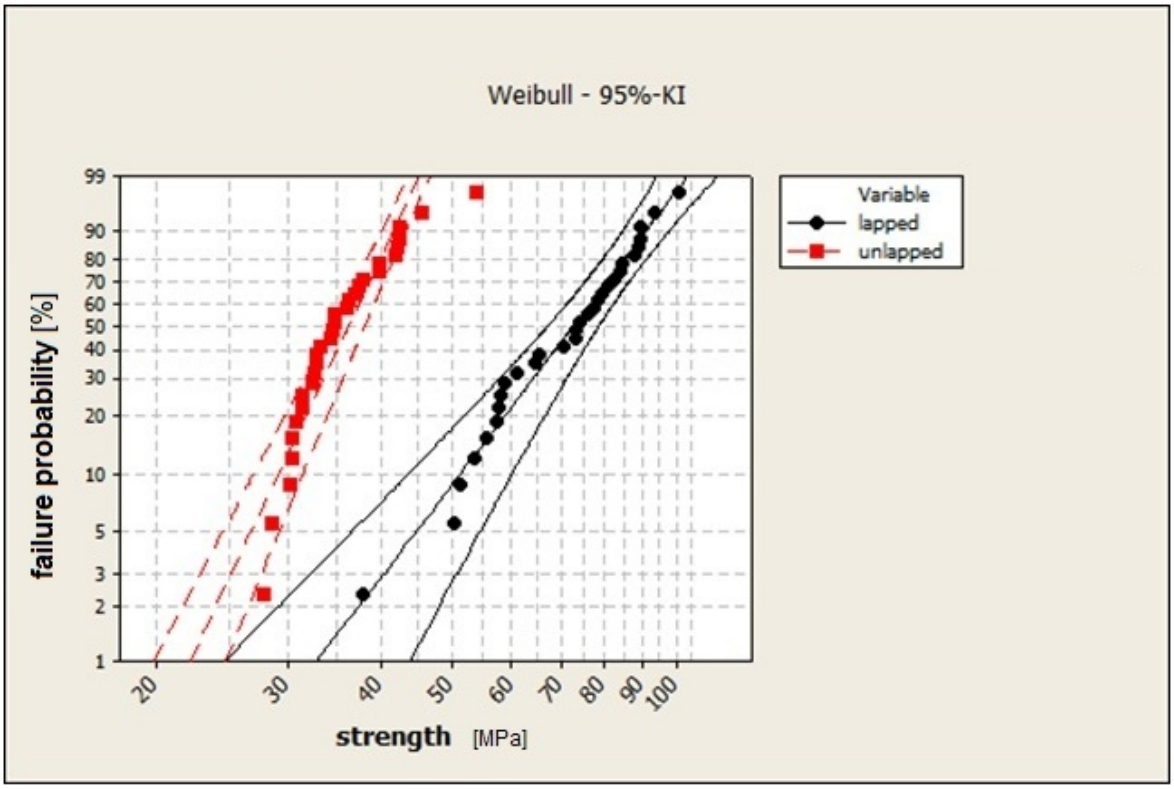

Figure 4.9.: Weibull diagram for the sample 5a: black:lapped, red:unlapped (as sintered)

4.2.3. Microstructure

The section microstructure gives a short overview of all investigated samples regarding their pores, precipitations, cracks and grain size distributions.

Sample 1a and 1b consist of the same material and are sintered with the same sintering

Table 4.4.: comparision of lapped and unlapped 5a NTC

Sample ID	5a unlapped	5a lapped
Weibull strength [MPa]$\Delta\sigma = 2MPa$	38	78
Weibull module m	7.6	5.5
Archimedes density $[g/cm^3]$	5.06 ± 0.02	4.99 ± 0.01
Total Porosity [%]	7 ± 1	6 ± 1

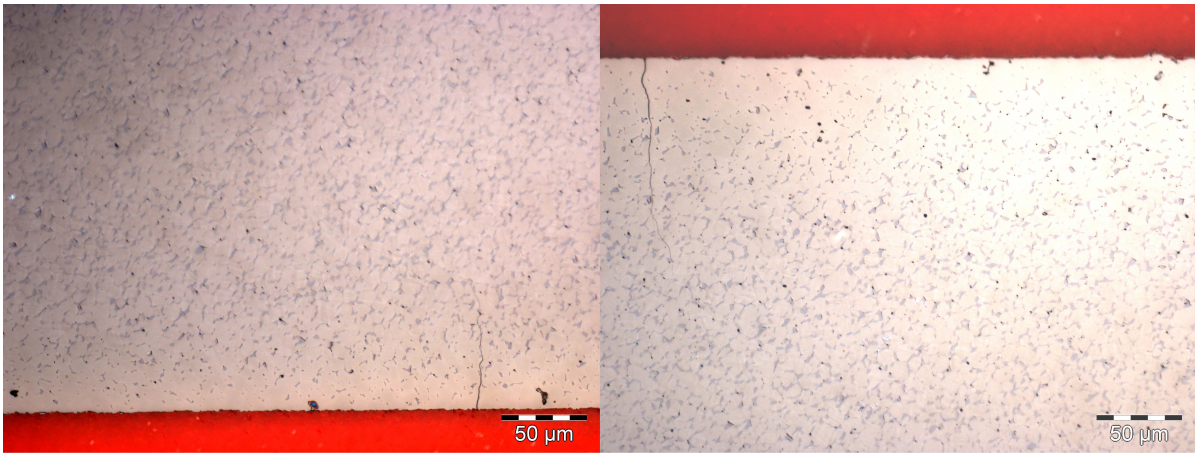

Figure 4.10.: microstructure of samples 1a and 1b

parameters. The only difference between those samples is the thickness. Sample 1a has a thickness of 0.439 ± 0.002 mm and sample 1b has a thickness of 0.839 ± 0.003 mm. Figure 4.10 shows photos from both samples taken with the light optical microscope. Attention should be paid to the cracks (Craquelure) in the samples , which are found all over the sample surface. Cracks are propagating perpendicular in the samples from the surface to the middle of the sample. Possible reason for the development of those cracks is the cooling phase during sintering. Rapid cooling can cause cracks. Cracks are possible failure causes and lower the strength of a sample. Also a sintered skin is visible on sample 1a and 1b at the edge of the samples. The amount and size of precipitations are much smaller in this region.

Figure 4.11 shows pictures of sample 2 taken with the light optical microscope on the left side and taken with the electron microscope in BSE mode on the right side. It is obvious, that a high amount of precipitations occur in this sample. Moreover the sintered skin is visible in both pictures, which may lead to lower strength.

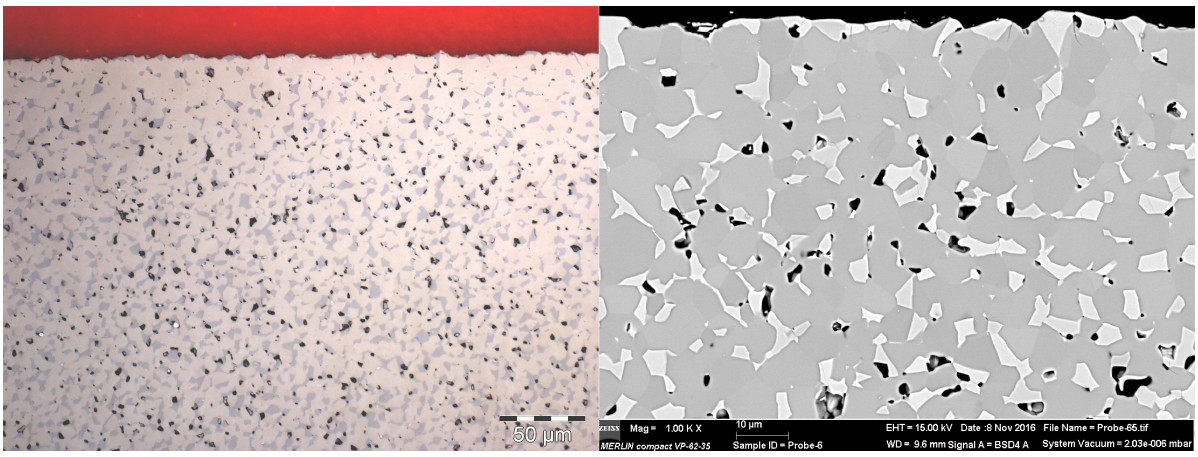

Figure 4.11.: microstructure of sample 2: left: LoM picture, right: SEM picture in BSE mode

Sample 3 (see figure 4.12) exhibits a high porosity and low amount of precipitations. Sample 4 in figure 4.12 shows no precipitations but pores ordered in chains. The origin of this pore chains can be found in the manufacturing process. The reason could be a low amount of pressure force, when pressing the green foils.

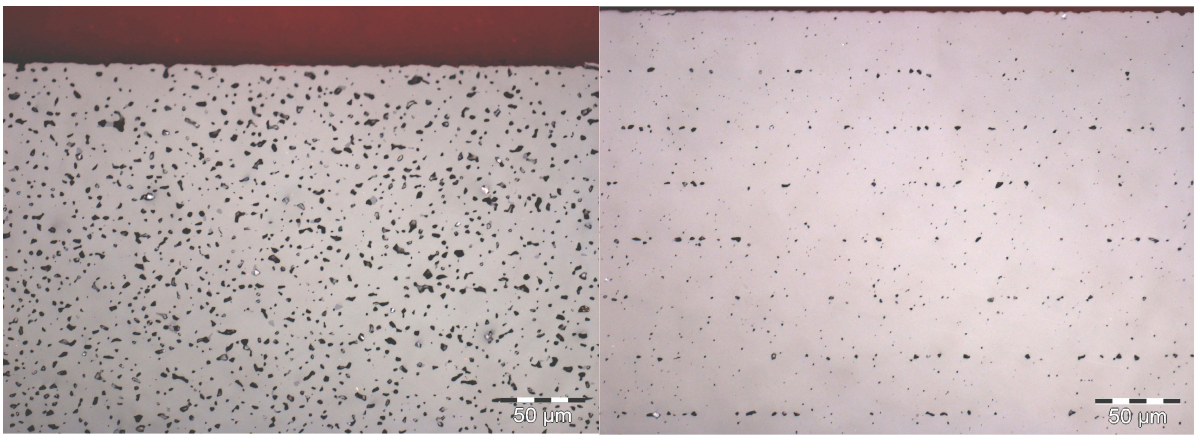

Figure 4.12.: microstructure of samples 3 and 4

Samples 5a and 5b (in figure 4.13) exhibit a high amount of Ni rich precipitations and fine dispersed pores. In sample 5a a sintered skin of $10 - 15\mu m$ can be determined.

The difference in composition between the edge of a sample and the intermediate layer can lead to stress, which also can lower the strength of a sample.

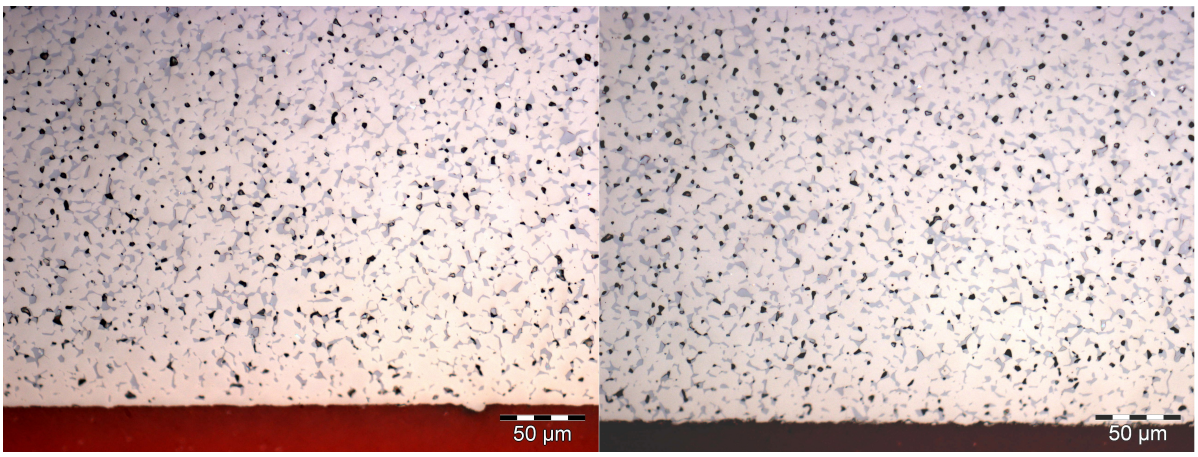

Figure 4.13.: microstructure of samples 5a and 5b

4.2.4. Influence of the Porosity Distribution

Following section takes a closer look to the porosity of the samples. In some literature like in [9] it is suggested, that porosity is a main influencing factor on strength. To examine this statement, pictures were taken with the Electron microscope in BSE mode and are shown in figure 4.14 to 4.20.

The analysis of the porosity distribution was carried out with the software Analyze (as described in section 3.7.2) and represented to the right side of the microscope pictures in a plot. The x axis discribes the distance from the edge of the sample in μm and the y axis shows the amout of pores in this area in percent.

Samples 1a and 1b (see figure 4.14 and 4.16) have rather low porosity and show a low distribution of pores all over the sample. Only tiny pores occure in the sintered skin.

Sample 2 (see figure 4.16) has a higher porosity than samples 1a and 1b and also bigger pore size. The distribution of pores is consistent all over the sample.

Sample 3 (see figure 4.17) has the highest amount of porosity of the investigated samples. In the range of $30-40\mu m$ from the edge and also in the range of $60-70\mu m$, the amount of pores is higher. This could be a hint of a pore chain, which could originate from the production process as already seen in figure 4.12 sample 4 or more obviouse in figure 4.18 sample 4.

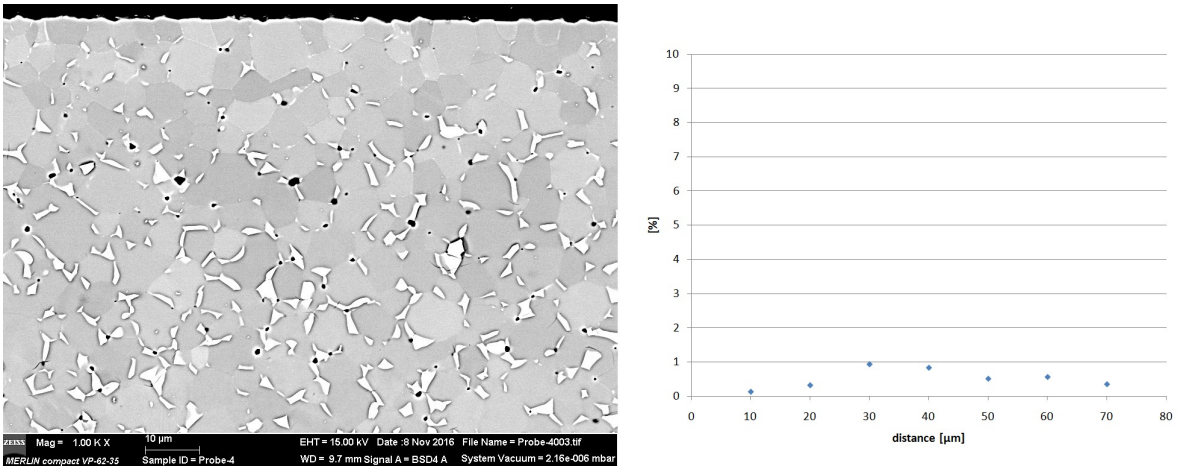

Figure 4.14.: porosity distribution of sample 1a

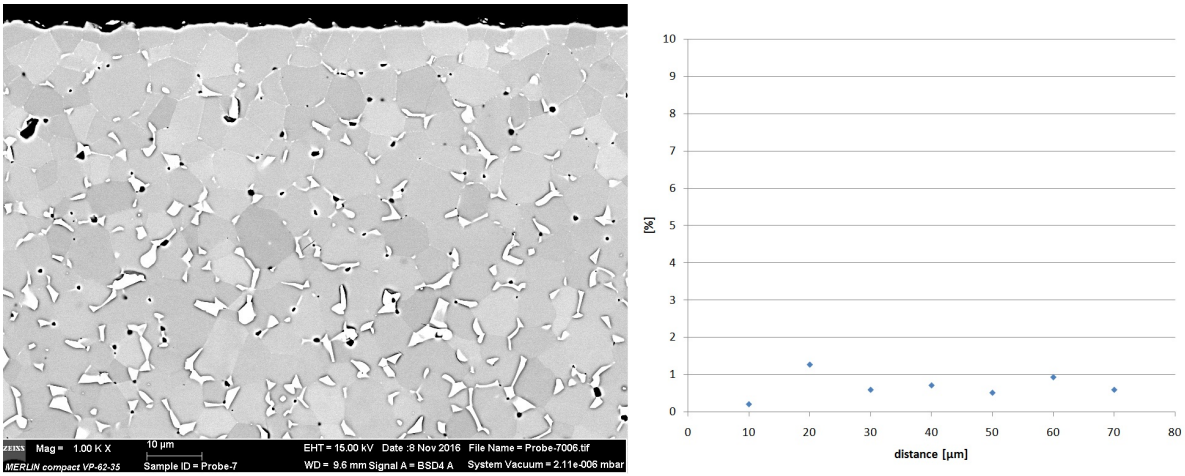

Figure 4.15.: porosity distribution of sample 1b

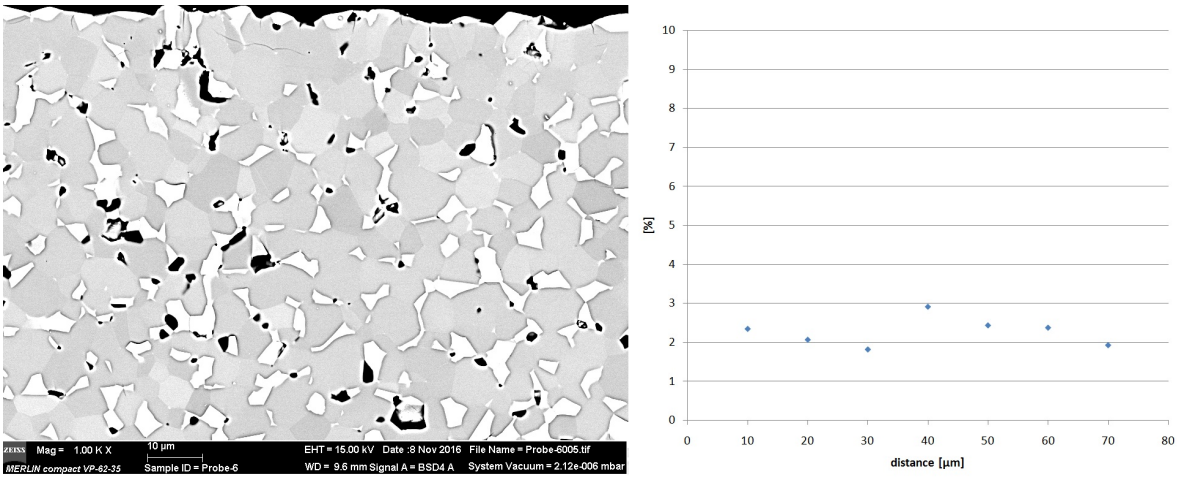

Figure 4.16.: porosity distribution of sample 2

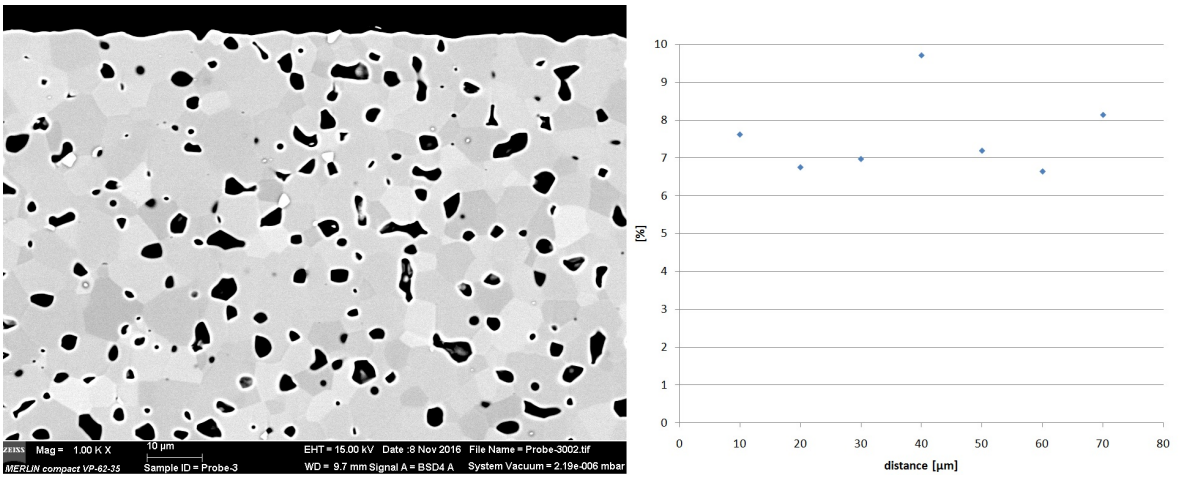

Figure 4.17.: porosity distribution of sample 3

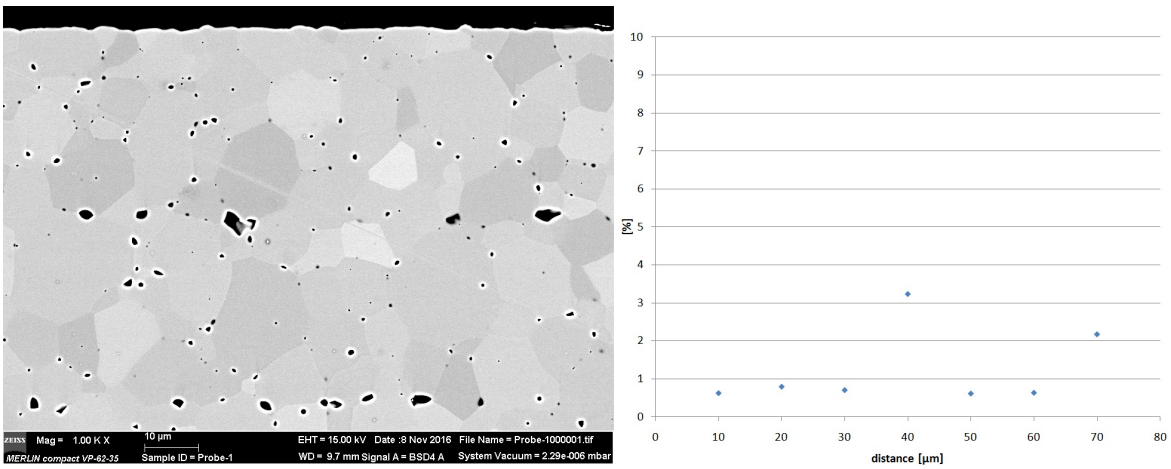

Figure 4.18.: porosity distribution of sample 4

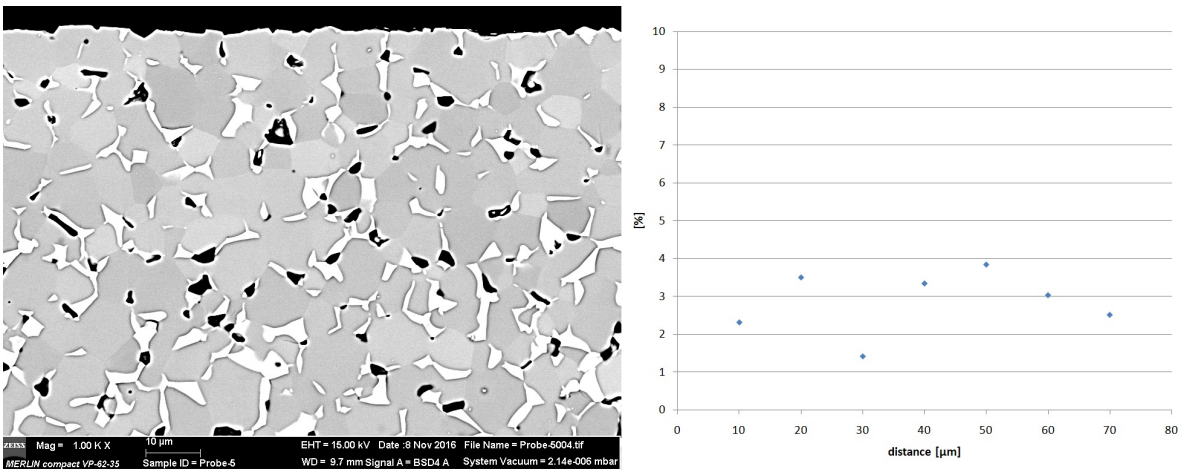

Figure 4.19.: porosity distribution of sample 5a

Samples 5a and 5b (see figure 4.19 and 4.20) show a rather homogeneous pore distribution, although sample 5b has a higher porosity at 20-30 and $50 - 60\mu m$, which could be a hint for a pore chain due to tape productions.

As a fazit we can say, that the porosity distribution among the investigated samples is more or less homogeneous. There is no striking distribution of pores over the samples.

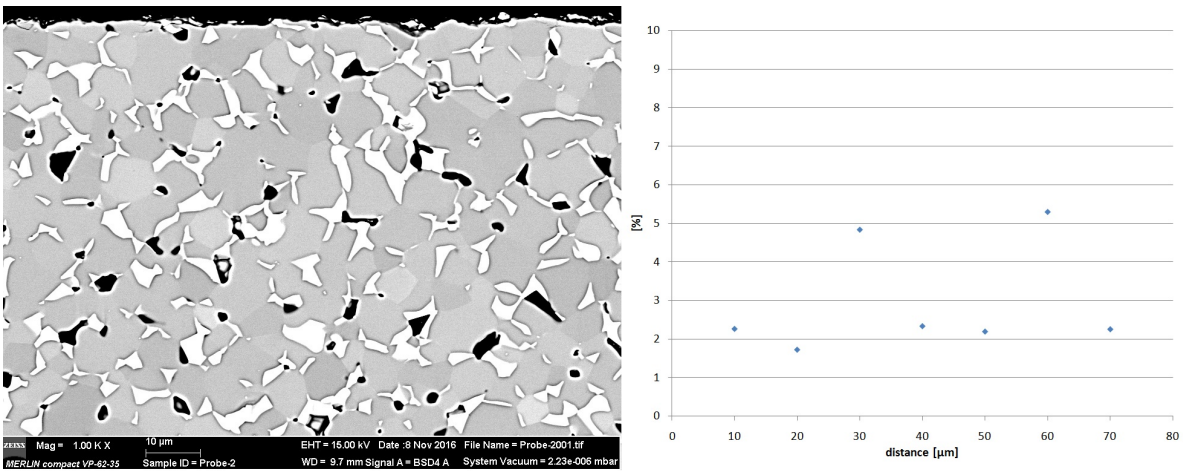

Figure 4.20.: porosity distribution of sample 5b

Table 4.5.: EDX Spectrum of selected areas of sample 5a

Spectrum Nr	O [Wt%]	Mn [Wt%]	Fe [Wt%]	Ni [Wt%]
22	23.44	50.37	6.53	19.67
23	18.11	8.23	-	73.65
24	16.66	5.90	-	77.44

4.2.5. Influence of the Precipitation Distribution

The next section exam the influence of Ni rich precipitations and their distribution from the edge of the sample to the inner side of the sample on the mechanical strength.

Looking at figure 4.21 and table 4.5 it could be proved with EDX analysis that precipitations (light areas) are Ni enriched. Those NiO precipitations are forming out of the Spinel phase when sintering at temperatures of the two phase region (see phase diagram in figure 2.2) according to formula 4.1 [9]. It is obvious, that oxygen is emitted during gas phase. Conversely at back reaction oxygen has to be gathered by the ceramic, although it is densified from sintering.

$$(3-y)Mn_{3-x}Ni_xO_4 \rightarrow (3-x)Mn_{3-4}Ni_yO_4 + 3(x-y)NiO + \frac{1}{2}(x-y)O_2 \qquad (4.1)$$

In figures 4.22 to 4.27 one can see SEM pictures in BSE mode from the sample edges on the left side. The right side shows the distribution of precipitation in a plot from 0 to 70 μm. Section 3.7.2 shows how the measurement was performed.

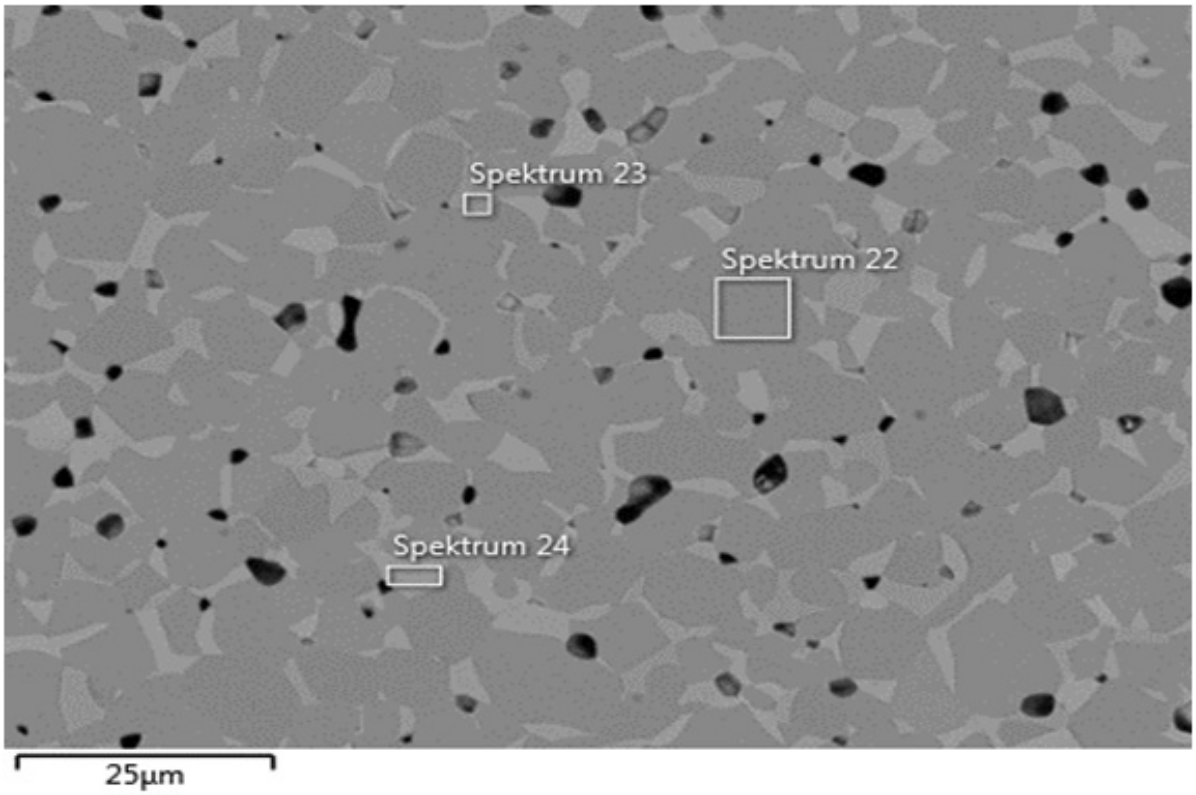

Figure 4.21.: EDX analysis of sample 5a

For sample 1a and sample 1b (see figure 4.22 and 4.23) the precipitations rise from 2% at the edge of the sample up to 9% in the middle of the sample. Together with the cracks all over the samples as already discussed in chapter 4.2.3, this adds to the very poor strength of 1a and 1b, which have the lowest measured Weibull strength of all investigated samples.

In sample 2 (see figure 4.24), the precipitations show an ascending behavior from 9 to 20 % in the area between the edge of the sample and 70 μm. This sample has a higher strength than sample 1a and 1b (see figure 4.22 and 4.23), but does not reach the strength of samples like sample 3 (see 4.25) or sample 4 which have the highest measured weibull strength and little precipitations.

Sample 3 has a distribution of precipitationon at very low level, which can be seen in figure 4.25. The amount of precipitations all over the sample with $0.7 \pm 0.5\%$ is rather low.

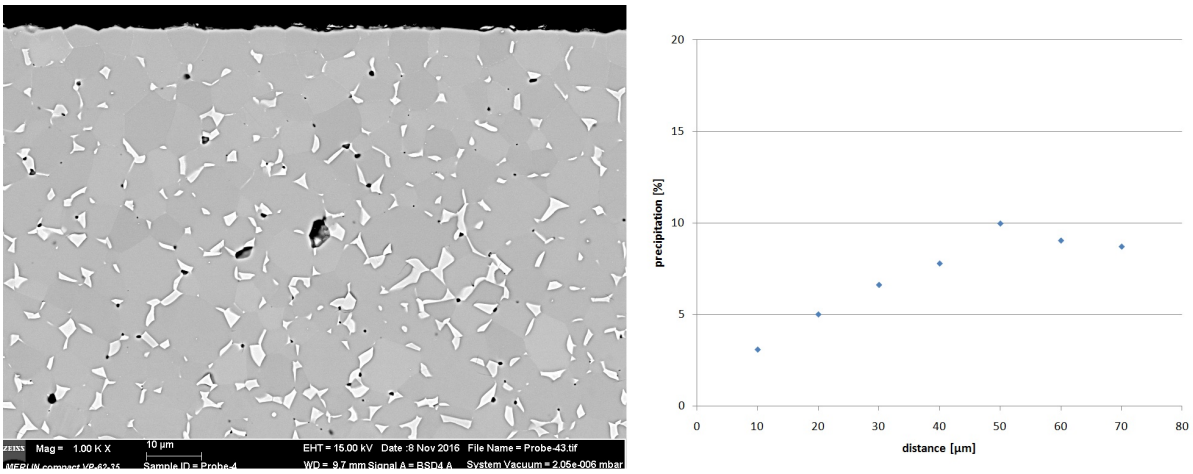

Figure 4.22.: precipitation distribution of sample 1a

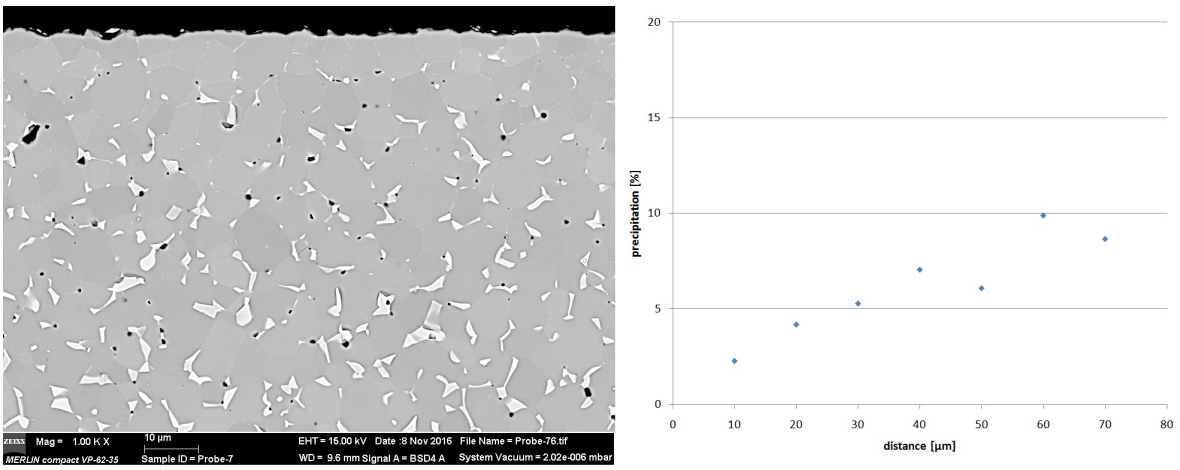

Figure 4.23.: precipitation distribution of sample 1b

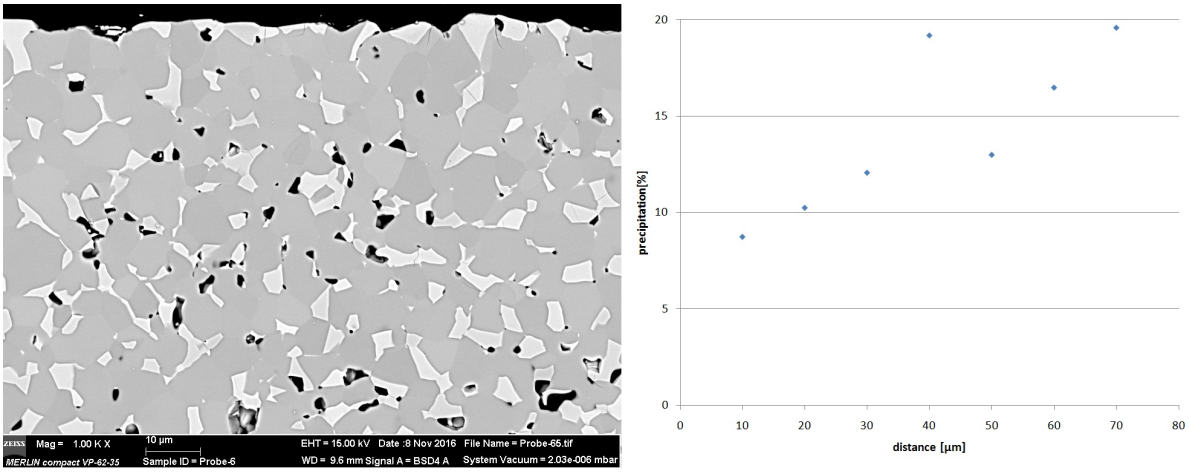

Figure 4.24.: precipitation distribution of sample 2

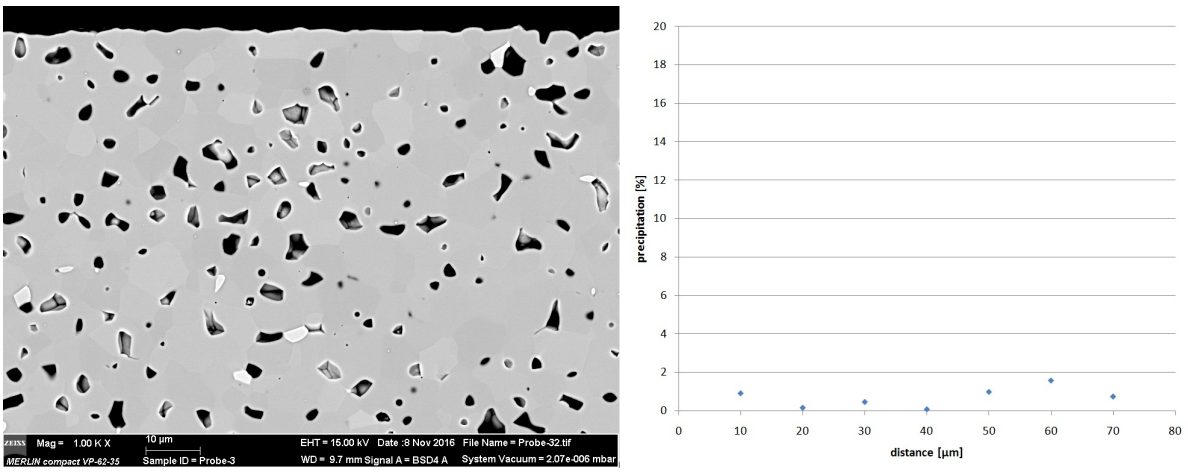

Figure 4.25.: precipitation distribution of sample 3

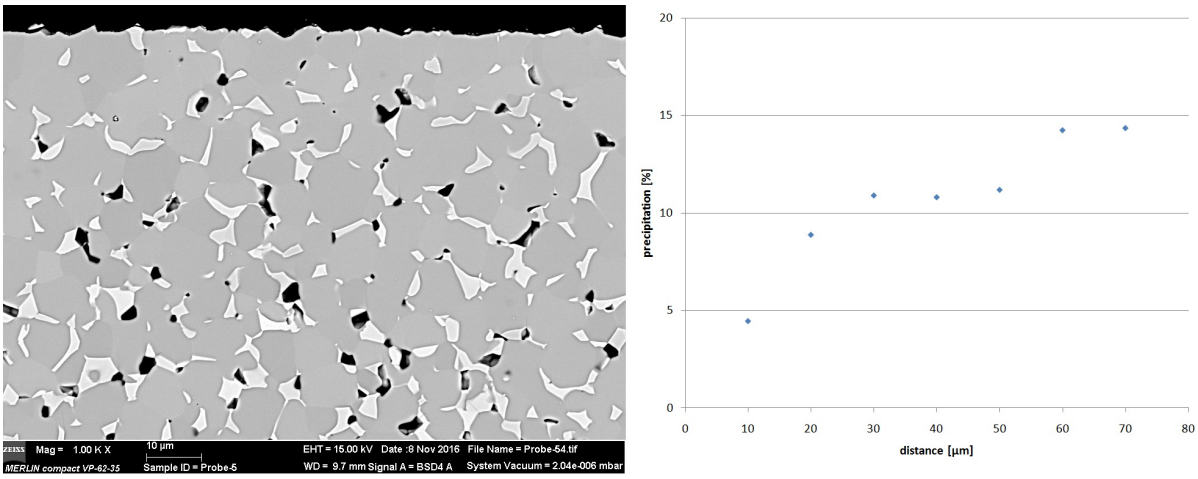

Figure 4.26.: precipitation distribution of sample 5a

Sample 5a (see figure 4.26) shows a precipitation distribution from 4 to 14 % in the area between the edge of the sample and 70 μm.

In contrast to that sample 5b has a stable precipitation distribution in the area between the edge of the sample and 70 μm and the mean area of precipitation is $14 \pm 1\%$. The reason for the missing sintered skin is, that sample 5b is a lapped sample. Furthermore sample 5b shows a higher Weibull strength of 64 ± 2 MPa in contrast to sample 5a with 32 ± 2 MPa.

This leads to the assumption, that the sintered skin is a main influencing factor of the mechanical strength for all samples.

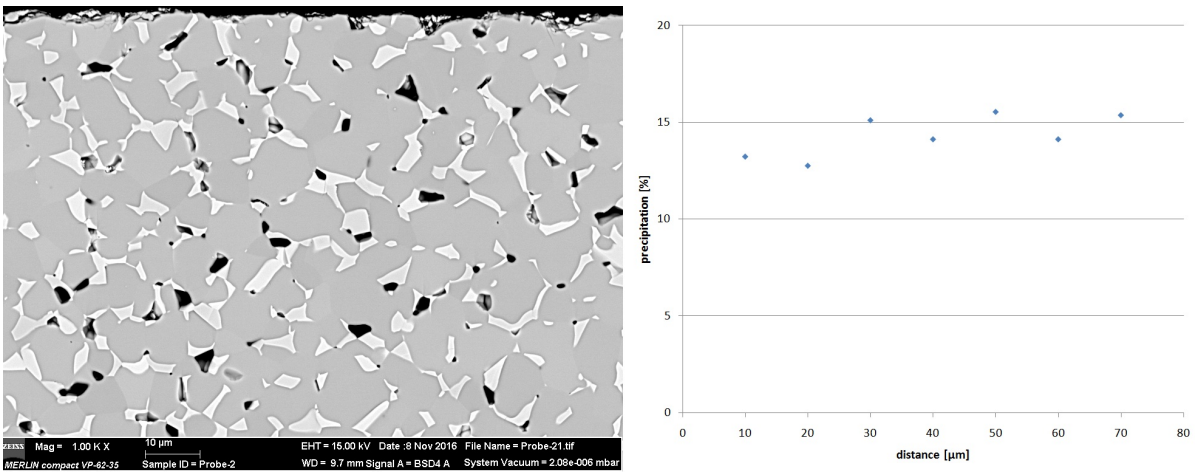

Figure 4.27.: precipitation distribution of sample 5b

4.2.6. Fractography

Fractography is a tool to analyze fractured ceramics. With fractography it is possible to identify the cause of the failure and moreover it is possible to calculate the size of the failure cause.

In figure 4.28 a typical fractography picture taken with the stereo microscope from sample 5a can be seen. The for ceramics typical fracture mirrors as described in [15] are visible starting from the origin of the fracture.

Using formula 2.6 from the fundamentals section, it is possible to calculate the size of the origin of the fracture. It can be assumed, that the geometical factor Y equals one and the critical fracture toughness equals 1.2 $MPa\sqrt{m}$. This approximation is based upon data from [13], where K_{IC}=1.2-1.9 $MPa\sqrt{m}$ for the Spinel structured $MgAl_2O_4$.

The as sintered sample 5a exhibits a mechanical strength of σ_c=32 MPa. This would lead to a fracture origin of about 450 μm. Using the strength of the lapped sample of 5a with σ_c=78 MPa, the facture origin would be 75 μm. The calculated 75 μm could be the possible fracture origin in figure 4.29, considering that the critical fracture toughness and the geometrical factor are estimations. This could be a crack, that develops in form of a half circle. A crack origin with a size of about 450 μm could not be found in 5a samples.

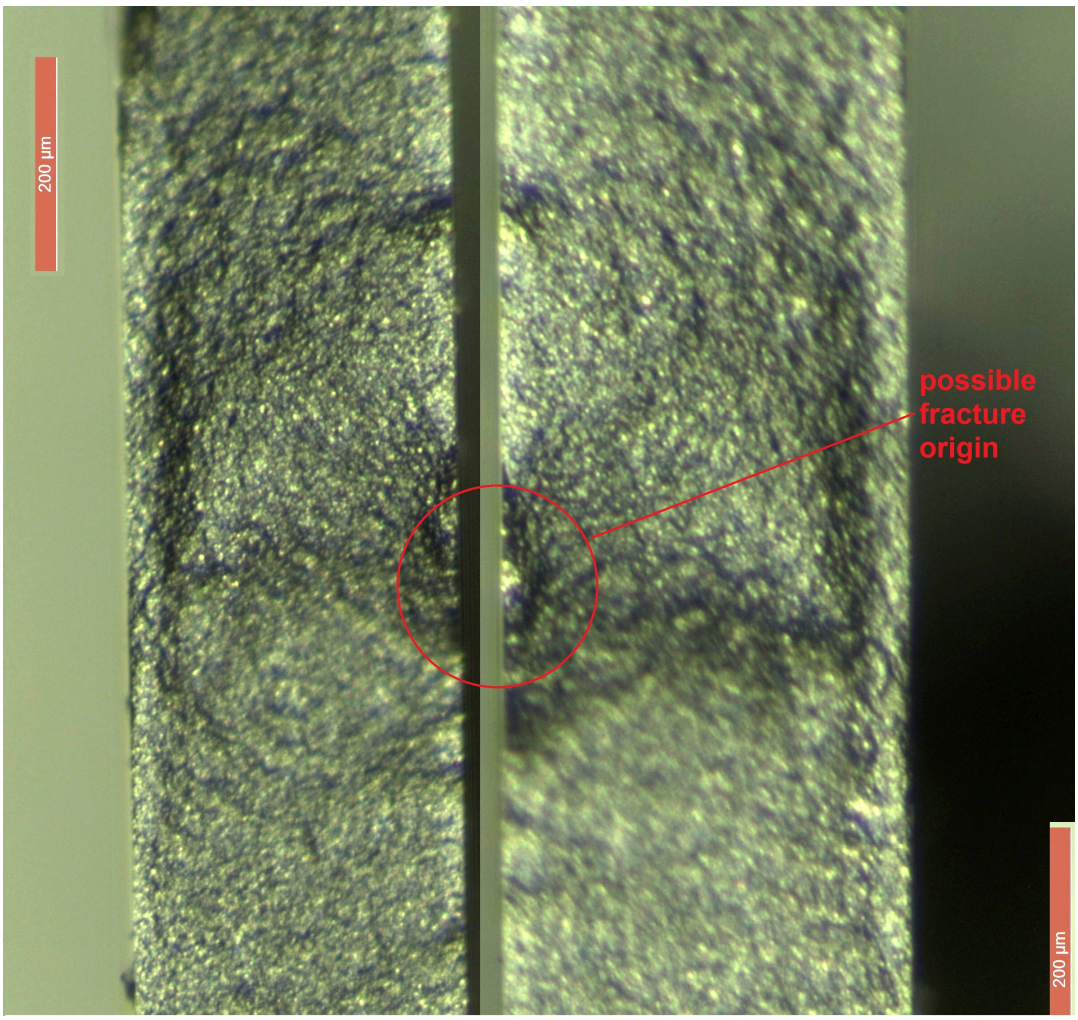

Figure 4.28.: fracture surface of sample 5a taken with the stereo microscope

These calculations show that besides cracks and pores another factor has to be responsible for the lower Weibull strength. This indicates on the sintered skin which lowers the strength of about one half due to the formation of stress between sintered skin and the intermediate layer. Considering the size of the fracture origin a higher porosity does not lead to a lower strength like described in literature like [9], because the pores of sample 5a have a diameter of 1.2 μm, whereas the fracture origin has a size of 75 μm.

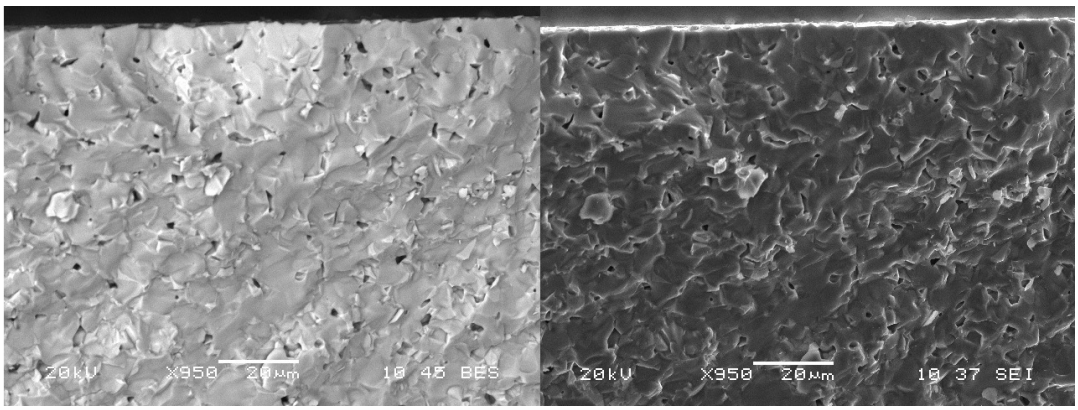

Figure 4.29.: fracture surface of sample 5a taken with the electron microscope: left: BSE mode, right: SE mode

4.2.7. Determination of Internal Stresses

The internal stresses were investigated as described in the methods section 3.6. The results of the measurement are shown in figure 4.30.

It is obviouse, that the warping after grinding (red line) is higher than the warping before grinding (blue line). This could be justified with internal stresses caused by the sintered skin. The sintered skin causes a tensile stress, which is schematically illustrated in figure 3.11.

Before grinding the substrate is in an equilibrium situation, where the sintered skin occures on both sides of the substrate and balances itself. If one side is worn off, only one sintered skin remains on the substrate and releases the tensile stress, which leads to the warping of the substrate.

This experiments can only indicate, that there are internal stresses within the substrate. The dimensions of the internal stresses cannot be quantified, because the method is not accurate enough. Besides every substrate was grinded by hand and the thickness of the substrate after grinding could not be adjusted precisely.

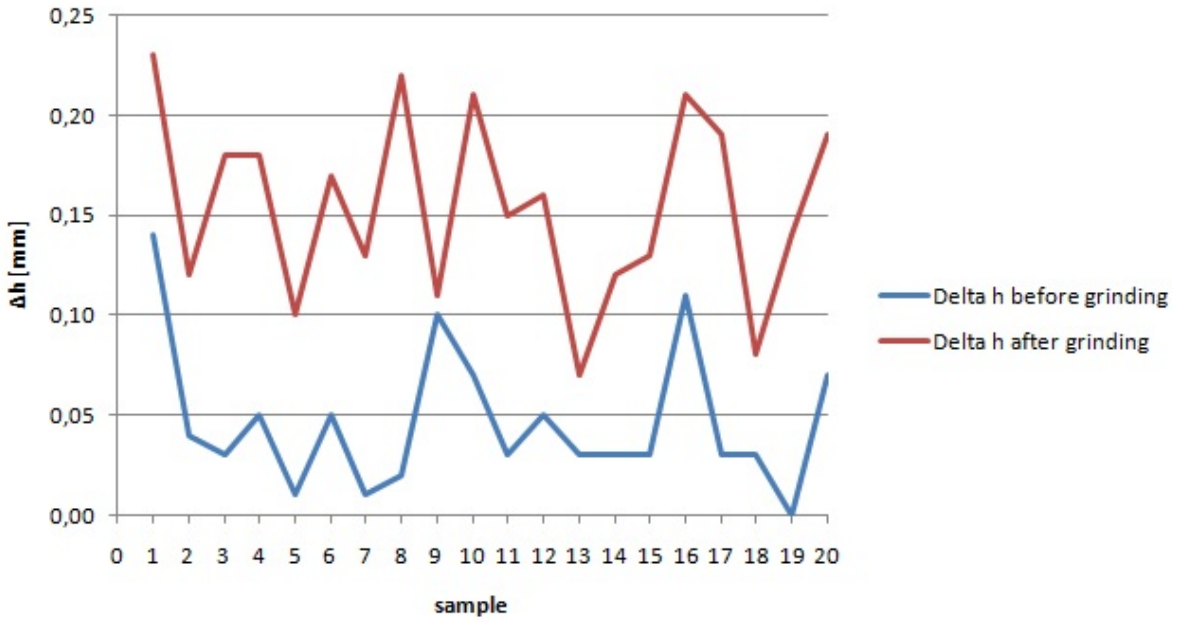

Figure 4.30.: warping before and after grinding of 20 DoE samples: blue: warping before grinding, red: warping after grinding

4.2.8. Origin of the Sintered Skin

The so called sintered skin is on the surface of a substrate, and exhibits a lower amount of precipitations as the inner sample.

In sample 5a, the precipitations in the first $10\mu m$ are 4%, whereas in the section between $60 - 70\mu m$ the precipitations are 14 % of the whole area (see also figure 4.26).

Looking at the phase diagram of figure 2.2 in the fundamentals section there could be made an assumption, how this sintered skin is built. Nevertheless it should be considered, that the phase diagram is only valid for systems with $NiO - Mn_2O_3 - O_2$ compositions. NTCs investigated in this diploma thesis also contain iron, so this phase diagram was only used for an estimation.

The compositions of investigated NTCs are around R=0.3. Sintering such green body up to about 1200°C leads to the two phase area of Spinel and $Ni_xMn_{1-x}O$, where Ni enriched precipitations are built. During sintering the outer pores are closing (closed porosity). After sintering the cooling with a predetermined cooling rate follows. For a

rebuild of the single phase Spinel, oxygen would be needed. But as the outer pores are closed, only the skin of a sample is able to rebuild the single phase. The inner side of the sample says in two phases, because the needed oxygen is absent. So the diffusion of oxygen into the sample is hindered by a dense sintered skin.

4.2.9. Summary

In table 4.6 and 4.7 the summarized data for the iron containing and non iron containing NTCs is given.

Sample 1a and 1b as well as sample 5a and 5b have the same composition and are sintered with the same temperature curve. The only difference is the thickness. Furthermore sample 5b is lapped (see also figure 4.1) and sample 5a is investigated as sintered.

The non iron containing samples 1a and 1b from table 4.6 show a nearly similar strength value, although the Weibull modulus for 1b is much higher than for 1a, which means that 1b is much more homogeneous than 1a. As it is the same material, the Archimedes density, the total porosity, the mean pores size and the grain size are not significantly different.

Sample 2 has a significantly different density, total porosity, mean pores size and grain size compared to sample 1a and 1b, as it is a different material. Furthermore the strength of sample 2 is higher that that of samples 1a and 1b, but compared with the iron containing samples, it has a moderate strength. A possible reason for the low strength of samples 1a and 1b are the cracks on the surface of the samples, which can be seen in figure 4.10.

Sample 2 has a rather high amout of precipitations ,but the precipitations have a distribution from 9% at the edge of the sample to 19% in the middle of the sample, which is obvious in figure 4.24. This distribution of precipitations is caused by a decomposition of the spinel during sintering and a back reaction during cooling of the material and could lead to internal stresses, which lower the strength of the material (see also section 4.2.7). Guillement-Fritsch et. al. [9] assumes, that in polyphased nickel-manganite-based ceramics containing a nickel oxide phase as second phase, the strength decreases as the quanitity of NiO increases.

Moreover the grain sizes of the non iron containing ceramics are generally smaller than the grain sizes of the iron containing ceramics. In general smaller grains lead to higher strength, but for the investigated ceramics, the grain size is not the main influencing factor for the strength.

Sample 4 is an iron containing ceramic. The microstructure is quite homogeneous and the pores are small and fine dispersed and allocated in rows (see also figure 4.12). Sample 4 has the largest grain size compared to the other samples and no precipitations (see figure 4.12). It is the sample with the highest measured strength, which is another hint, that the amount and distribution of precipitation is a main influencing factor of the strength. Sample 3 also has a high strength but in comparision to sample 4 it has a higher total porosity, larger pores and smaller grain sizes. Moreover sample 3 has few precipitations which are homogeneously dispersed throughout the sample, which may lead to a high strength.

Sample 5a and 5b have the same material composition and the only difference between them is the thickness of the samples (amount of stacked layers). Furthermore sample 5b is lapped. The density with open pores, the mean pores size, the total porosity and the grain size are not significantly different between the two samples. Nevertheless the strength of 5b is twice as high as 5a. The reason could be the different distribution of precipitation, as it can be seen in figure 4.26 and 4.27. The distribution of precipitation in 5a from 4% at the edge to 14% in the middle of the sample (see figure 4.26) could lead to inner tensions, which weake the strength. The detatching of the sintered skin leads to a tensile stress free surface of the samples.

Within the iron containing ceramics (see table 4.3), sample 3 has the lowest density and the highest porosity. Guillement-Fritsch et. al. [9] described for nickel manganite based ceramics used as NTCs, that the strength decreases with increasing porosity. This could not be proved in current diploma thesis, as sample 3 with the highest porosity has also the second highest strength. Moreover no regression for strength and total porosity for the reference NTC ceramics could be found. On the contrast to that, sample 4 has low total porosity and this sample has the highest strength of all samples measured. An explanation can be found in section 4.2.6.

Table 4.6.: main properties of non iron containing NTCs

	1a	1b	2
thickness [mm]	0.439 ± 0.002	0.839 ± 0.003	0.479 ± 0.003
strength [MPa] $\Delta\sigma = 5MPa$	32	27	55
Weibull modul m	9.7	15.0	7.1
Density with open pores $[g/cm^3]\Delta\rho = 0.002g/cm^3$	5.252	5.217	5.155
Total porosity [%]	2.1 ± 0.2	2.1 ± 0.2	6.4 ± 0.6
Mean pores size $[\mu m^2]$	1.00 ± 0.72	0.89 ± 0.55	3.96 ± 3.65
Grain size (area) $[\mu m^2]$	5.49 ± 8.59	4.62 ± 8.65	7.38 ± 8.11

Table 4.7.: main properties of iron containing NTCs

	3	4	5a	5b
thickness [mm]	0.441 ± 0.003	0.35 ± 0.02	0.629 ± 0.004	0.646 ± 0.002
strength [MPa] $\Delta\sigma = 2MPa$	79	85	32	64
Weibull modul m	7.4	5.1	6.8	5.9
Density with open pores $[g/cm^3]\Delta\rho = 0.002g/cm^3$	4.753	5.041	5.143	5.105
Total porosity	9.1 ± 0.3	2.1 ± 0.2	4.4 ± 0.2	4.6 ± 0.3
Mean pores size $[\mu m^2]$	4.88 ± 5.16	1.66 ± 1.95	4.48 ± 3.85	4.66 ± 4.05
Grain size (area) $[\mu m^2]$	15.19 ± 16.23	31.42 ± 43.52	12.36 ± 12.83	12.11 ± 14.57

4.3. Experiments for Optimization of Mechanical Properties

4.3.1. DoE examination

As discovered in the Pareto analysis (chapter 4.1.5), the factors "Maximum Temperature ","Hold time" and "Cooling rate" should be investigated in DoE A full factorial DoE with these 3 factors and 2 steps was chosen for DoE because linear as well as not linear dependencies should be investigated. With $2^3 = 8$ a cubic designed DoE is given, where the corner points of the cube are the DoE points to be investigated.

As a next step this DoE was enlarged to a Central Composite Design DoE with 8 cube points and 6 star points as described in section 2.4.1. The actual sintering parameters from fabrication department were chosen as center point with Maximum temperature=1194°C, Hold time=10 h and Cooling rate=4.7K/min. The Center point was tested 6 times. Based on these data a DoE was established in Minitab and is represented in table 4.8.

4.3.2. DoE Evaluation

4.3.2.1. Full DoE with All Strength Values

In this section the DoE including cube and star points was evaluated with every strength value available (30 values per point). The estimated regression coefficients for the strength are shown in table 4.9. The p values of the regression are all below 0.1 and therefore significant. The value R-Qd, which is a quality factor for the regression, is 23.75%. This means that the quality of the regression is not very good. DoE 18 was recognized as runaway value.

4.3.2.2. Full DoE with Weibull Strength Values

In this section the DoE including cube and star points was evaluated with the Weibull strength values. The estimated regression coefficients for the strength are shown in table

Table 4.8.: Central Composite Designed DoE

DoE number	Maximum Temperature[°C]	Hold time[min]	Cooling rate[K/min]
1	1244	900	1.7
2	1194	600	4.7
3	1244	900	7.7
4	1244	300	7.7
5	1244	300	1.7
6	1144	300	7.7
7	1144	900	7.7
8	1144	900	1.7
9	1144	300	1.7
10	1194	95.46	4.7
11	1109.91	600	4.7
12	1194	600	0.3
13	1194	600	4.7
14	1194	600	9.75
15	1194	600	4.7
16	1194	600	4.7
17	1194	600	4.7
18	1194	1104.54	4.7
19	1278.09	600	4.7
20	1194	600	4.7

Table 4.9.: Regression for full DoE with all strength values

	Coef	t	p
Constant	-1087.43	-3.253	0.001
Max Temp	1.88	3.351	0.001
Hold time	-0.04	-5.274	0.000
Cooling rate	4.54	7.046	0.000
Max Temp*Max Temp	-0.00	-3.351	0.001
Hold time*Hold time	0.00	7.059	0.000
Cooling rate*Cooling rate	-0.33	-5.130	0.000

Table 4.10.: Regression for full DoE with Weibull strength values

	Coef	t	p
Constant	63.0613	1.096	0.290
Max Temp	-0.0167	-0.352	0.730
Hold time	-0.0613	-1.943	0.071
Cooling rate	1.5965	2.018	0.062
Hold time*Hold time	0.0001	2.463	0.026

4.10. The p values of the regression for Hold time, Cooling rate and Hold time*Hold time are below 0.1 and therefore significant. The p values of the regression for the constant and the Maximum Temperature are not significant. The value R-Qd is 47.08%. That means that the quality of the regression is not very good. DoE 18 was recognized as runaway value.

4.3.2.3. Cubic DoE with Weibull Strength Values

In this section the DoE including the cube points was evaluated with Weibull strength values.

The estimated regression coefficients for the strength are shown in table 4.11. The p values of the regression are all, except of the hold time, below 0.1 and therefore significant. The value R-Qd is 83.98%,which means that the quality of the regression is good.

The contour plots for the dependence of the strength from Maximum Temperature, Hold time and Cooling rate can be seen in figure 4.31. Comparing Hold time to the Maximum Temperature, it is visible that above a hold time of 700 minutes, the Maximum Temperature is irrelevant. Below 700 minutes the strength is higher when substrates are sintered between 1170°C and 1220°C.

The plot, which shows the Cooling rate in dependence of the Maximum Temperature shows, that faster Cooling rates generally lead to higher strength values almost independet from Maximum Temperature. Also the plot with the dependency of Cooling rate and Hold time shows that the faster the Cooling rate the higher the strength independent from hold time.

Table 4.11.: Regression for cubic DoE with Weibull strength values

	Coef	t	p
Constant	-2074.82	-2.158	0.059
Max Temp	3.53	2.193	0.056
Hold time	-0.00	-0.792	0.449
Cooling rate	2.38	6.451	0.000
Max Temp*Max Temp	-0.00	-2.198	0.056

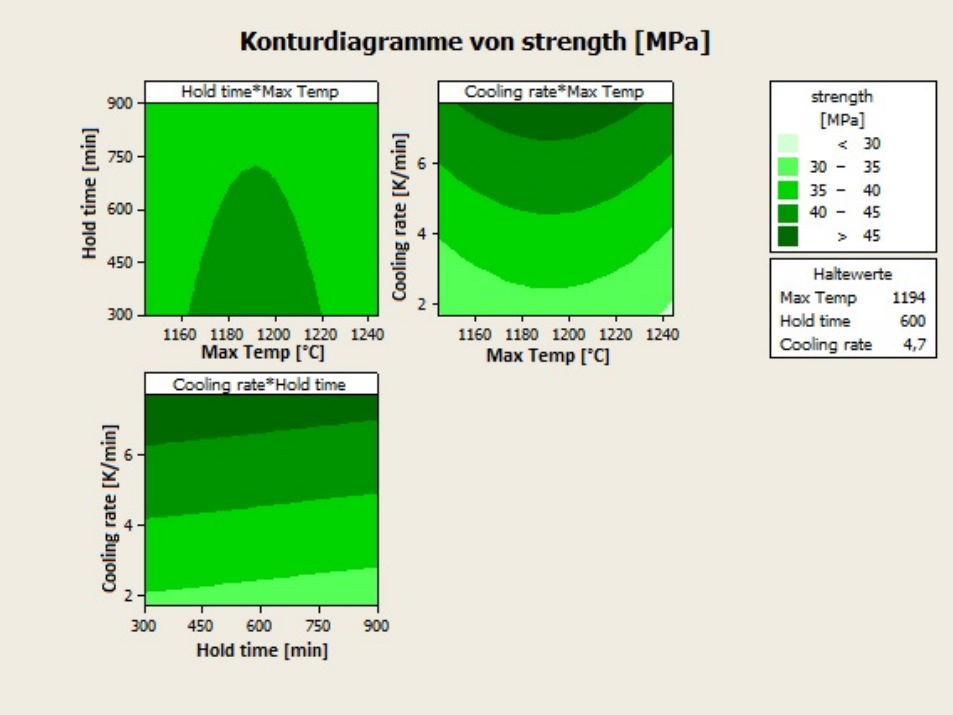

Figure 4.31.: contour plot for the cubic DoE with the Weibull strength: strength in dependence from Maximum Temperature, Hold time and Cooling rate

The parameter R25 is the resistance measured at 25°C, as described in section 2.1. The estimated regression coefficients for the R25 are shown in table 4.12. The p values are all below 0.1 and therefore significant. The value R-Qd is 99.92%, which means that the quality of the regression is very good.

Looking at the plot with the hold time in dependence of the Maximum Temperature (figure 4.32), it is visible, that the R25 value rises with Maximum Temperature, nearly independent from the Hold time. A higher Cooling rate on the other side leads to a higher R25 in combination with a higher Maximum Temperature. Also the third plot shows that a higher Cooling rate leads to a higher R25, independet from the Hold time.

Table 4.12.: Regression for cubic DoE with R25 values

	Coef	t	p
Constant	-714.176	-4.464	0.007
Max Temp	1.270	4.906	0.004
Hold time	-0.053	-3.118	0.026
Cooling rate	-31.681	-18.305	0.000
Max Temp*Max Temp	-0.001	-5.016	0.004
Max Temp*Hold time	0.000	3.262	0.022
Max Temp*Cooling rate	0.029	21.292	0.000
Hold time*Cooling rate	-0.001	-2.330	0.067

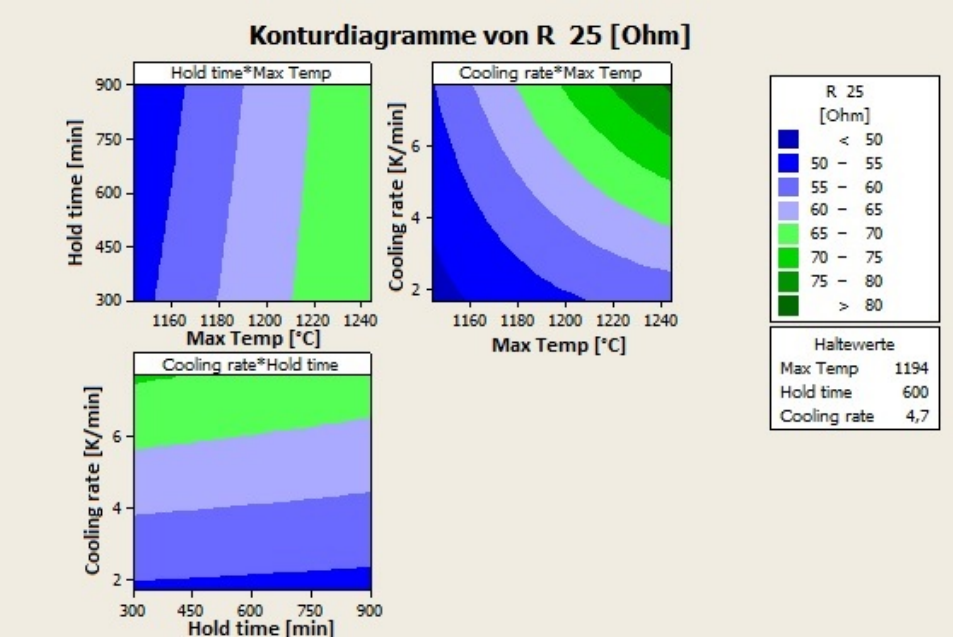

Figure 4.32.: contour plot for the cubic DoE with the R25 values: R25 in dependence from Maximum Temperature, Hold time and Cooling rate

The parameter R100 is the resistance measured at 100°C, as described in section 2.1. The estimated regression coefficients for the R100 are shown in table 4.13, where the p values are all below 0.1 (significant), except from the constant.The value R-Qd is 99.80%, which means that the quality of the regression is very good. Regarding figure 4.33, it can be seen, that with a higher Maximum Temperature, the R100 gets higher, nearly independent from the Hold time. The R100 also rises with a higher Cooling rate, nearly independet from the Hold time. Faster Cooling rates in combination with higher Maximum Temperatures lead to higher R100 values.

Table 4.13.: Regression for cubic DoE with R100 values

	Coef	t	p
Constant	-18.9933	-1.627	0.155
Max Temp	0.0399	2.082	0.082
Hold time	-0.0054	-4.631	0.004
Cooling rate	-1.8579	-16.046	0.000
Max Temp*Max Temp	-0.0000	-2.221	0.068
Max Temp*Hold time	0.0000	4.447	0.004
Max Temp*Cooling rate	0.0017	17.528	0.000

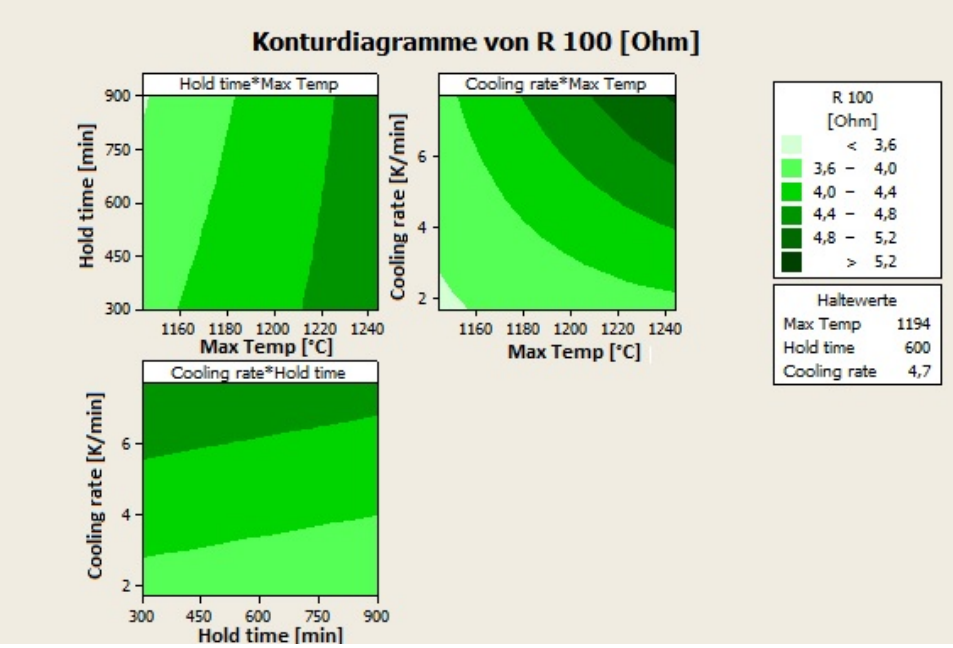

Figure 4.33.: contour plot for the cubic DoE with the R100 values: R100 in dependence from Maximum Temperature, Hold time and Cooling rate

The parameter B is described in section 2.1.The estimated regression coefficients for the B value are shown in table 4.14, where the p values are all below 1.1 and therefore significant.

The value R-Qd is 99.86%, which means that the quality of the regression is good.

Regarding figure 4.34, it can be seen, that with a higher Maximum Temperature, the B value gets higher, nearly independent from the Hold time. The B value also rises with a faster Cooling rate, nearly independet from the Hold time. Higher Cooling rates in combination with higher Maximum Temperatures moreover lead to higher B values.

Table 4.14.: Regression for cubic DoE with B values

	Coef	t	p
Constant	-9172.67	-11.625	0.000
Max Temp	21.35	16.348	0.000
Hold time	0.02	3.570	0.012
Cooling rate	-96.16	-11.724	0.000
Max Temp*Max Temp	-0.01	-16.047	0.000
Max Temp*Cooling rate	0.09	13.604	0.000
Hold time*Cooling rate	-0.00	-2.422	0.052

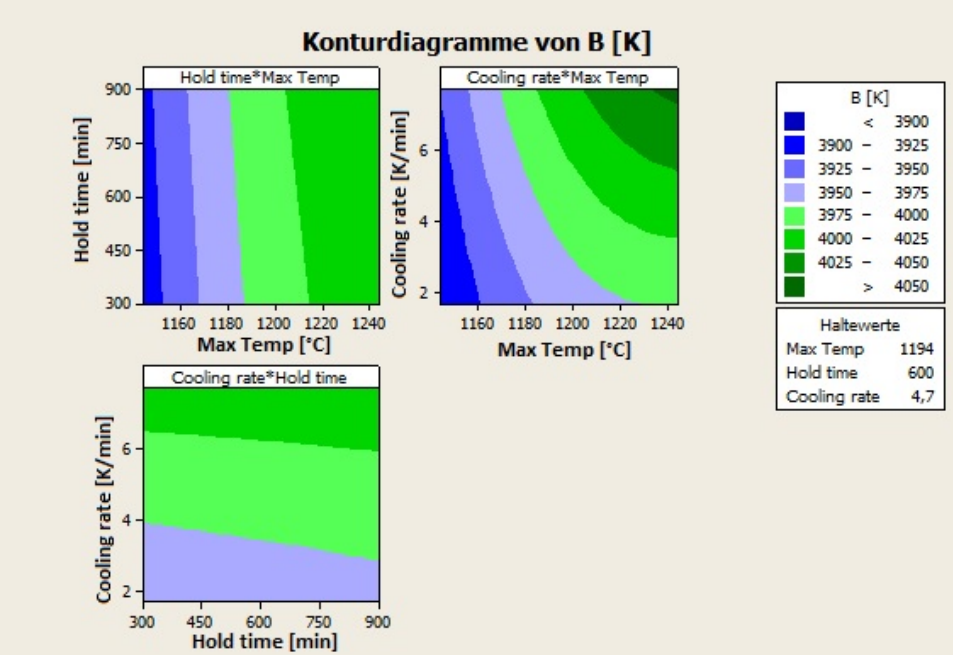

Figure 4.34.: contour plot for the cubic DoE with the B values: B in dependence from Maximum Temperature, Hold time and Cooling rate

4.3.2.4. Runaway Sample

One reason for the low R-Qd value of the full DoE was the runaway sample DoE 18. With a Weibull strength of 79 ± 10 MPa it did not fit into the regression of DoE. Although the B-value as well as the R25 and the R100 do not fit into the specifications. It is worth to take a closer look at this sample because the strength is much higher than for the other samples. Sample DoE 18 was sintered with 1194°C Maximum Temperature, 4.7 K/min Cooling rate and 1104 min Hold time, so the Hold time was much longer compared to the other DoE samples.

In figure 4.35 one can see, that DoE 18 has less precipitations in comparision to DoE 13, which is sintered at the Center Point. Furthermore DoE 18 has many fine dispersed pores with a porosity of 10.3±1.5% in contrast to DoE 13 with a porosity of 5.7±1.7%.

Considering that the sample of DoE 18 is out of the regression of the whole DoE, one could assume that the change in the fraction of the secondary phase is due to external factors that have not been taken into account in the experimental design. The changes in the fraction of the secondary phase with extremly long Hold time gives rise to the assumption, that evaporation of some components or reaction with the base plate (alumina) interferes with the sintering process.

Due to the low amount of precipitations and furthermore no distribution of precipitations from the edge to the inner side of the sample, the strength of DoE 18 is very high. On the other hand, the R_{25}, R_{100} and the B value are below the specifications.

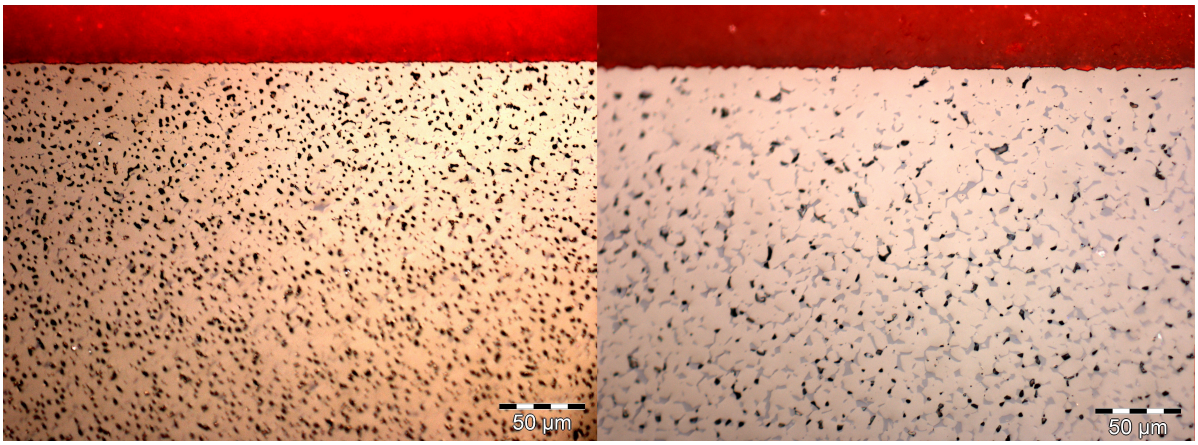

Figure 4.35.: microstructure of sample DoE 18:R25=27 Ω, R100=2 Ω, B=3744 K (left) and DoE 13: R25=61 Ω, R100=3984 Ω, B=3984 K (right)

Another peculiarity is the phase distribution in DoE 18 in comparision to a Center Point sintered sample (see table 4.15). The material distribution in DoE 18 is homogeneous due to the long hold time. On the contrary the phase distribution in DoE 13 (Center Point) is not homogeneous. Comparing the two sides of a sample with XRD measurement, side 2 exhibits a higher amount of $NiMn_2O_4$ and less NiO (see table 4.15). This could be the reason for the warping of the as sintered substrates.

Table 4.15.: XRD data from the Center Point sample DoE 13 and the runaway sample DoE 18

	DoE 13	DoE 18
$NiMn_2O_4$ side 1[%]	87.8	95.5
$NiMn_2O_4$ side 2[%]	96.6	95.3
NiO side 1 [%]	12.2	4.5
NiO side 2 [%]	3.4	4.7

4.4. Validation of Design of Experiments

Figure 4.36 shows the optimized values of Maximum Temperature=1162°C, Hold time=760 min and Cooling rate=7.7 K/min to achieve the maximum strength.

The specified values are $B = 3946K \pm 0.5\%$, $R_{25} = 59.45\Omega \pm 8.2\%$ and $R_{100} = 4.085\Omega \pm 8.2\%$. The calculated maximum strength is 45.7 MPa, whereas the B value amounts to 3964 K, the R_{25} value is 59.5Ω and the R_{100} value is 4.1Ω.

The validation of the calculated data was performed with another sintering run with the optimized values of Maximum Temperature, Hold time and Cooling rate. As an experimental result the strength was improved to 43 MPa, B=3951.58 K, $R_{25} = 55.14\Omega$ and $R_{100} = 3.84\Omega$.

Specified, calculated and measured values can also be seen in table 4.16 and it is obvious, that all measured values lie within the range of the specified values. Therefore an enhancement of the mechanical strength from 32 MPa up to 43 MPa is possible.

Table 4.16.: Specified, calculated and measured value for Mechanical strength, B, R_{25} and R_{100}

	Specified value	Calculated value	Measured value
Strength [MPa]	Max	46	43
B [K]	$3946K \pm 0.5\%$	3964	3952
R_{25}	$59.45\Omega \pm 8.2\%$	59.5	55.14
R_{100}	$4.085\Omega \pm 8.2\%$	4.1	3.840

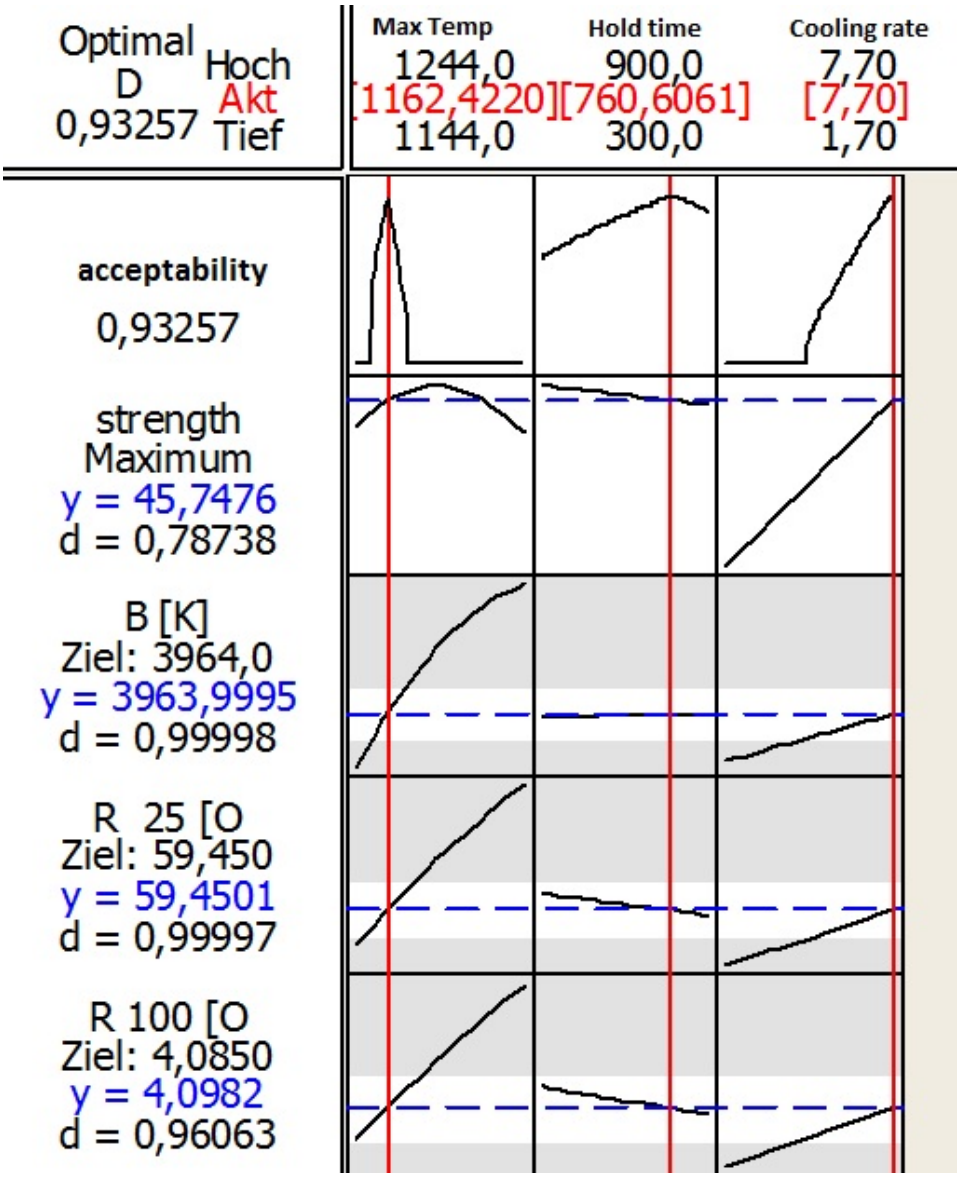

Figure 4.36.: optimization of the target values strength, B, R25 and R100

5. Summary and Outlook

The goal of current diploma thesis was to investigate the mechanical strength of NTC substrates and its influencing factors. Furthermore strength should be improved for one specific composition by variation of sintering parameters, but maintaining electrical specifications.

Comparing the investigated iron containing and non iron containing ceramics, it is obvious that the density for all ceramics lies around 5 g/cm^3. Sample 3 exhibits the lowest density with 4.753 g/cm^3 and has the highest porosity of 9.1 %, but it also shows the second highest mechanical strength of 79 MPa. On the contrary the samples with the highest density and lowest porosity are sample 1a and 1b. But these samples show very poor mechanical strength. In many scientific papers it is published, that a higher porosity leads to a lower mechanical strength. This could not be confirmed for the investigated NTC ceramics. Taking a closer look at the fractography section it can be seen, that the pore size of the investigated ceramics is far too low to be the origin of a fracture. Also the distribution of the pores is mostly homogeneous in the substrates. Only sample 4 shows a pore chain which originates probably from fabrication and this sample has the highest mechanical strength. Therefore porosity has no significant influence on mechanical strength for the investigated NTC substrates.

The grain sizes of the non iron containing ceramics are generally lower than the grain sizes of the iron containing ceramics. Smaller grains normally lead to higher strength, which again is not observed in the samples of this investigation. So grain sizes cannot be regarded as the main influencing factor on strength.

Sample 5 was investigated in a lapped status (sample 5b) and as sintered (sample 5a). The mechanical strength of the lapped sample was twice as high as for the as sintered sample, which was quite astonishing at a first glimpse, because lapping causes scratches

on the surface of the sample. After further investigations of lapped and as sintered samples it became obvious that the distribution of precipitations has a high influence on the mechanical strength. After sintering samples showed a so called sintered skin, which is a distribution of precipitation from the edge to the middle of the sample. Precipitations at the surface of a sample are far less than in the middle of a sample.

If a sample is lapped, the sintered skin is worn off and the mechanical strength rises. Experiments show, that the sintered skin causes tensile stresses, which can lower the mechanical strength of a sample. The existence of the sintered skin can be explained with the $NiO - Mn_2O_3 - O_2$ phase diagram (figure 2.2), although the investigated NTCs are also contaning Fe, Ni and more elements. Sintering a composition with a ratio Ni/(Ni+Mn) of 0.3 above 1000°C leads to a two phase area representing a decomposition of the spinel phase to NiO under release of oxygen. Hence sintering at 1200°C will cause NiO precipitations. Furthermore pore structure is changing from open porosity to closed porosity during sintering. After sintering the cooling with a predetermined cooling rate follows. For dissolving the precipitates in a back reaction during cooling oxygen would be needed. But in the state of closed porosity the oxygen can enter the material only by diffusion in bulk and along grain boundaries. That is why only in a thin surface layer ("skin") this back reaction takes place. The inner part of the sample stays in two phases, because the needed oxygen is absent.

After a process analysis according to Six Sigma standards, an insufficient mechanical strength was identified as root cause for edge breakouts. As an outcome the mechanical strength of sample type 5a should be improved by variation of the sintering parameters "Maximum Temperature", "Hold time" and "Cooling rate". As design of experiments a central composite design with 20 experiments was chosen, to consider linear as well as not linear influencing factors. For evaluation of DoE, only the cubic DoE could be used, because the star points included a runaway sample, which did not fit into regression. As an outcome it was possible to improve mechanical strength within electrical specifications with lower Maximum Temperature, higher Hold Time and a higher Cooling Rate, than sintering is now performed in production line.

Sample DoE 18 was sintered with a long Hold time, compared to the other DoE samples and exhibits a very high strength compared to other samples. It is therefore a runaway sample, which could not be considered in DoE. For better understanding of the mechanical strength of the 5a ceramic, it is useful to take a closer look at this sample. DoE

18 has less precipitations in comparison to Center Point sintered samples. Furthermore DoE 18 has many fine dispersed pores with a high porosity in contrast to Center Point sintered samples. One could assume that the change in the fraction of the secondary phase is due to external factors that have not been taken into account in the experimental design. Due to the low amount of precipitations and furthermore no distribution of precipitations, the strength of DoE 18 is very high. On the other hand, the R_{25}, R_{100} and the B value are far out of specifications.

For the future it could be useful to change the whole sintering process. The suggestion is to sinter the samples first and temper them afterwards to remove precipitations, which are the main problem of strength. But it has to be taken into account, that mainly the electrical parameters have to be within specifications. To do so, a new DoE would be needed. One could also think that quenching after the specified Hold Time instead of a special Cooling Rate, could also lead to non distributed precipitations in the sample. This may be true but quenching of ceramics causes cracks, which would lower the mechanical strength.

Another proposal is to lap off the sintered skin of every substrate after sintering, which would influence the thickness of the sample. This also has to be considered when designing the NTC.

For future investigations one should also bear in mind the oxygen distribution in sintering oven. More or less ogygen during sintering could also lead to diverse microstructures and precipitation behavior.

A. Appendix

Table A.1.: experimental results for DoE

DoE	Max. Temp.[°C]	Hold time[min]	Cooling rate[K/min]	Weibull strength [MPa]	R25 [Ω]	B [K]	R100 [Ω]
1	1244	900	1.7	29	57.00	3981	3.89
2	1194	600	4.7	40	61.91	3984	4.22
3	1244	900	7.7	40	80.02	4055	5.20
4	1244	300	7.7	46	81.44	4056	5.29
5	1244	300	1.7	30	56.52	3969	3.89
6	1144	300	7.7	46	56.89	3923	4.04
7	1144	900	7.7	43	52.81	3930	3.74
8	1144	900	1.7	31	47.15	3906	3.39
9	1144	300	1.7	28			
10	1194	95.46	4.7	41	59.50	3948	4.15
11	1109.91	600	4.7	42	47.37	3881	3.46
12	1194	600	0.3	33	42.2	3891	3.06
13	1194	600	4.7	46	61.44	3984	4.19
14	1194	600	9.75	38	66.43	3999	4.48
15	1194	600	4.7	38	61.97	3985	4.22
16	1194	600	4.7	36	61.30	3989	4.16
17	1194	600	4.7	43	60.91	3986	4.15
18	1194	1104.54	4.7	79	37.35	3744	2.19
19	1278.09	600	4.7	37	79.30	4052	5.16
20	1194	600	4.7	39	61.26	3987	4.17

Table A.2.: table of formulas

ρ	specific resistivity	Ω m
T	temperature	K
B	energy dependent constant	1/K
α_R	temperature coefficient of resistance	$1/K^3$
U	voltage	V
I	current	A
P	power	W
k_{th}	mounting, shape and surface finish constant	
F	failure load	N
S	distances between load rolls	m
W	sample height	m
b	sample width	m
σ_c	bending strength	Pa
σ_0	characteristic mechanical strength	Pa
K_{Ic}	fracture toughness	$Pa\sqrt{m}$
Y	geometry factor	
G(x)	probability that a measured value turns out the be x	
Q(x)	probability that a measured value not turns out the be x	
μ	arithmetic mean	
σ	standard deviation	
a	length of the initial crack size	m
a_0	smallest assumed crack size	m
m	Weibull modulus	
α	level of significance	
V_{sample}	volume of a NTC sample	cm^3
m_{sample}	mass of a NTC sample	g
m_{water}	mass of a NTC sample in a water bath	g
m_{air}	mass of a NTC sample wiped off after water bath	g
$\rho_{Archimedes}$	density of a NTC sample	g/cm^3
ρ_t	theoretical density of a NTC sample	g/cm^3
π_a	open porosity	
π_t	total porosity	

Bibliography

[1] Ametek. *Electron Backscatter Diffraction*. John Wiley and Sons, 2014.

[2] Carter C. Barry and Norton M. Grant. *Ceramic Materials- Science and Engineering*. Springer, 2007.

[3] Robert Danzer. On the relationship between ceramic strength and the requirements for mechanical design. *Journal of the European Ceramic Society*, 34:3435–3460, 2014.

[4] Robert Danzer, Peter Supancic, and Walter Harrer. Biaxial tensile strength test for brittle rectangular plates. *Journal of the Ceramic Socienty of Japan*, 114:1054–1060, 2006.

[5] Robert E. Dinnebier and Karin Friese. *Modern XRD methods in mineralogy*. 2003.

[6] Antonio Feteira. Negative temperature coefficient resistance (ntcr) ceramic thermistor: An industrail perspective. *J. Am. Ceram. Soc.*, 92:967–983, 2009.

[7] TEQ Technologietransfer & Qualitätssicherung GmbH. Trainingsprogramm six sigma black belt. Chemnitz, 2006.

[8] Yu V Golikov and V F Balakirev. Phase euilibrium diagram of the system ni-mn-o. *Journal of Phys. Chem. Solids*, 49:329–332, 1988.

[9] Sophie Guillement-Fritsch, Joaouad Salmi, Joseph Sarrias, Abel Rousset, Sophie Schuurman, and Andre Lannoo. Mechanical properties of nickel maganites-based ceramics used as negative temperature coefficient thermistors. *Materials Research Bulletin*, 39:1957–1965, 2004.

[10] Horst Scholze Hermann Salmang. *Keramik*. Rainer Telle, 2007.

[11] T. Holstein. Studies of polaron motion. *Annals of Physics*, 281:725–773, 2000.

[12] A.J. Moulson and J.M. Herbert. *Electroceramics: Materials, Properties, Applications*. 2003.

[13] Dietrich Munz and Theo Fett. *Mechnisches Verhalten keramischer Werkstoffe*. Springer, 1989.

[14] Lothar Papular. *Mathematische Formelsammlung*. Vieweg, 2014.

[15] George Quinn. *Fractography of Ceramics and Glasses*. National Institute of Standards and Technology, 2007.

[16] M.N. Rahman. *Ceramics Processing and Sintering*. 1995.

[17] Hanno Schaumburg. *Werkstoffe und Bauelemente der Elektrotechnik-Sensoren*. 1992.

[18] Hanno Schaumburg. *Werkstoffe und Bauelemente der Elektrotechnik-Keramik*. 1994.

[19] Peter Fritz Schmidt. *Praxis der Rasterelektronenmikroskopie and Mikrobereichsanalyse*. Wilfried J. Bartz, 1994.

[20] Karl Siebertz, David van Bebber, and Thomas Hochkirchen. *Statistische Versuchsplanung*. Springer, 2010.

[21] Gouglas A. Skoog, James F. Holler, and Stanley R. Crouch. *Instrumentelle Analytik: Grundlagen-Geräte-Anwendungen*. Springer Spektrum, 2013.

[22] Johann Wappis and Berndt Jung. *Taschenbuch Null-Fehler-Management*. Hanser, 2008.

List of Figures

List of Tables

Danksagung

Hiermit möchte ich mich für die sehr gute wissenschaftliche Betreuung bei Herrn Ao.Univ.Prof. Dipl.-Ing. Dr.techn. Klaus Reichmann (TU Graz) und Frau Dr. Christl Mead (Fa. Epcos) bedanken, die mir immer mit neuen Ideen und Rat und Tat zur Seite gestanden sind.

Der gesamten Abteilung SEN NTC gebührt ebenfalls anerkennender Dank, allen voran Herrn Dr. Jan Ihle für die Bereitstellung des Themas.

Ich möchte mich des Weiteren noch bei meiner Familie bedanken, die mir in dieser anstrengenden Zeit viel Verständnis entgegen gebracht hat.

Graz, Mai 2017 Petra Christöfl

AFFIDAVIT

I declare that I have authored this thesis independently, that I have not used other than the declared sources/resources, and that I have explicitly indicated all material which has been quoted either literally or by content from the sources used. The text document uploaded to TUGRAZonline is identical to the present master's thesis

Date ....

Signature